IMPACT RESISTANCE OF STEEL FIBER REINFORCED CONCRETE SLABS

A Thesis Submitted to the
Graduate School of Engineering and Sciences of
İzmir Institute of Technology
in Partial Fulfillment of the Requirements for the Degree of

MASTER OF SCIENCE

in Civil Engineering

by
Süleyman YAŞAYANLAR

July 2015
İZMİR

We approve the thesis of **Süleyman YAŞAYANLAR**

Examining Committee Members:

Assist. Prof.Dr. Selçuk SAATCI
Department of Civil Engineering, İzmir Institute of Technology

Assoc. Prof. Dr. Engin AKTAŞ
Department of Civil Engineering, İzmir Institute of Technology

Assist. Prof. Dr. Mert Yücel YARDIMCI
Department of Civil Engineering, Gediz University

13 July 2015

Assist. Prof.Dr. Selçuk SAATCI
Supervisor, Department of Civil Engineering
İzmir Institute of Technology

Prof.Dr. Gökmen TAYFUR
Head of the Department of
Civil Engineering

Prof.Dr. Bilge KARAÇALI
Dean of the Graduate School of
Engineering and Sciences

ACKNOWLEDGMENTS

First of all, I would like to express my gratitude for my supervisor Assist. Prof. Dr. Selçuk SAATCI for his endless support, guidance and patience over the course of this thesis and the laboratory work required.

I would like to thank our laboratory technician Cemal Kılıç, CE Research Assistant Hasan Yavuz Ersöz and my beloved fiancé Yonca Arsan for their help in and out of the laboratory.

My special thanks to the technicians of our neighbor laboratory, Laboratory of Mechanics, for sharing their experience, guidance and assistance.

ABSTRACT

IMPACT RESISTANCE OF STEEL FIBER REINFORCED CONCRETE SLABS

As rare as it may seem, impact loads can act on a structure in its lifespan. For structures such as nuclear energy facilities, industrial facilities, and military buildings design for impact loads may be required. Steel fibers are increasingly used in the design and construction of such reinforced concrete structures. However, studies on the effect of steel fibers on the impact resistance of reinforced concrete structures are rare in the literature. This study investigates the global behavior of reinforced concrete slabs with different ratios of steel fibers under static and impact loading.

10 steel fiber reinforced concrete slabs with dimensions of 2150x2150x150 mm were tested with varying steel fiber volume ratios of 0.5 %, 1.0 % and 1.5 %. Specimens were manufactured as twins, as one to be tested under static loading and one to be tested under impact loading. Static tests were carried out by applying a static load at the midpoint with a hydraulic jack, whereas impact tests were applied through free falling drop-weights.

Observed behavior and collected data were compared with companion studies of Batarlar (2013) and Arsan (2014), as they have used the same test setup with different parameters. As a result, it was seen that even steel a fiber addition of 0.5 % in volume was sufficient to provide a ductile behavior both under static and impact loading. Steel fibers significantly enhanced the impact behavior by increasing the strength and resiliency of the specimens.

ÖZET

ÇELİK FİBER KATKILI BETONARME DÖŞEMLERİN DARBE DAYANIMI

Her ne kadar ender görülse de yapılar kullanım ömürleri boyunca darbe yüklerine maruz kalabilirler. Nükleer enerji tesisleri, endüstriyel tesisler ve askeri binalar gibi yapıların darbe yüklerine karşı tasarımları gerekebilir. Bu tür betonarme yapıların tasarım ve inşalarında çelik fiberler artan oranda kullanılmaktadır. Ancak literatürde çelik fiberlerin betonarme yapıların darbe dayanımı üzerine olan etkilerini inceleyen çalışmalar çok azdır. Bu çalışma değişen çelik fiber oranına sahip betonarme döşemelerin statik ve darbe yükleri altındaki global davranışını incelemektedir.

2150x2150x150 mm boyutlarında 10 adet betonarme döşeme,% 0.5, % 1.0 ve % 1.5 oranlarında çelik fiber katkısı ile imal edilmiş ve test edilmişlerdir. Numuneler biri statik yük diğeri darbe yükü altında test edilmek üzere ikiz olarak imal edilmişlerdir. Statik yük orta noktaya hidrolik kriko yardımıyla uygulanırken darbe yükü serbest düşen darbe kütleleri vasıtasıyla uygulanmıştır.

Testler sırasında oluşan mesnet reaksiyonları, donatılar üzerinde oluşan gerinimler, yerdeğiştirmeler ve ivmeler yüksek hızlı bir veri toplama cihazıyla kaydedilmiştir..Test düzeneği kenarlarda basit mesnet koşulları oluşturacak şekilde imal edilmiştir.

Gözlemlenen davranış ve elde edilen veriler aynı test düzeneğini farklı numunelerle kullanan Batarlar (2013) ve Arsan'ın (2014) tamamlayıcı nitelikteki çalışmaları ile karşılaştırılmıştır. Sonuç olarak hacimce %0.5 oranındaki çelik fiber katkısının dahi hem statik hem darbe yükleri altında sünek bir davranış sağladığı görülmüştür. Çelik fiberler numunelerin darbe davranışını hem dayanımlarını hem de eski durumunu alma yeteneklerini geliştirerek önemli ölçüde iyileştirmiştir. Ayrıca çelik fiber oranının arttırılmasının darbe davranışını iyileştirmekle birlikte elde edilen faydanın aynı oranda olmadığı da gözlemlenmiştir.

TABLE OF CONTENTS

LIST OF FIGURES viii

LIST OF TABLES xiv

CHAPTER 1. INTRODUCTION 1

CHAPTER 2. LITERATURE REVIEW 4

2.1. Introduction 4

2.2. Impact Loading on RC Slabs 4

2.3. Companion Studies 17

CHAPTER 3. EXPERIMENTAL PROGRAM 24

3.1. Test Specimens 24

3.2. Slabs with Steel Fiber 26

3.3. Material properties 27

3.4. Test Setup 27

3.5. Instrumentation 28

3.5.1. Load Cells 29

3.5.2. Strain Gauges 29

3.5.3. Resistive Linear Position Transducers (RLPT's) 31

3.5.4. Accelerometers 32

3.5.5. Drop Weight 33

3.5.6. Data Acquisition System 34

3.5.7. High Speed Camera 34

3.6. Static Testing 35

3.6.1. SY100f05-a 36

3.6.2. SY150f05-a 36

3.6.3. SY150f15-a 37

3.6.4. SY200f05-a 38

3.6.5. SY200f15-a 39

3.6.6. YA200fa (Arsan, 2014) 40

3.6.7. BB100a (Batarlar ,2013) 41
3.6.8. BB200a (Batarlar, 2013) 42
3.7. Dynamic Testing 43
3.7.1. SY100f05-b 43
3.7.2. SY100f10-b 44
3.7.3. SY100f15-b 45
3.7.4. SY200f05-b 46
3.7.5. SY200f15-b 47
3.7.6. YA200fb (Arsan, 2014) 49
3.7.7. BB100b (Batarlar, 2013) 50
3.7.8. BB200b (Batarlar, 2013) 50

CHAPTER 4. DISCUSSION OF RESULTS 51
4.1. Static Tests 51
4.1.1. SY100f05-a SY150f10-a SY150f15-a BB100-a 53
4.1.2. SY200f05-a SY200f15-a YA200fa BB200a 58
4.2. Impact Tests 63
4.2.1. SY100f05-b, SY100f10-b, SY100f15-b, BB100b 63
4.2.2. SY200f05-b SY200f15-b YA200fb BB200b 70
4.3. Displaced Shapes 75
4.4. Support Reactions 89

CHAPTER 5. CONCLUSIONS 95

REFERENCES 97

APPENDIX A. TECHNICAL DATA SHEETS 99

LIST OF FIGURES

Figure **Page**

Figure 1.1. a) Penetration, b) Cone cracking, c) Spalling, d) Cracks on i) proximal face ii) distal face, e) Scabbing, f) Perforation and g) Overall target response 2
Figure 2.1. Overall view of the modified Charpy impact machine 5
Figure 2.2. Results from static uniaxial compression test 6
Figure 2.3. Metallic frame supporting a specimen 7
Figure 2.4. Drop-weight impact test setup 8
Figure 2.5. Failure of plain concrete slab 9
Figure 2.6. Failure patterns of slabs containing 0.5% volume fraction of fibers 10
Figure 2.7. Failure patterns of slabs containing 2.0% volume fraction of fibers 11
Figure 2.8. Effects of V_f and fiber type on the fracture energy: (a) fracture energy by observed load; (b) fracture energy by bending load 11
Figure 2.9. Test setup 12
Figure 2.10. Crack pattern on slab tension side: (a).Shear failure; (b).Flexural failure . 13
Figure 2.11. Load-versus-deflection response: (a). 10cm spacing; (b). 15cm spacing .. 14
Figure 2.12. Three dimensional views of (a) control specimen; (b) proposed system ... 15
Figure 2.13. Experimental setup (a) elevation; (b) top view 15
Figure 2.14. Cracking patterns at the tension side of the specimens: (a) CON-2T-2L; (b) SPE-2T-2L; (c)TOR-2T-2L; and (d)PVA-2T-2L 16
Figure 2.15. Impact test setup 17
Figure 2.16. Batarlar's reinforcement layout 18
Figure 2.17. RLPT's locations for static case 19
Figure 2.18. RLPT's locations for dynamic case 19
Figure 2.19. Hydraulic jack with the load cell 20
Figure 2.20. Crack distributions at the tension side of specimen in BB100a 21
Figure 2.21. Crack distributions at the tension side of specimen in BB150a 21
Figure 2.22. Crack distributions at the tension side of specimen in BB200a 22
Figure 2.23. Drop weights (210 and 320 kg respectively) 22
Figure 2.24. Shear stud used in Arsan, 2014 23
Figure 2.25. Layout of shear studs 23

Figure 3.1. Naming methodology 25
Figure 3.2. Geometric details of steel fibers 26
Figure 3.3. Steel fibers 26
Figure 3.4. Test Setup 28
Figure 3.5. Test Setup 28
Figure 3.6. (a) 10ton; (b) 5ton capacity load cells 29
Figure 3.7. Hydraulic piston with 50 ton capacity load cell on top 29
Figure 3.8. Strain gauges before coating 30
Figure 3.9. Strain gauges after coating 30
Figure 3.10. Final state of the strain gauge 31
Figure 3.11. General view of RLPT 31
Figure 3.12. Positions of RPLT's under the slab 32
Figure 3.13. Connection of the pivot head to the specimen before impact test 32
Figure 3.14. Locations of the accelerometers on top face 33
Figure 3.15. Two types of accelerometers; (a) Kistler Group accelerometers, (b) PCB Piezotronics accelerometers 33
Figure 3.16. (a) Former Drop Weight (320 kg), (b) Current Drop Weight (555 kg) 34
Figure 3.17. General view of Data Acquisition System 34
Figure 3.18. Mikroton EoSens high speed camera 35
Figure 3.19. SY100f05-a, (a) after 1st stop; (b) after 2nd stop; (c) after 3rd stop (Given numbers are crack widths in millimeter.) 36
Figure 3.20. SY150f10-a, (a) after 1st stop; (b) after 2nd stop; (c) after 3rd stop (Given numbers are crack widths in millimeter.) 37
Figure 3.21. SY150f15-a, (a) after 1st stop; (b) after 2nd stop; (c) after 3rd stop (Given numbers are crack widths in millimeter.) 38
Figure 3.22. SY200f05-a, (a) after 1st stop; (b) after 2nd stop; (c) after 3rd stop (Given numbers are crack widths in millimeter.) 39
Figure 3.23. SY200f15-a, (a) after 1st stop; (b) after 2nd stop; (c) after 3rd stop (Given numbers are crack widths in millimeter.) 40
Figure 3.24. YA200fa, (a) after 1st stop; (b) after 2nd stop; (c) after 3rd stop (Given numbers are crack widths in millimeter.) 41
Figure 3.25. BB100a, (a) after 1st stop; (b) after 2nd stop; (c) after 3rd stop; (d) after 4th stop 42

Figure 3.26. BB200a, (a) after 1st stop; (b) after 2nd stop; (c) after 3rd stop;
(d) after 4th stop; (e) after 5th stop 43
Figure 3.27. Bottom side of specimen SY100f05-b after 1st, 2nd and 3rd impacts
(Given numbers are crack widths in millimeter.) 44
Figure 3.28. Top side of specimen SY100f05-b after 1st, 2nd and 3rd impacts..... 44
Figure 3.29. SY100f10-b, (a) after 1st drop; (b) after 2nd drop; (c) after 3rd drop
(Given numbers are crack widths in millimeter.) 45
Figure 3.30. SY100f10-b, top side of the specimen (a) after 1st drop;(b) after 2nd drop 45
Figure 3.31. SY100f15-b, (a) after 1st drop; (b) after 2nd drop; (c) after 3rd drop
(Given numbers are crack widths in millimeter.) 46
Figure 3.32. SY100f15-b, top side of the specimen (a) after 2nd drop; (b) after 3rd
drop 46
Figure 3.33. SY200f05-b, (a) after 1st drop; (b) after 2nd drop
(Given numbers are crack widths in millimeter.) 47
Figure 3.34. SY200f05-b, top side of the specimen
(Given numbers are crack widths in millimeter.) 47
Figure 3.35. (a) after 1st drop; (b) after 2nd drop, (c) after 3rd drop
(Given numbers are crack widths in millimeter.) 48
Figure 3.36. SY200f15-b, top side of the specimen 48
Figure 3.37. YA200f10-b, after 1st and 2nd drop
(Given numbers are crack widths in millimeter.) 49
Figure 3.38. YA200f10-b, top side of the specimen (a) after 1st drop;
(b) after 2nd drop (Given numbers are crack widths in millimeter.) 49
Figure 3.39. BB100f00-b, (a) after 1st drop; (b) after 2nd drop; (c) after 3rd drop
(Given numbers are crack widths in millimeter.) 50
Figure 3.40. BB200f00-b, (a) after 1st drop; (b) after 2nd drop
(Given numbers are crack widths in millimeter.) 50
Figure 4.1. Load vs. midpoint displacement responses for static loading..... 52
Figure 4.2. Midpoint deflection vs. applied load responses for specimens
SY100f05-a, SY150f10-a, SY150f15-a and BB100-a..... 56
Figure 4.3. Tension face of specimen SY100f05-a after testing
(Numbers indicate crack widths in millimeters)..... 56
Figure 4.4. Tension face of specimen SY150f10-a after testing
(Numbers indicate crack widths in millimeters)..... 57

Figure 4.5. Tension face of specimen SY150f15-a after testing (Numbers indicate crack widths in millimeters) 57
Figure 4.6. Tension face of control specimen BB100-a after testing 57
Figure 4.7. Midpoint deflection vs. applied load responses for specimens SY200f05-a, SY200f15-a, YA200f00-a, YA200f-a and BB200-a 61
Figure 4.8. Tension face of specimen SY200f05-a after testing (Numbers indicate crack widths in millimeters) 61
Figure 4.9. Tension face of specimen SY200f15-a after testing (Numbers indicate crack widths in millimeters) 62
Figure 4.10. Tension face of the specimen YA200fa, after testing (Numbers indicate crack widths in millimeters) 62
Figure 4.11. Tension face of the control specimen BB200a, after testing 62
Figure 4.12. Bottom face of SY100f05-b after 1st, 2nd and 3rd impacts (Given numbers are crack widths in millimeter.) 64
Figure 4.13. Impacted face of SY100f05-b after 1st, 2nd and 3rd impacts 65
Figure 4.14. Bottom face of SY100f10-b after 1st, 2nd and 3rd impacts (Numbers indicate crack widths in millimeters) 66
Figure 4.15. Impacted face of SY100f10-b after 2nd and 3rd impacts 66
Figure 4.16. Bottom face of SY100f15-b after 1st, 2nd and 3rd impacts (Numbers indicate crack widths in millimeters) 67
Figure 4.17. Impacted face of SY100f15-b after 2nd and 3rd impacts 68
Figure 4.18. Crack profiles of bottom face for BB100b 68
Figure 4.19. Bottom face of (a) SY100f05-b, (b) SY100f10-b and (c) SY100f15-b at final state (Numbers indicate crack widths in millimeters) 69
Figure 4.20. Bottom face of specimen SY200f05-b after 1st and 2nd impacts (Numbers indicate crack widths in millimeters) 70
Figure 4.21. Top face of specimen SY200f05-b after 1st and 2nd impacts (Numbers indicate crack widths in millimeters) 71
Figure 4.22. Bottom face of specimen SY200f15-b after 1st, 2nd and 3rd impacts (Numbers indicate crack widths in millimeters) 72
Figure 4.23. Impacted face of specimen SY200f15-b after 1st, 2nd and 3rd impacts (Numbers indicate crack widths in millimeters) 72
Figure 4.24. Bottom face of specimen BB200b after 1st and 2nd impacts 73

Figure 4.25. Bottom face of specimen YA200f-b after 1st, 2nd, 3rd and 4th impacts (Numbers indicate crack widths in millimeters) 74
Figure 4.26. Impacted face of specimen YA200fb after 2nd, 3rd and 4th impacts (Numbers indicate crack widths in millimeters) 75
Figure 4.27. Placement of RLPTs on the bottom face of the specimens 75
Figure 4.28. Chosen RLPTs for specimens SY100f05-b, SY100f10-b and SY200f05-b for the first impacts 76
Figure 4.29. Chosen RLPTs for SY100f15-b and SY200f15-b for the first impacts 77
Figure 4.30. Deformation profile of specimen SY100f05-b after 1st impact 77
Figure 4.31. Deformation profile of specimen SY100f10-b after 1st impact 78
Figure 4.32. Deformation profile of specimen SY100f15-b after 1st impact 78
Figure 4.33. Deformation profile of specimen SY200f05-b after 1st impact 78
Figure 4.34. Deformation profile of specimen SY200f15-b after 1st impact 78
Figure 4.35. Deformation profile of specimen BB100b after 1st impact 79
Figure 4.36. Deformation profile of the specimen BB200b after 1st impact 79
Figure 4.37. Deformation profile of specimen of YA200fb after 1st impact 79
Figure 4.38. Maximum downwards displacement of the specimens with 0.4% longitudinal reinforcement ratio (Group 1) 81
Figure 4.39. Maximum downwards displacement of the specimens with 0.2% longitudinal reinforcement ratio (Group 2) 81
Figure 4.40. Comparison of static and dynamic displacements of specimens for same mid-point displacements 82
Figure 4.41. Time vs. Midpoint displacements for specimens with 0.2% and 0.4% longitudinal reinforcement ratio 83
Figure 4.42. Time vs. Midpoint displacements for specimens for all specimens 84
Figure 4.43. Maximum displacements of the specimens withe same longitudinal reinforcements and corresponding static tested control specimens 84
Figure 4.44. Shape of the specimen under static and impact loading 85
Figure 4.45. Displacement profile of each specimen under impact loading and the corresponding mid-point displacement at static loading 85
Figure 4.46. SY100f10 dynamic vs static displacements 87
Figure 4.47. SY100f15 dynamic vs static displacements 87
Figure 4.48. SY200f05 dynamic vs static displacements 88
Figure 4.49. SY200f15 dynamic vs static displacements 88

Figure 4.50. Total reaction force – time histories for SY100f05-b after each impact 89
Figure 4.51. Total reaction force – time histories for SY100f10-b after each impact 89
Figure 4.52. Total reaction force – time histories for SY100f15-b after each impact 90
Figure 4.53. Total reaction force – time histories for SY200f05-b after each impact 90
Figure 4.54. Total reaction force – time histories for SY200f15-b after each impact 91
Figure 4.55. Positions of the accelerometers and a typical tributary area used for the calculation of the inertia force of related mass 93
Figure 4.56. Load cell readings, inertia forces and impact forces for specimen SY100f10-b for first 60 ms 93
Figure 4.57. Load cell readings, inertia forces and impact forces for specimen SY100f15-b for first 60 ms 93
Figure 4.58. Load cell readings, inertia forces and impact forces for specimen SY200f05-b for first 60 ms 94
Figure 4.59. Load cell readings, inertia forces and impact forces for specimen SY200f15-b for first 60 ms 94

LIST OF TABLES

Table **Page**

Table 2.1. Details of the experimental program 5
Table 2.2. Thickness, fiber content and number of plates 7
Table 2.3. Summary of test results 16
Table 3.1. Details of specimens 24
Table 3.2. Mechanical properties of materials 27
Table 3.3. Peak load and related displacements 35
Table 4.1. Stopping displacements and related loads 52
Table 4.2. Peak loads and related displacements 52
Table 4.3. Peak load and relative displacement of the specimen Group 1 54
Table 4.4. Increase in the failure load and failure displacement 54
Table 4.5. Peak load and corresponding displacement of the specimen Group 2 58
Table 4.6. Increase in the failure load and failure displacement relative to BB200a 59
Table 4.7. Final load and related displacement of all the specimens 60
Table 4.8. Drop weight and drop heights for specimens 63
Table 4.9. Dropped RLPTs in each axis of each specimen for the first impacts 76
Table 4.10. Maximum, minimum and residual displacements of each specimen 80
Table 4.11. Normalized maximum and residual displacements of the specimens 83
Table 4.12. Displacement values of the RLPTs under dynamic and static loading 86
Table 4.13. Maximum positive support reactions after each impact 91
Table 4.14. Maximum negative support reactions after each impact 92

CHAPTER 1

INTRODUCTION

Civil engineering applications have been improving in accordance with harmony and desires of humanity. As a result of the improvements in composite materials, reinforced concrete became the material of choice in the majority structures. In addition to gravity loads, various types of load combinations can be taken into account in the design of such structures, such as impact, earthquake and blast. Impact resistant design have been an objective for many researchers and designers. Vehicle collisions, rocks falls, accidental events in industry, military actions and terrorist attacks can cause impact loads in structures. During an impact event, target absorbs a large amount of energy in a short time. Depending on the energy absorption capacity of the structure affected by the impact, member penetration, scabbing or spalling can occur. Alternatively, the system may respond globally (Figure 1.1). Due to the damage state of the target and projectile, impact can be categorized in two: a soft impact, when the projectile deforms more than the target, and a hard impact, when the target deforms more than the projectile. The state of the damage on the structure is the main interest in most studies. For military studies local damage is the main interest, whereas for civil studies global failure of the target is the main interest.

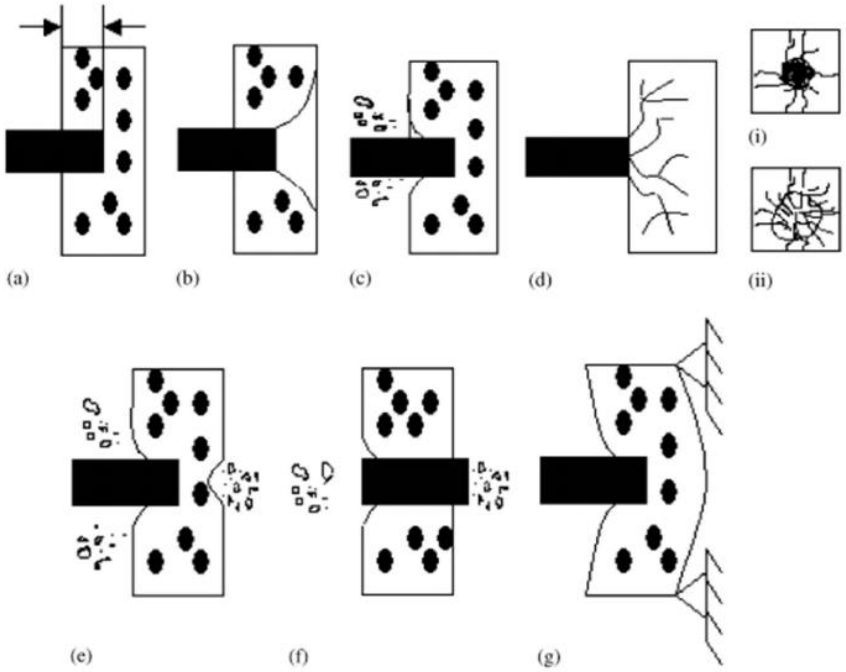

Figure 1.1. a) Penetration, b) Cone cracking, c) Spalling, d) Cracks on i) proximal face ii) distal face, e) Scabbing, f) Perforation and g) Overall target response (Source: Li et al, 2005)

Reinforced concrete (RC) slabs are typically designed for gravity loads and live loads, which are smaller in magnitude and act for a long duration compared to impact loads. In case of impact loading, a large amount of energy is applied to the slab for a very short time. As a result of impact load, the structure can lose the ability to transfer the force to other structural elements such as columns and beams. Thus, after the impact the slab can locally fail or in a worst case scenario, global failure of the structure can occur.

In literature numerous studies on the impact loading on structures exist. Many of the studies investigated the local failure of the specimens due to the demands of the military and nuclear energy industry. Such studies investigated the effects of the high velocity missiles on structures. On the other hand, global failure of the structures is the main concern for civil structures. Research on the global response of the structures under impact loading is very limited.

The study presented here is a work that precedes the work by Batarlar (2013) and Arsan (2014). Like the companion studies, this study aimed towards understanding the global behavior of the RC members under impact loading. In Batarlar's study, which investigated the behavior of RC slabs under impact loads, a brittle punching failure

mechanism was observed. In Arsan's study, in order to increase the punching capacity of specimens, two approaches were followed: steel fibers added to concrete mix, and shear studs added around the impact area. This study concentrated on the effect of steel fibers to the impact behavior of RC slabs and expanded Arsan's study on the subject. 0.5%, 1.0% and 1.5% steel fiber ratio by volume were used in the specimens and compared to the companion studies.

In the following chapter, a literature review of the subject is provided. Details of the experimental program are presented in Chapter 3. Discussions and comparisons with companion studies are presented in Chapter 4. Conclusion and further studies are presented in Chapter 5.

CHAPTER 2

LITERATURE REVIEW

2.1. Introduction

For the past few decades, impact event has been investigated by many researchers. Here in this study, response of the slabs with steel fibers under impact loading will be investigated. Therefore, in this chapter some important studies which investigated the response of reinforced slabs with steel fibers will be summarized. Finally, companion studies by Batarlar (2013) and Arsan (2014) will be investigated in more detail.

2.2. Impact Loading on RC Slabs

Impact on the structures can be categorized as either soft or hard impacts. If the projectile penetrates the target without suffering any damage, it is called hard impact. In case of soft impact, the projectile is damaged while the target remains relatively undamaged.

After a hard impact event, different types of failure modes can be observed. Kennedy (1976) stated possible modes of failure as presented in Figure 1.1.

Impact resistance of concrete could be increased by adding sufficient amount of fiber. American Concrete Institution (ACI) Committee 544 recommends repeated impact drop weight test to obtain the impact resistance of concrete members. The results from this test method have some drawbacks. The obtained results rely on the geometry of the specimen, boundary condition and prescribed failure criteria. In order to overcome these drawbacks, an experimental study was carried by Gopalaratnam and Shah (1986). In this study, modified charpy test machine (Figure 2.1) was used to measure the impact resistance of steel fiber reinforced concrete specimens.

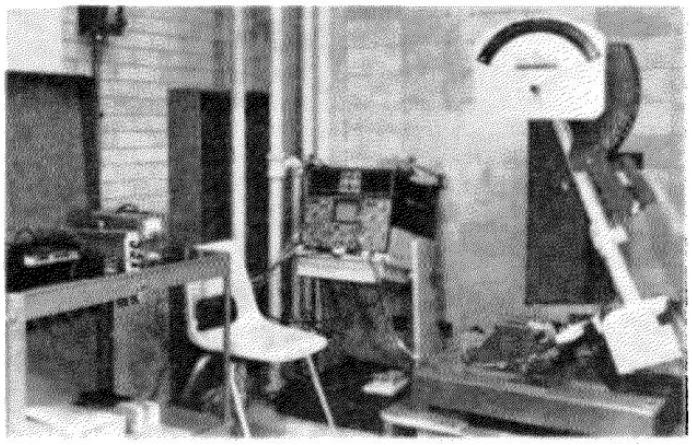

Figure 2.1. Overall view of the modified Charpy impact machine
(Source: Gopalaratnam and Shah, 1986)

Specimens, 229 mm long, 25 mm wide and 76 mm deep flexural beams, were tested under four different strain rates. Furthermore, four different mix proportions were used in those beams. The mix proportions could be seen from the Table 2.1.

Table 2.1. Details of the experimental program
(Source: Gopalaratnam and Shah, 1986)

Mix*	Fiber content v_f, percent	Flexural tests[1]							Compression tests[2] number of specimens
		Net cross section depth × width, in. (mm)	Span, in. (mm)	Number of specimens					
				$\dot{\epsilon}_1$	$\dot{\epsilon}_2$	$\dot{\epsilon}_3$	$\dot{\epsilon}_4$	$\dot{\epsilon}_5$	$\dot{\epsilon}_1$
1	0.0	3 × 1 (76 × 25)	8 (203)	4	4	4	4	4	4
		½ × 1 (64 × 25)	8 (203)	4	—	—	—	—	
2	0.5	½ × 1 (64 × 25)	8 (203)	4	4	4	4	4	4
3	1.0	½ × 1 (64 × 25)	8 (203)	4	4	4	4	4	4
4	1.5	½ × 1 (64 × 25)	8 (203)	4	4	4	4	4	4

*Matrix 1:2:0:0.5 (C:S:A:W, by weight); fibers ℓ = 1 in. (25 mm); d = 0.016 in. (0.4 mm).
[1]$\dot{\epsilon}_1 = 1 \times 10^{-6}$/sec, $\dot{\epsilon}_2 = 1 \times 10^{-4}$/sec, $\dot{\epsilon}_3 = 0.09$/sec, $\dot{\epsilon}_4 = 0.17$/sec, $\dot{\epsilon}_5 = 0.3$/sec. Flexural tests at $\dot{\epsilon}_1$ and $\dot{\epsilon}_2$ were conducted using a closed-loop machine under displacement control. Flexural tests at $\dot{\epsilon}_3$, $\dot{\epsilon}_4$, and $\dot{\epsilon}_5$ were conducted using the modified instrumented Charpy setup.
[2]Compression tests were conducted on 3 × 6 in. (76 × 152 mm) cylinders.

Compression tests were done by universal test setup. In case of plain concrete mix, softening was observed. By adding fibers, strength was increased. As presented in Figure 2.2 the biggest contribution of the fibers during compression tests was increased toughness after the peak load.

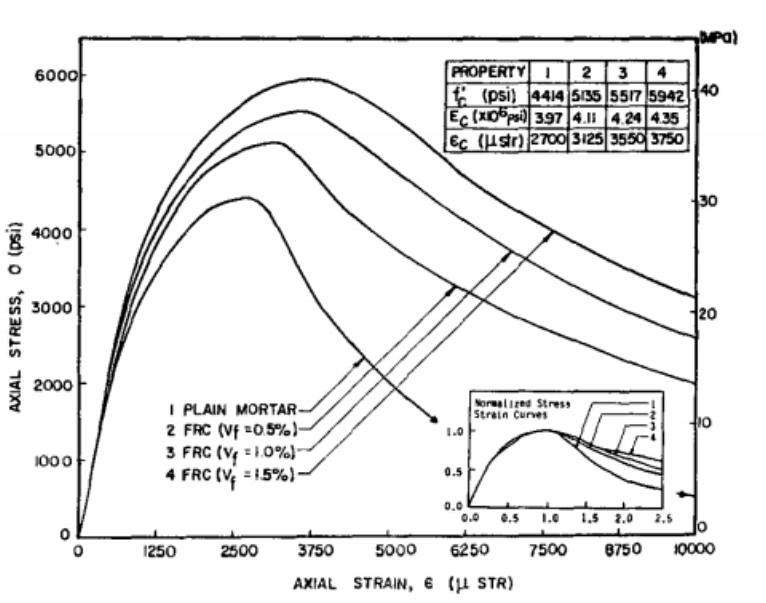

Figure 2.2. Results from static uniaxial compression test
(Source: Gopalaratnam and Shah, 1986)

It was observed that, specimens with fiber were more rate sensitive than the ones without fiber. This phenomenon was related to presence of additional cracks.

At higher strain rates, all the specimens exhibited increased flexural strength. As mentioned earlier, fiber reinforced concrete (FRC) members showed more rate sensitive behavior than plain concrete. Improvement of flexural strength in specimens with 0.5%, 1.0% and 2.0% fiber contents were 79%, 99% and 111%, respectively. Furthermore energy absorption capacity was increased up to 80% with increased fiber fraction.

It is concluded that, using static flexural test on FRC to estimate the impact strength and toughness of specimen under impact was an approximate and conservative method. However, using static method to estimate the behavior under impact loading is not straightforward.

Almansa and Cánovas (1999) carried out a study to determine the response of steel fiber reinforced concrete to small projectiles. In their study, fibers with the length of 50mm and diameter of 0.5mm were added to concrete mix. Portland cement with 28 day compressive strength of 45 MPa was used. Fibers were added to the concrete mix by 0.5%, 1.0% or 1.5% volume fractions. Both length and height of the specimens were 60 cm. The depths of the specimens were varied. Details were presented in Table 2.2.

Table 2.2. Thickness, fiber content and number of plates
(Source: Almansa and Canovas, 1999)

	Quantity of fibers (kg/m^3)			
Thickness (cm)	0	40	80	120
4	4	0	4	1
6	10	2	10	2
8	8	0	8	2
10	10	0	10	2
12	8	0	8	0
14	0	2	2	2
18	0	2	0	2
20	0	0	0	2

The specimens (Figure 2.3) were subjected to 5.56 mm projectile at least 5 times, 7.62 mm armor piercing (AP) projectile at least 3 times and 12.7 mm armor piercing projectile 1 time.

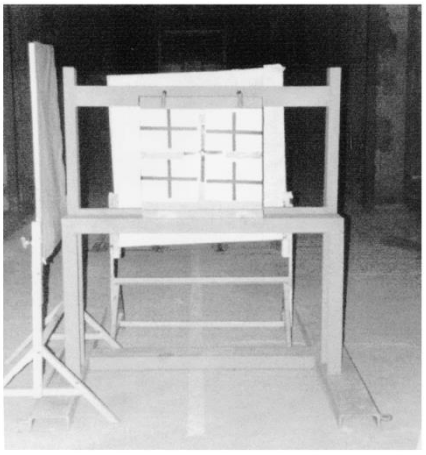

Figure 2.3. Metallic frame supporting a specimen
(Source: Almansa and Canovas , 1999)

It was observed that, without fibers scabbing occurred at about 80-90% of the required energy for perforation. Although specimens without fibers resisted only 50% of penetration without scabbing, penetration of specimens with fibers could have reached 70% of thickness without scabbing. Furthermore, by adding fibers the crater volume, which was the result of impact event on the surface, was reduced.

Experimental studies on larger scale members were also carried out in the literature to observe the performance of steel fibers under impact loading, such as the one carried out by Ong et al. (1999). In this study, effectiveness of different kinds of

fibers under impact loading was investigated. Mixtures with 1:1.3:2.1 cement: coarse aggregate: fine aggregate and 0.4 water –cement ratio were used in this study. Three different types of fibers were used in exactly same mixtures. Ordinary Portland cement and crushed aggregate of maximum ten millimeters were used. Specimens with area of $1m^2$ and depth of 30 mm were cast. Varying amounts of fiber (0.5%, 1.0% and 2.0% by weight) were added to the concrete mix. Slabs were simply supported at all four edges. Impact loading was applied by a fabricated guide (Figure 2.4). The specimens were tested by dropping hemi-spherical nose shaped projectile of mass 43 kg from a height of 4000 mm. Test setup was presented in Figure 2.4.

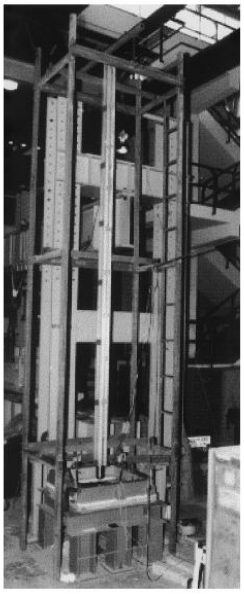

Figure 2.4. Drop-weight impact test setup
(Source: Ong et al., 1999)

In case of plain concrete members, the result of the impact event was catastrophic. As presented in Figure 2.5 the projectile penetrated the slab, and then shear cone shaped fracture was formed. Slab lost its integrity and gained momentum as a result of radial crack formation. As presented in Figure 2.6 Similar results were obtained in the specimens with the fraction of 0.5% for both polyolefin and PVA fibers. But in case of steel fibers, no such catastrophic results were observed; no penetration was occurred in concrete members with steel fibers.

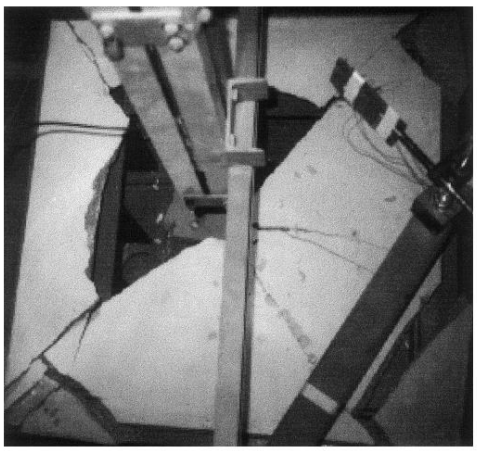

Figure 2.5. Failure of plain concrete slab
(Source: Ong et al., 1999)

In case of members with polyolefin 0.5% in volume, penetration was occurred. By adding the fiber between the amounts of 0.5% to 2.0% some improvements, such as improvement in integrity, number of cracks or width of cracks, were obtained. Members with PVA fibers could not keep their integrity after impact event. They failed in a similar manner to plain concrete members.

Members with steel fibers were performed significantly better than other members. In case 0.5% steel fiber addition, penetration, shear cone and radial cracks were occurred. In case of 1.0% and 2.0% steel fiber case, size of shear cone and the width of cracks were decreased with respect to specimens with 0.5% fiber contents. For 0.5%, 1.0% and 2.0% steel fiber contents, 24 mm, 12 mm and 4.5 mm residual displacements were obtained. Thus, by adding more steel fiber the stiffness of the member could be increased. Furthermore, in case of 2.0% steel fiber no crack was observed on bottom side.

Firstly the formation of frustum shaped fracture zone was observed and then formation of flexure cracks from center to corners was observed before failure. Polyolefin fibers specimens failed due to pullout and rupture, whereas both steel and PVA fibers failed due to only pullout effect only along fracture surfaces. In Figure 2.7 it was presented that, adding 2.0% fibers resulted well than, 0.5% and 1.0% ones.

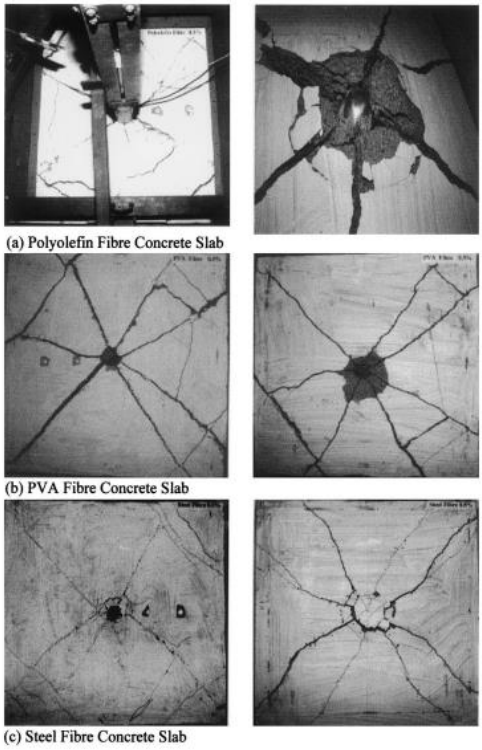

Figure 2.6. Failure patterns of slabs containing 0.5% volume fraction of fibers (Source: Ong et al., 1999)

As a result of increased fiber content both the duration of impact event and maximum peak load of the specimens were reduced. Thus stiffer response was obtained by adding more fibers. For example 36% and 56% reduction in displacement was obtained by increasing volume fraction of steel fiber from 0.5% to 1.0% and 1.0% to 2.0% respectively. Furthermore the duration of impact in 2.0% steel fiber was 50% of that of 0.5% steel fiber member. Increasing fiber fraction from 0.5% to 2.0%, observed damage after the impact event was decreased. Difference of the damage could be seen from the comparison of Figure 2.6 and Figure 2.7.

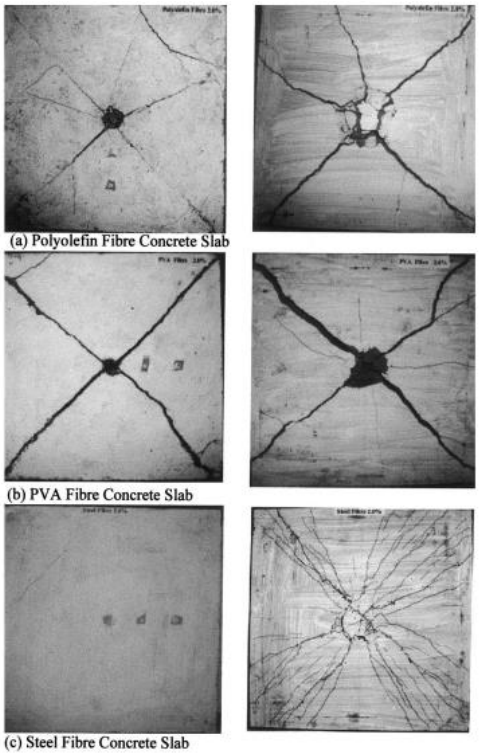

Figure 2.7. Failure patterns of slabs containing 2.0% volume fraction of fibers
(Source: Ong et al., 1999)

Fracture energy until 20 mm deflection was used for comparing the slabs. From Figure 2.8, it can be seen that steel fibers were performed much better than both PVA and POF fibers.

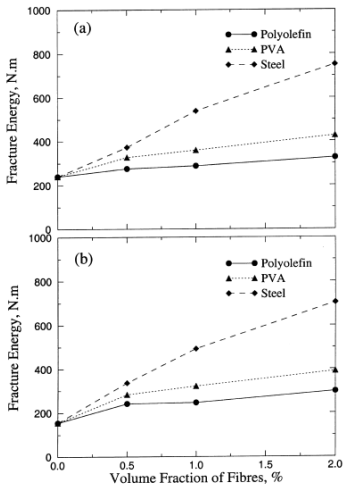

Figure 2.8. Effects of V_f and fiber type on the fracture energy: (a) fracture energy by observed load; (b) fracture energy by bending load
(Source: Ong, et al., 1999)

Beside the impact tests, static tests carried out on slabs can also provide an understanding of the contribution of steel fibers to the overall structural performance. For example, an experimental study was carried out by Cheng and Parra-Montesinos (2010) to investigate the effect of using steel fibers on slab-column connections.

Ten specimens with 1.50m x 1.50m x 0.15m with a square column stub at the center were tested under monotonically increased loading. The test setup was presented in Figure 2.9. Rate of the loading was 3.8 mm/min. The 28 day strength of the concrete was around 35 MPa. Only tension sides of the slabs were reinforced. Two different longitudinal reinforcement ratios, 0.83% or 0.56%, were used in the study Geometry, strength, and the volume fraction of the fibers and reinforcement ratio were the main parameters in this study. The slabs used in this study were simply supported.

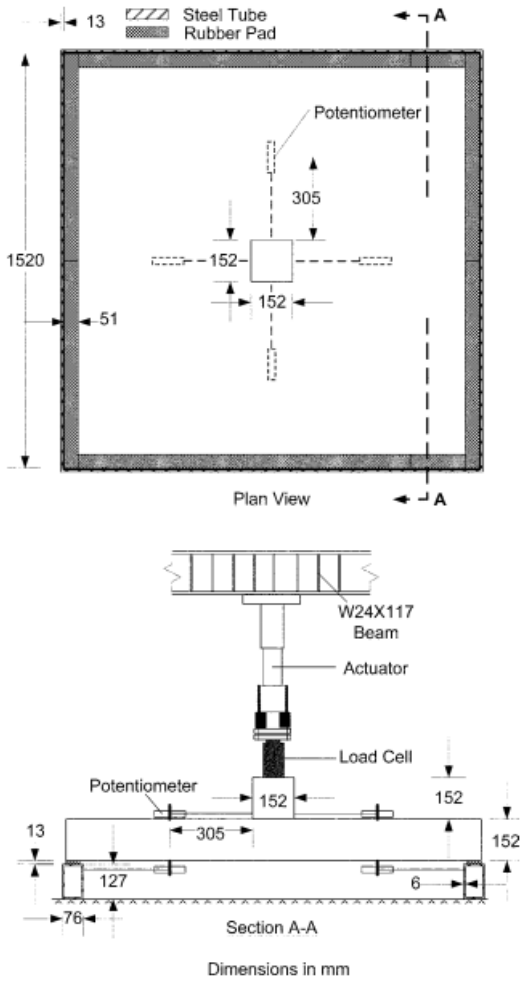

Figure 2.9. Test setup
(Source: Cheng and Parra-Montesions, 2010)

After each test, specimens were filliped over to see the crack distribution. From the observed data, it was seen that, some specimens showed shear failure, and some showed flexural type of failure. Different types of failures were presented in Figure 2.10. The reason of different failure types could be related to the membrane like behavior of flexural reinforcement. In other words, as a result of membrane like behavior of flexural reinforcement high displacements were prevented after shear failure.

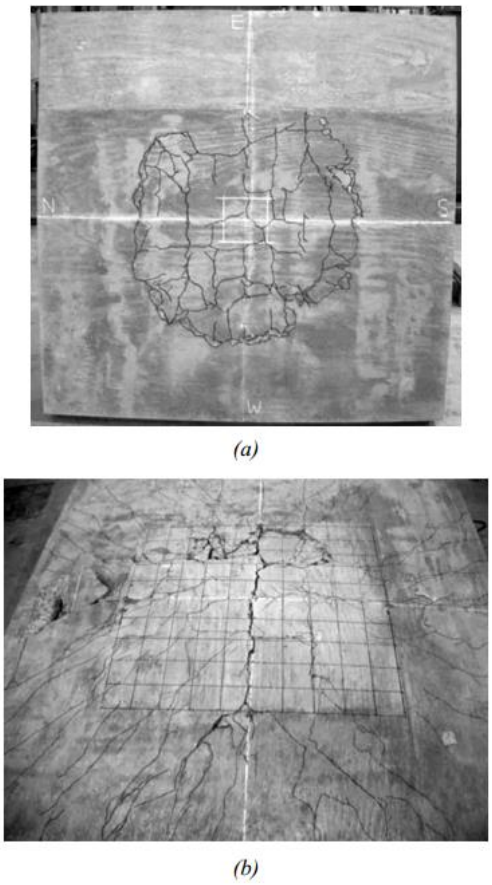

Figure 2.10. Crack pattern on slab tension side: (a).Shear failure; (b).Flexural failure (Source: Cheng and Parra-Montesions, 2010)

Initial stiffness and peak load of the slabs with 10 cm spacing between longitudinal reinforcement was higher than slabs with 15 cm reinforcement spacing. Slabs with 10 cm spacing showed little or no ductility due to the limited flexural yielding capacity. On the other hand, specimens with 15 cm reinforcement spacing

showed more ductile behavior as the fiber ratio increased. Load vs. deflection graphics of all specimens were presented in Figure 2.11.

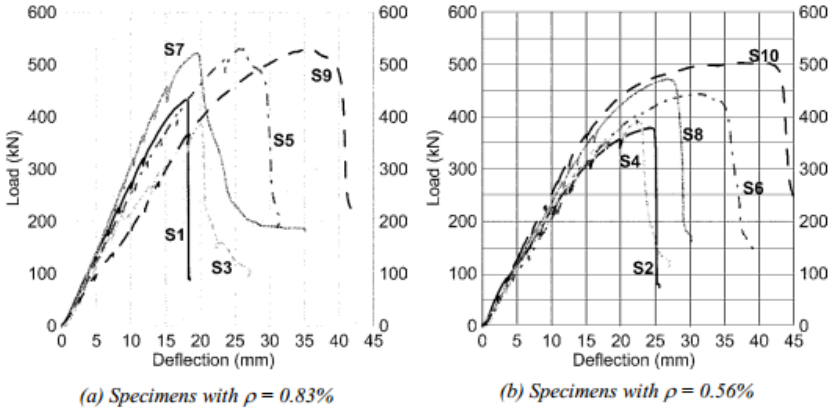

Figure 2.11. Load-versus-deflection response: (a). 10cm spacing; (b). 15cm spacing (Source: Cheng and Parra-Montesions, 2010)

Slabs with regular strength steel fibers showed best performance among all other slabs. Increment in shear strength by adding twisted steel fibers and hooked steel fibers in 1.50% volume fraction with respect to control specimen were 11% and 50%. Thus, it was observed that with same amount of fiber, hooked steel fibers were more efficient than twisted steel fibers.

Increment of the fiber content resulted as increased flexural strength of slabs prior to punching. Therefore, adding fiber changed the mode of failure from brittle to ductile manner.

Another experimental study was carried out by Naaman et al. (2007) to evaluate the shear resistance in high performance fiber reinforced cement composite structures.

A slab, which had two top and bottom layers of reinforcement, was employed as a control specimen. Then, by removing some layers of reinforcement and adding fiber other test specimens were obtained. Control specimen and the proposed systems were presented in Figure 2.12. Finally, the response of the each specimen, under concentrated centrally monotonic loading was compared

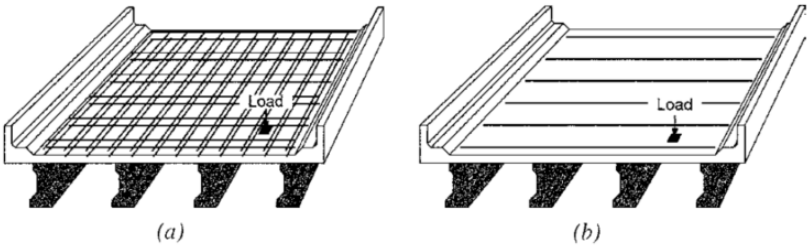

Figure 2.12. Three dimensional views of (a) control specimen; (b) proposed system (Source: Naaman et al., 2007)

All slab specimens were 810 x 810 x 50 mm and simply supported. Test setup was presented in Figure 2.13. Three linear voltage differential transformers and two transducers were used to record the test data. Loading process was achieved by servo-controlled hydraulic testing machine with 0.25 mm/min speed.

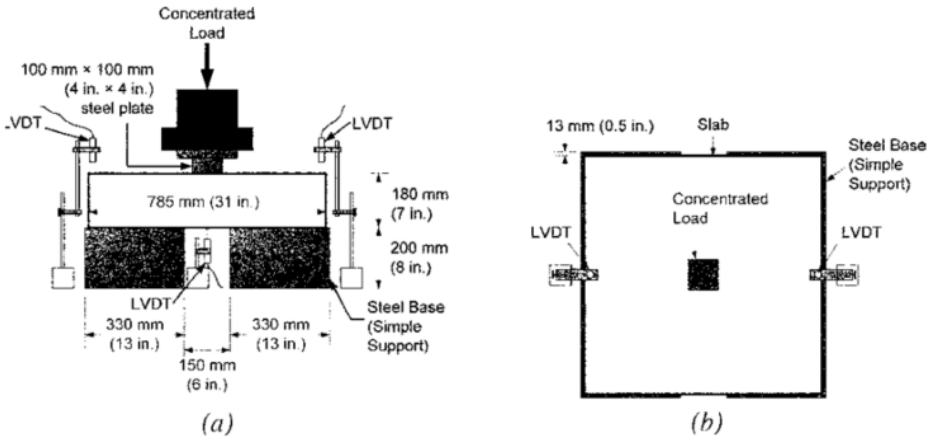

Figure 2.13. Experimental setup (a) elevation; (b) top view (Source: Naaman et al., 2007)

Peak load, displacement at peak load, residual strength, energy absorption capacity up to 45mm, type of failure and angle of punching surface (if exists) could be seen from Table 2.3. CON, PVA, SPE and TOR stand for control specimen, specimens with polyvinyl alcohol fibers, and specimens with ultra-height polyethylene fibers and specimens with twisted steel fibers, respectively. Second term, which was in the form of #T stood for number of layers in transverse direction. Final term, which was in the form of #L stood for number of layers in longitudinal direction.

Table 2.3. Summary of test results
(Source: Naaman et al., 2007)

ID	Peak Load P, kN(kips)	Displacement at peak load, mm(in)	Residual strength kN(kips)	Energy absorption up to 45 mm displacement kN-mm (kips-in.)	Failure mode	Angle of punching surface, degrees
CON-2T-2L	383(86)	2,8(0,11)	134(30)	6210(55)	Punching shear	41
PVA-2T-2L	500(113)	5,1(0,20)	245(55)	13220(117)	Punching shear	41
PVA-0T-0L	209(47)	5,1(0,20)	-	3160(28)	Flexural	-
SPE-2T-2L	549(124)	8,1(0,32)	307(69)	16950(150)	Punching shear	34
SPE-1T-1L	440(99)	7,1(0,28)	178(40)	11750(104)	Punching shear	34
SPE-0T-0L	205(46)	6,1(0,24)	138(31)	4750(42)	Flexural	-
TOR-2T-2L	759(171)	11(0,42)	347(78)	23500(208)	Punching shear	38
TOR-1T-1L	614(138)	13(0,50)	267(60)	20000(177)	Flexural	-
TOR-0T-1L	592(133)	7,0(0,27)	-	15030(133)	Flexural	-
TOR-0T-0L	569(128)	7,0(0,27)	-	11750(104)	Flexural	-

It was concluded that, by adding PVA, SPE or TOR type of fiber one can significantly increase the energy absorption capacity. Furthermore, unlike the control specimen, no clear cover spalling was observed in large deflections for specimens with fibers. The cracking patterns of the specimens in failure state were presented in Figure 2.14.

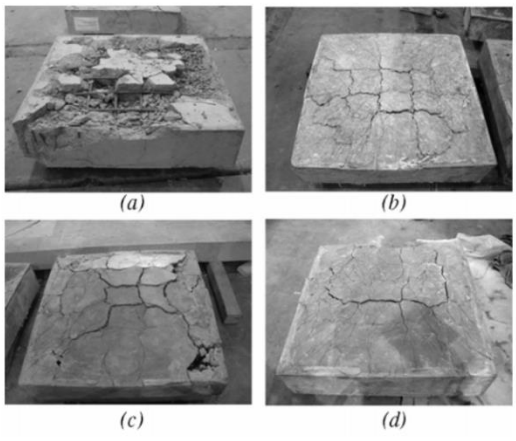

Figure 2.14. Cracking patterns at the tension side of the specimens: (a) CON-2T-2L; (b) SPE-2T-2L; (c)TOR-2T-2L; and (d)PVA-2T-2L
(Source: Naaman et al., 2007)

2.3. Companion Studies

The study carried out by Batarlar (2013) was the leading study of a series of experimental studies on the impact resistance of reinforced concrete slabs, including this study. Same test setup was used in all studies as presented in Figure 2.15. Furthermore, boundary conditions, specimen dimensions, ratio of longitudinal reinforcement, method of loading and the method of obtaining data were also almost identical. Due to these similarities, plain concrete specimens tested by Batarlar were used as control specimens in this study.

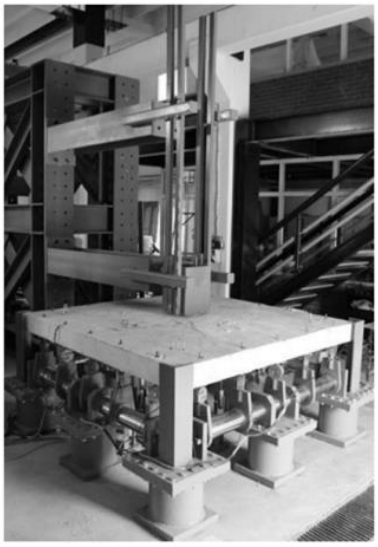

Figure 2.15. Impact test setup
(Source: Batarlar, 2013)

In Batarlar's study, as presented in Figure 2.15**,** three identical pairs of reinforced concrete slabs with ϕ 8 mm reinforcing bar with different reinforcement ratios were casted. Longitudinal reinforcement spacing was 100, 150 and 200 mm for different ratios. Each specimen had one layer of reinforcement on the top and one layer reinforcement on the bottom face. One member of the pair was used in static test, and the other one used impact test.

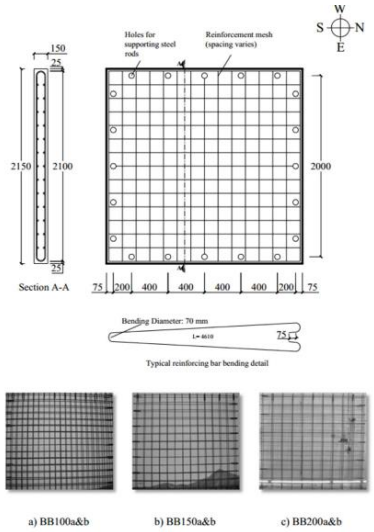

Figure 2.16. Batarlar's reinforcement layout
(Source: Batarlar, 2013)

Dimension of specimens were 2150x2150x150 mm. Simply supported boundary conditions were provided by 20 hinges along the edges of the specimens. In order to prevent lifting of the edges and enable to the free rotation of the slabs, hinges and load cells were connected to a circular shaft.

To record the deflection of the specimens' resistive linear positioning transducers (RLPT) were used. The RLPT's were elongated with extension rods and attached to the specimens' bottom faces. Locations of the RLPTs can be seen from the Figure 2.17 for static case, and Figure 2.18 for dynamic case. To record the displacement of center point in static loading, an RLPT was placed at the center top of the specimen.

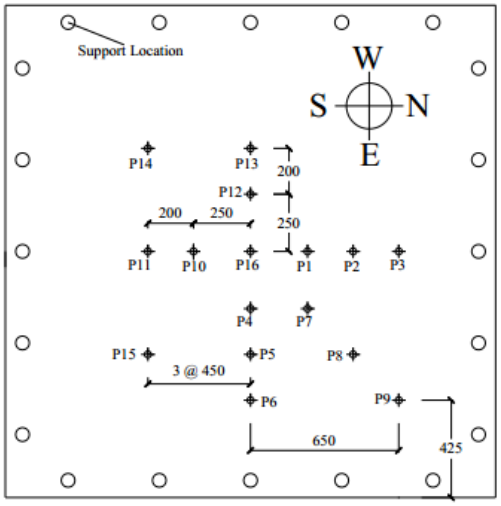

Figure 2.17. RLPT's locations for static case
(Source: Batarlar, 2013)

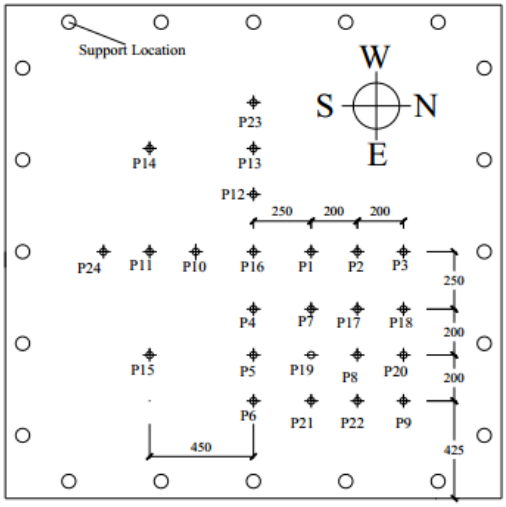

Figure 2.18. RLPT's locations for dynamic case
(Source: Batarlar, 2013)

In order to obtain strain values from the specimens' 12 strain gauges were used. All the data from RLPTs, strain gauges and load cells were recorded by data acquisition system.

A hydraulic jack was used to apply the load during static tests. The hydraulic jack (Figure 2.19) was placed under the center bottom of the specimen and used manually. During test, the loading was halted few times in order to see the crack pattern

of the specimen and the change of the cracks widths. A load cell was placed between hydraulic jack and specimen, in order to monitor the applied load.

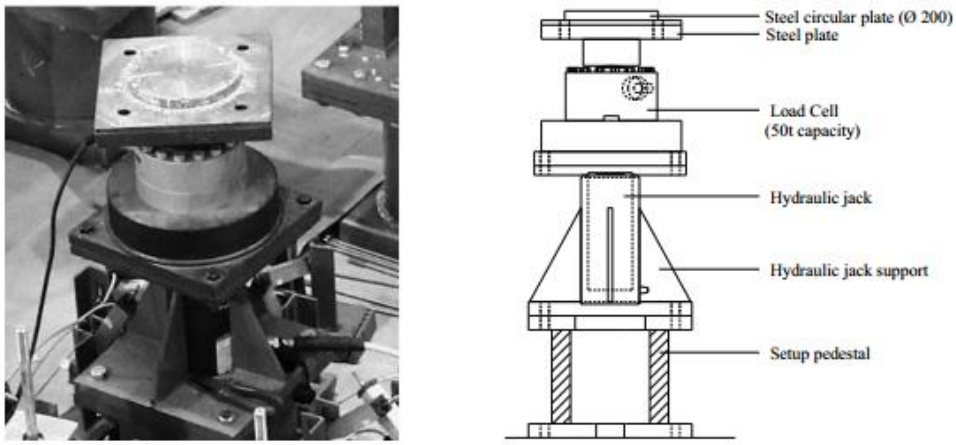

Figure 2.19. Hydraulic jack with the load cell
(Source: Batarlar, 2013)

In the static phase of the tests, all the specimens were failed due to punching failure. From the obtained data during after the static tests, following results were obtained;

1. With the increased spacing between longitudinal reinforcement, load bearing capacity was decreased, but ductility was increased.
2. Punching cone was formed in all specimens. Formation of these cones could be seen from the crack distribution in tension side of the specimen. The crack distribution of the specimens in each step was presented in Figure 2.20, Figure 2.21 and Figure 2.22.
3. Specimens with less reinforcement ratio had wider cracks than specimens with more reinforcement.
4. Specimens with more reinforcement ratio resulted in more and narrower crack distribution.

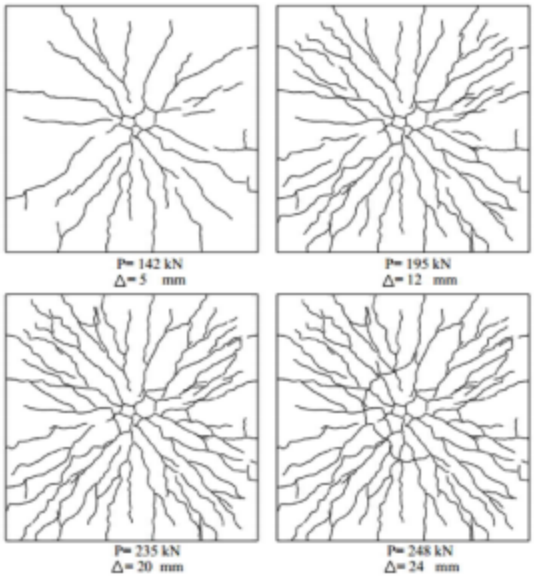

Figure 2.20. Crack distributions at the tension side of specimen in BB100a (Source: Batarlar, 2013)

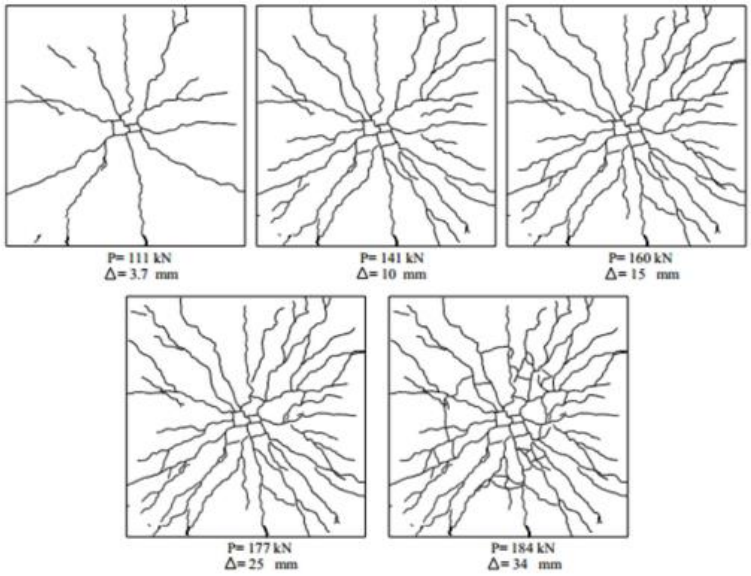

Figure 2.21. Crack distributions at the tension side of specimen in BB150a (Source: Batarlar, 2013)

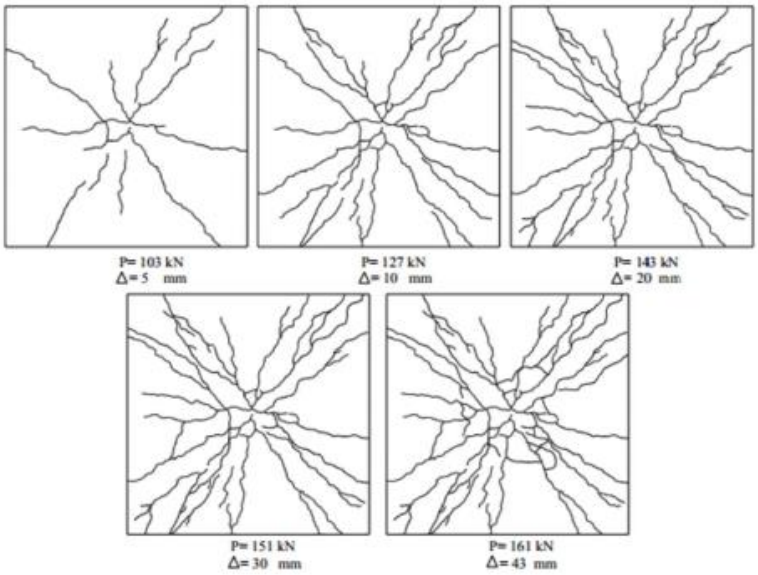

Figure 2.22. Crack distributions at the tension side of specimen in BB200a
(Source: Batarlar, 2013)

For impact test, some modifications were applied to the test setup. Firstly a drop tower, with a height of 2.50 m, was installed in order to guide the projectile. In order to both provide more space for RLPTs and prevent hydraulic jack from any damage, hydraulic jack was removed under the specimen. Two accelerometers were placed on the drop weight and five accelerometers were placed on the specimen to obtain data from impact event.

Two drop weights were used in this study, light one with 210 kg mass and heavy one with 320 kg mass. (Figure 2.23) Impact tests were repeated until punching failure was seen. Failure occurred as a result of widened cracks and formation of punching cone. On the contact area between specimen and drop weight, local penetration was seen due to the impact.

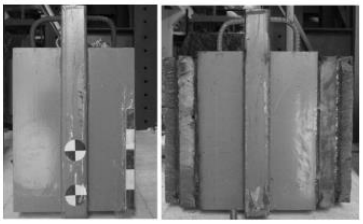

Figure 2.23. Drop weights (210 and 320 kg respectively)
(Source: Batarlar, 2013)

The same test setup was used by Arsan (2014) as well. Dimensions of test specimens and the ratio of longitudinal reinforcements were the identical in these two studies. In Arsan's study effects of shear studs (Figure 2.24) and steel fibers in reinforced concrete slabs under both static and impact loading were investigated. The layout of shear studs was presented in Figure 2.25. Like Batarlar (2013), static loading was applied to bottom middle point and impact loading was applied to top middle point of each specimen.

The effects of shear studs and steel fibers were compared in this study. The specimens with same longitudinal reinforcement ratios from Batarlar (2013) were employed as control specimens. Therefore, it was concluded in this study,

Both the shear studs and steel fibers changed the mode of failure of specimen from brittle to ductile manner,

Cracking was observed in impact load, due to bending. Further, as a result of steel fiber in concrete mix, evenly distributed cracks were formed.

Load carrying capacity was increased significantly with respect to the specimens without steel fiber addition.

Figure 2.24. Shear stud used in Arsan, 2014

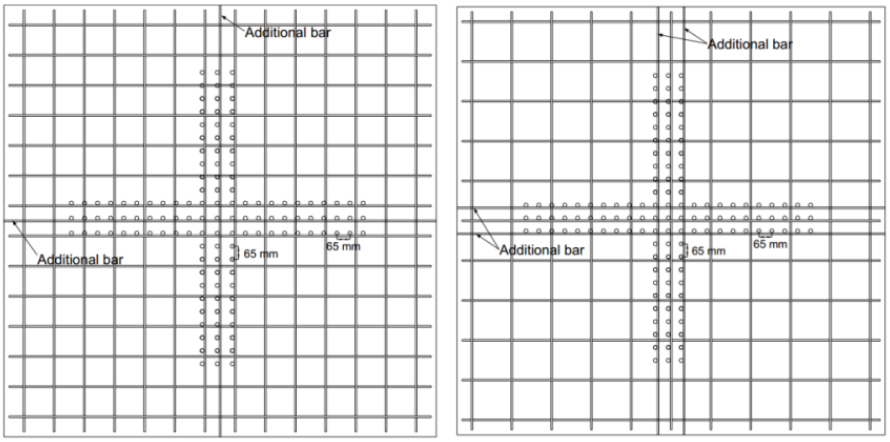

Figure 2.25. Layout of shear studs
(Source : Arsan, 2014)

CHAPTER 3

EXPERIMENTAL PROGRAM

In this study, to investigate the effects of steel fibers on the impact behavior of reinforced concrete slabs, ten slabs with different longitudinal reinforcement ratios and different fiber contents were tested under static and dynamic loading. Slabs were cast as twins. Thus, one was tested under static loading and its identical twin was tested under dynamic loading. Details of the experimental program were presented in the following sections.

3.1. Test Specimens

Ten specimens were cast in Civil Engineering Structural Mechanics Laboratory at İzmir Institute of Technology (IYTE). All specimens have dimensions of 2150x2150x150 mm and 25 mm clear cover. Static and impact loading procedures were applied to the mid-point of the specimens. As previously mentioned every slab had its twin. Thus, one pair was tested under static loading and the other one was tested under dynamic loading.

All the specimens had 2 layers of reinforcements in mesh form, one at the top and one at the bottom. . Those meshes were obtained by bending ϕ8 or ϕ10 steel bars. Only two specimens (SY150f10-a and SY150f15-a) were manufactured using ϕ10 bars due to the lack of ϕ8 bars during the manufacturing stage, but their spacing was adjusted such that their reinforcement ratios were identical to the ones manufactured with ϕ8 bars with 100 mm spacing. Reinforcement and fiber properties of the specimens were presented in Table 3.1.

Table 3.1. Details of specimens

Name of the specimen	Longitudial Reinforcement Layout and Ratio (for both principle directions)	Fiber fraction
SY100f10-b	ϕ 8 / 100 - 0.40 %	1.0 %
Sy100f05-a	ϕ 8 / 100 - 0.40 %	0.5 %
SY100f05-b	ϕ 8 / 100 - 0.40 %	0.5 %
SY100f15-b	ϕ 8 / 100 - 0.40 %	1.5 %
SY150f10-a	ϕ10/150 - 0.40 %	1.0 %
SY150f15-a	ϕ10/150 - 0.40 %	1.5 %
SY200f05-a	ϕ 8 / 200 - 0.20%	0.5 %
SY200f05-b	ϕ 8 / 200 - 0.20%	0.5 %
SY200f15-a	ϕ 8 / 200 - 0.20%	1.5 %
SY200f15-b	ϕ 8 / 200 - 0.20%	1.5 %
YA200f-b	ϕ 8 / 200 - 0.20%	1.0 %
YA200f-a	ϕ 8 / 200 - 0.20%	1.0 %
BB100a	ϕ 8 / 200 - 0.40 %	0.0 %
BB100b	ϕ 8 / 200 - 0.40 %	0.0 %
BB200b	ϕ 8 / 200 - 0.20 %	0.0 %
BB200a	ϕ 8 / 200 - 0.20 %	0.0 %

All the specimens were named according to the spacing between reinforcement, fiber content and type of loading. For example, in static case, specimens with 100 mm spacing and 1.0% fiber content was named as SY100f10-a. In this naming methodology, SY stands for the name of the author, 100 stands for spacing in millimeters, f10 stands for fiber content and –a stands for type of loading. In case of dynamic loading, -b was used instead of –a.

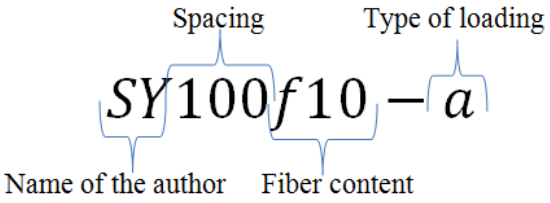

Figure 3.1. Naming methodology

3.2. Slabs with Steel Fiber

Steel fibers of 60 mm in length and 0.75 mm in diameter which had length diameter ratio of 80 were used in this study (Figure 3.2). Minimum tensile strength of the fibers is 1050 N/mm^2 and it comforted EN 10016-2 – C9D. General views of steel fibers are presented in the Figure 3.3.

Steel fibers were added to concrete batch during casting. Although no further investigation was made, it is safe to assume that steel fibers were randomly distributed inside specimen.

Steel fibers can fail due to pull out or rupture effects. The type of the failure of the steel fibers could change the behavior of the specimen significantly. However, due to the difficulties involved in breaking or cutting the specimens after tests, the mode of the failure of the steel fibers could not be investigated.

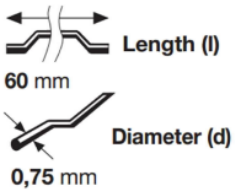

Figure 3.2. Geometric details of steel fibers

Figure 3.3. Steel fibers

3.3. Material Properties

Concrete was ordered from a local company. Concrete arrived in three batches. By adding sufficient amount of fiber to the mixer on site, 0.5%, 1.0% and 1.5% fiber fractions were achieved. Standard cylinder samples (150 mm in diameter, 300 mm in height) were casted for each batch during casting. Samples were cured for 28 days and tested at 28^{th} day. The mechanical properties of the materials are presented in Table 3.2.

Table 3.2. Mechanical properties of materials

	Compression Strength (Mpa)		Indirect Tensile Strength (Mpa)	Flexural Strength (Mpa)
Fiber fraction, %	28 days	12 months (experimental method)		
0	33,8	42,4	2,3	7,9
0,5	36,7	49,3	3,5	8,7
1	35,2	45,4	5,1	14,8
1,5	49,4	56,5	10,7	18,4

Reinforcement used in this study was tested before experiments. As a result the mean values of f_y=420 MPa yield strength and f_u=490 MPa rupture strengths were obtained.

3.4. Test Setup

The setup was manufactured and mounted at the strong floor at İzmir İnstitute of Technology as a part of previous studies Batarlar, 2013 and Arsan 2014). (Figure 3.4) With a few modifications both static and dynamic tests were done in this test setup.

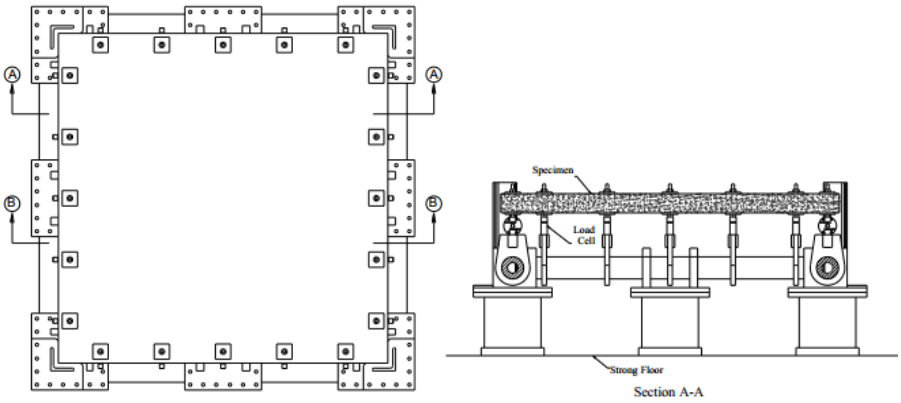

Figure 3.4. Test Setup

Test setup had eight footing and every one of them was fixed to the strong floor. All load cells were placed on a circular shaft. (Figure 3.5) Although the vertical movements of the edges were prevented, their free rotation was allowed. Thus, simply supported boundary conditions were obtained.

Figure 3.5. Test Setup

3.5. Instrumentation

All the instrumentation devices used for this study will be explained in this section.

3.5.1. Load Cells

Load cells with capacity of 5, 10 and 50 tons were employed in this study. In static tests, load cell with 50 ton capacity (Figure 3.7) was placed between hydraulic jack and specimen. In impact tests, eight load cells with 5 tons capacity and twelve load cells with 10 tons capacity were placed at the edges and corners. (Figure 3.6)

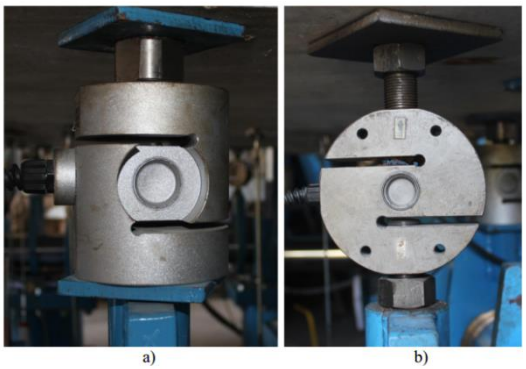

Figure 3.6. (a) 10ton; (b) 5ton capacity load cells

Figure 3.7. Hydraulic piston with 50 ton capacity load cell on top

3.5.2. Strain Gauges

Six Type FLA-5-11 strain gauges from Tokyo Sokki Kenkyujo Co. Ltd. were used to measure the strain in the reinforcement bars. Three of the strain gauges were glued at the top face and three of them were glued at the bottom face of the middle axis in WE directions onto the longitudinal reinforcement. The strain gauge at the center of

the specimen was numbered as 1 and the ones were numbered as 2 and 3, respectively. Therefore, strain gauges at the top face named as T1, T2 and T3 and the strain gauges at the bottom named as B1, B2 and B3.

Reinforcing bars were grinded at the strain gauge locations until a flat and smooth surface was obtained. Then, it was cleaned by basic and acidic solutions. After that, the strain gauges were glued with the special glue provided by the strain gauge manufacturer. Finally, strain gauges were covered with a thick layer of varnish, paraffin wax and insulation tape in order to prevent any external damage. All those procedures were presented in Figure 3.8, Figure 3.9 and Figure 3.10.

Despite the significant efforts spent, no dependable data was obtained after the impact testing from the strain gauges. As a result, the strain gauges measurements were not used in this study.

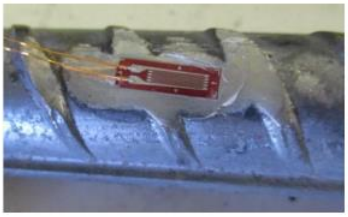

Figure 3.8. Strain gauges before coating

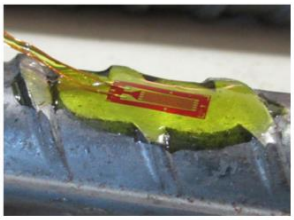

Figure 3.9. Strain gauges after coating

Figure 3.10. Final state of the strain gauge

3.5.3. Resistive Linear Position Transducers (RLPT's)

A total of 24 Resistive Linear Position Transducers (RLPT's) (Figure 3.11) were used to record the displacement of the specimen during testing (Figure 3.12). In order to connect the slab with the tip of the RLPT, a steel extension rod was used. A pivot head was put at the end of the extension rod in order to increase the rotation capacity of the rod. The pivot head was placed at the bottom of the specimen. In static testing, U profiles were screwed to the bottom face by using fixing plugs. However, in impact testing, chemical anchor was used instead of fixing plugs. (Figure 3.13) Despite all the efforts, some RLPT's have fallen in impact loading.

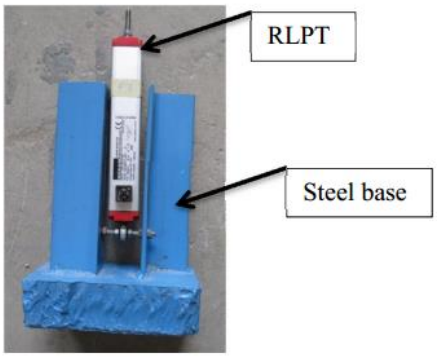

Figure 3.11. General view of RLPT

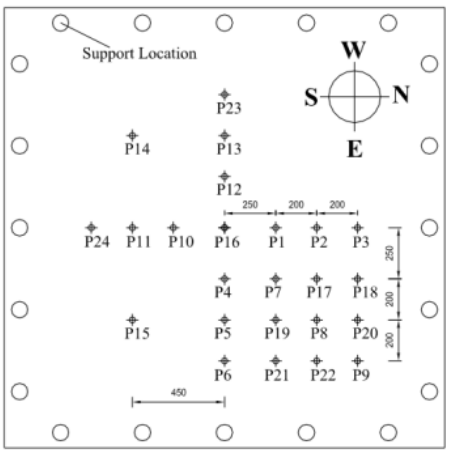

Figure 3.12. Positions of RPLT's under the slab

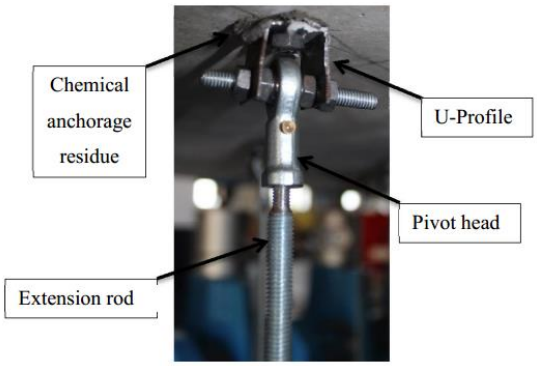

Figure 3.13. Connection of the pivot head to the specimen before impact test

3.5.4. Accelerometers

16 accelerometers were used to record acceleration. Two ± 50000g range, 8742A50 type from Kistler Group were mounted on the drop weight. Four ± 5000g range 8742A5 type from Kistler Group and ten models 350B04 from PCB Piezotronics with a range of ± 5000g were mounted on the top of the slab. (Figure 3.14)

Accelerometers were screwed to the specimen using delrin cylinders in order to prevent noise. These delrin cylinders were fixed to the slab with chemical anchorage to increase stability. (Figure 3.15)

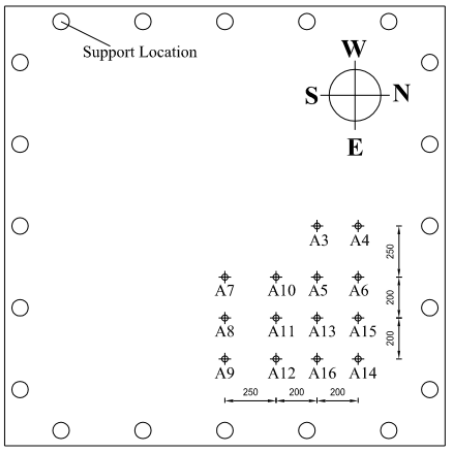

Figure 3.14. Locations of the accelerometers on top face

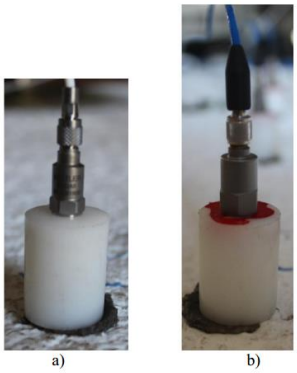

Figure 3.15. Two types of accelerometers; (a) Kistler Group accelerometers, (b) PCB Piezotronics accelerometers

3.5.5. Drop Weight

Drop weight was manufactured at IYTE structural lab using a steel bucket with 200 mm diameter circular bottom surface. In order to make the drop weight heavier, it was filled with steel plates and concrete. As a result, a drop weight of 320 kg was created. After the studies of Arsan (2014), it was concluded that the drop weight of 320 kg was not heavy enough to induce any significant damage to the steel fiber reinforced slabs. Then, in order to achieve a heavier drop weight, thick steel plates were placed on the top, reaching a maximum weight of 555kg. Both of the drop weights are presented in Figure 3.16.

Figure 3.16. (a) Former Drop Weight (320 kg), (b) Current Drop Weight (555 kg)

3.5.6. Data Acquisition System

In order to collect and record all data from the tests, a high speed data acquisition system with a 250 kS/s/channel sampling rate was employed. (Figure 3.17) Lab VIEW Academic Standard Suite program was used to manipulate and save all data obtained from experiments.

Figure 3.17. General view of Data Acquisition System

3.5.7. High Speed Camera

A high speed camera was used to record the impact event (Figure 3.18). In order to record the impact event MotionBLITZS high speed camera system, product of Mikroton GmbH, was used. The number of frames per second in this camera was

between 800 and 1262. Once the entire event was recorded, the records were used to calculate the speed of the mass at the impact moment.

Figure 3.18. Mikroton EoSens high speed camera

3.6. Static Testing

A monotonically increasing load from the bottom at middle of the specimen was applied as static load. Loading was stopped at several stages to mark and record the crack developments. These loads are presented in the Table 3.3. The maximum load and the corresponding displacement of the specimen presented in Table 3.3 as well. In this section the width and the distribution of the cracks will be presented.

Table 3.3. Peak load and related displacements

Name	Peak Load (kN)	Displacement (mm)
SY100f05-a	368	28,7
SY150f10-a	384	37,9
SY150f15-a	441	54,9
SY200f05-a	293	31,8
SY200f15-a	330	42,7
BB100a	248	24,0
BB200a	184	35,0
YA200fa	329	38,0

3.6.1. SY100f05-a

Specimen SY100f05-a reached a maximum load of 367.89 kN at 28.73 mm displacement and it reached 37.57 mm of displacement and 235.6 kN of load just before failure. Crack distribution and the width of the cracks are presented in Figure 3.19.

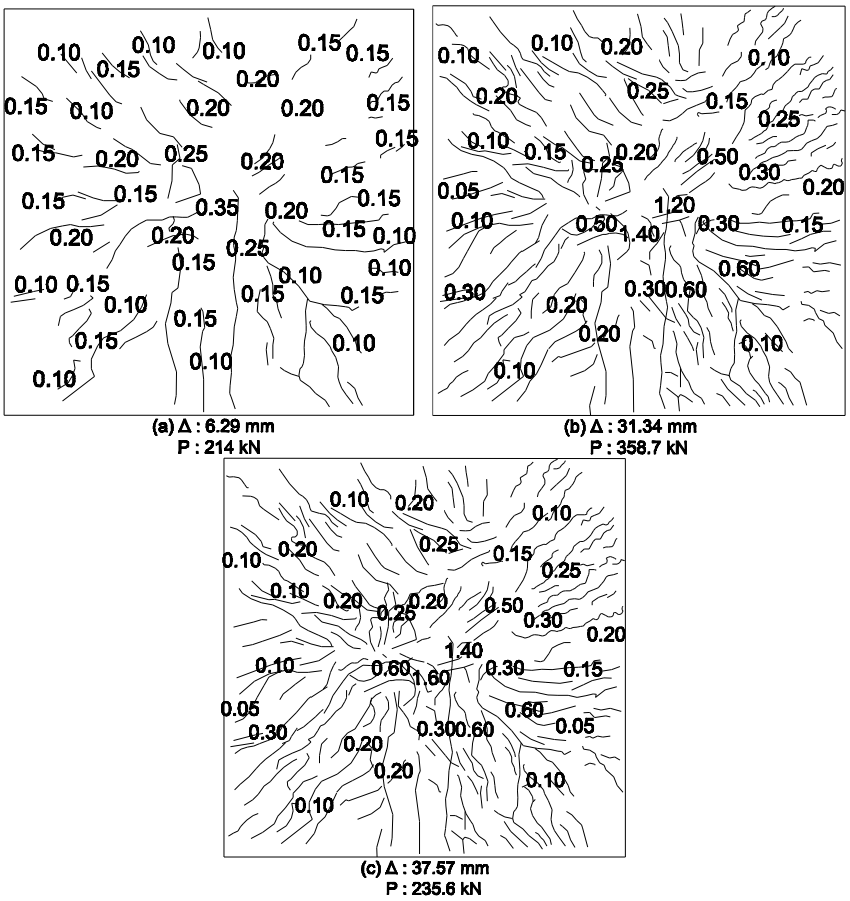

Figure 3.19. Crack patterns at the tension side of specimen SY100f05-a, (a) after 1st stop; (b) after 2nd stop; (c) after 3rd stop (Given numbers are crack widths in millimeter.)

3.6.2. SY150f05-a

Specimen SY150f10-a reached displacement of 37.88 mm and 383.87 kN load carrying capacity at the peak point. Furthermore, it reached 47.7 mm of displacement and 267.1 kN of load just before failure. Crack distribution and the width of the cracks are presented in Figure 3.20.

It must be noted that, in this specimen reinforcement with 10 mm diameter was used instead of 8 mm diameter. In order to keep same longitudinal reinforcement ratio with specimens manufactured with 8 mm bars, spacing between reinforcement bars were increased to 150 mm.

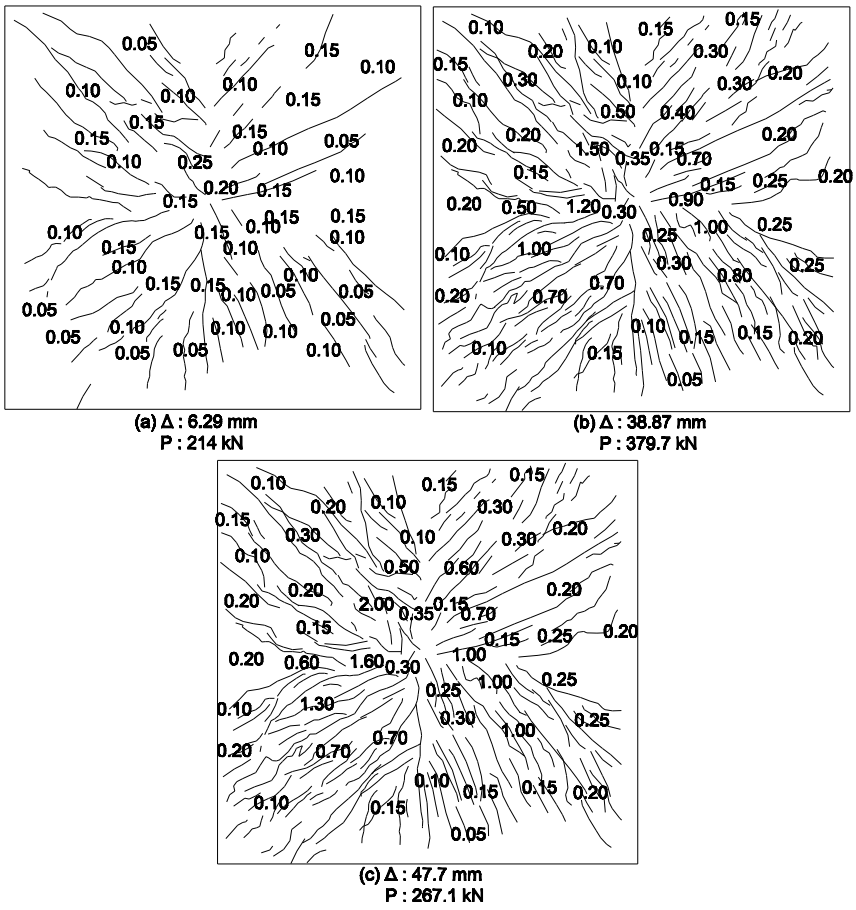

Figure 3.20. Crack patterns at the tension side of specimen SY150f10-a, (a) after 1st stop; (b) after 2nd stop; (c) after 3rd stop (Given numbers are crack widths in millimeter.)

3.6.3. SY150f15-a

Specimen SY150f15-a reached displacement of 54.89 mm and 440.54 kN load carrying capacity at the peak point. Furthermore, it reached 58.54 mm of displacement and 401.3 kN of load just before failure. Crack distribution and the width of the cracks are presented in Figure 3.21.

Similar to SY150f10-a, this specimen was also manufactured with 10 mm diameter bars at 150 mm spacing, but same reinforcement ratio was preserved with the specimens manufactured with 8 mm bars.

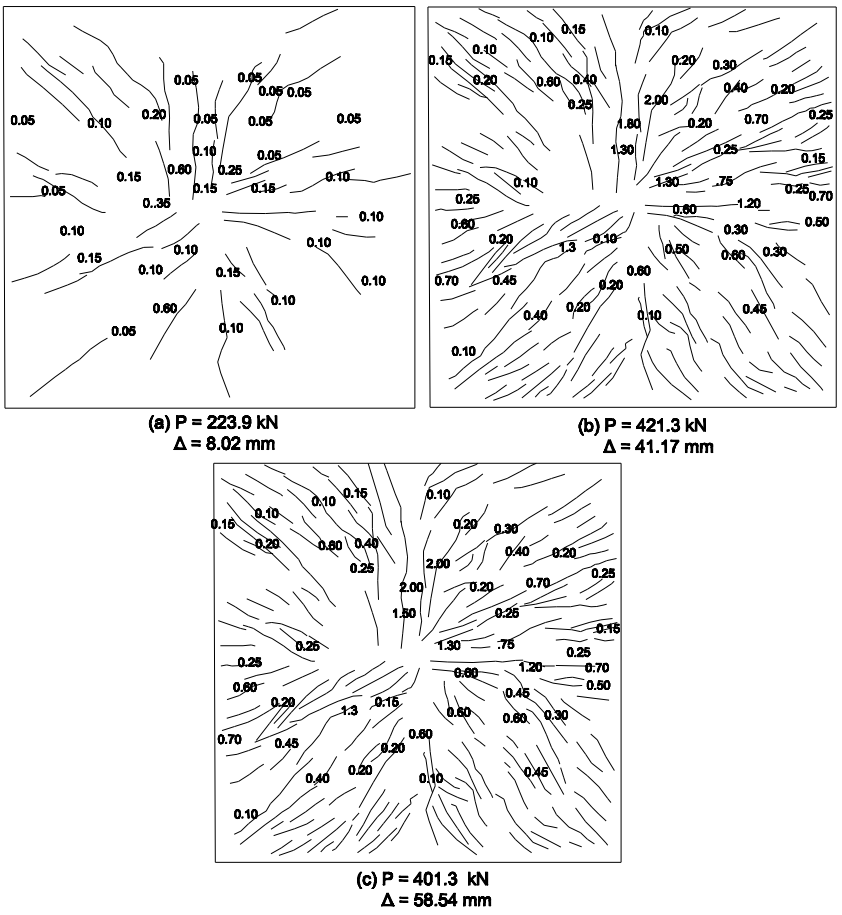

Figure 3.21. Crack patterns at the tension side of specimen SY150f15-a, (a) after 1st stop; (b) after 2nd stop; (c) after 3rd stop (Given numbers are crack widths in millimeter.)

3.6.4. SY200f05-a

Specimen SY200f05-a reached displacement of 31.81 mm and 292.67 kN load carrying capacity at the peak load. Furthermore, it reached 46.95 mm of displacement and 190 kN of load just before failure. Crack distribution and the width of the cracks are presented in Figure 3.22.

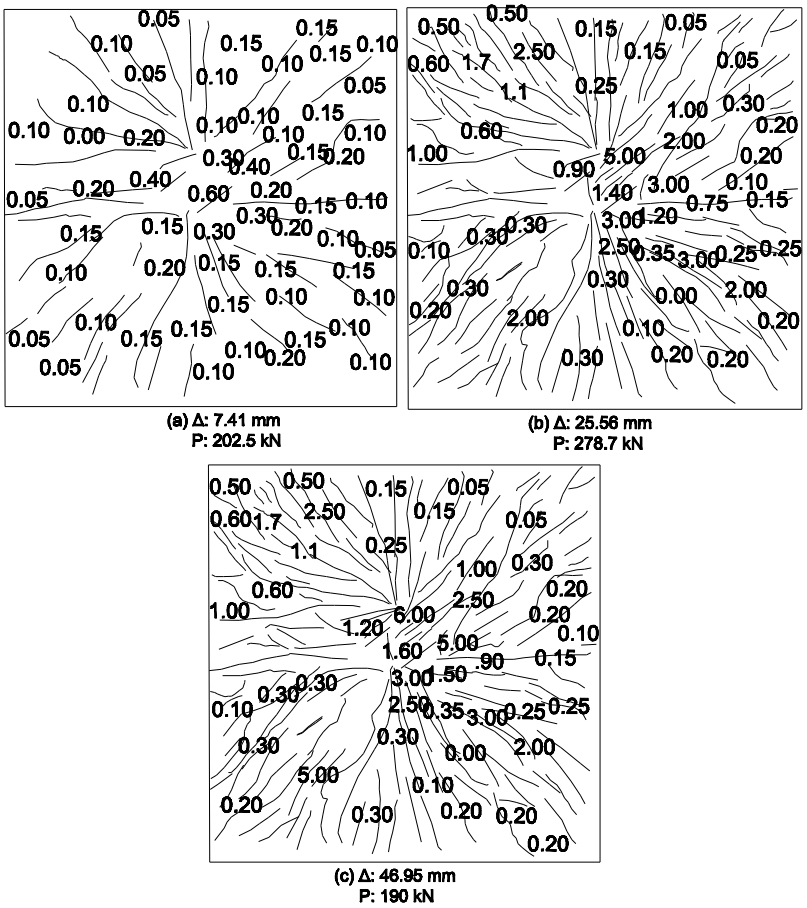

Figure 3.22. Crack patterns at the tension side of specimen SY200f05-a, (a) after 1st stop; (b) after 2nd stop; (c) after 3rd stop (Given numbers are crack widths in millimeter.)

3.6.5. SY200f15-a

Specimen SY100f05-a reached displacement of 42.66 mm and 329.64 kN load carrying capacity at the peak point. Furthermore, it reached 59.26 mm of displacement and 289.6 kN of load just before failure. Crack distribution and the width of the cracks are presented in Figure 3.23.

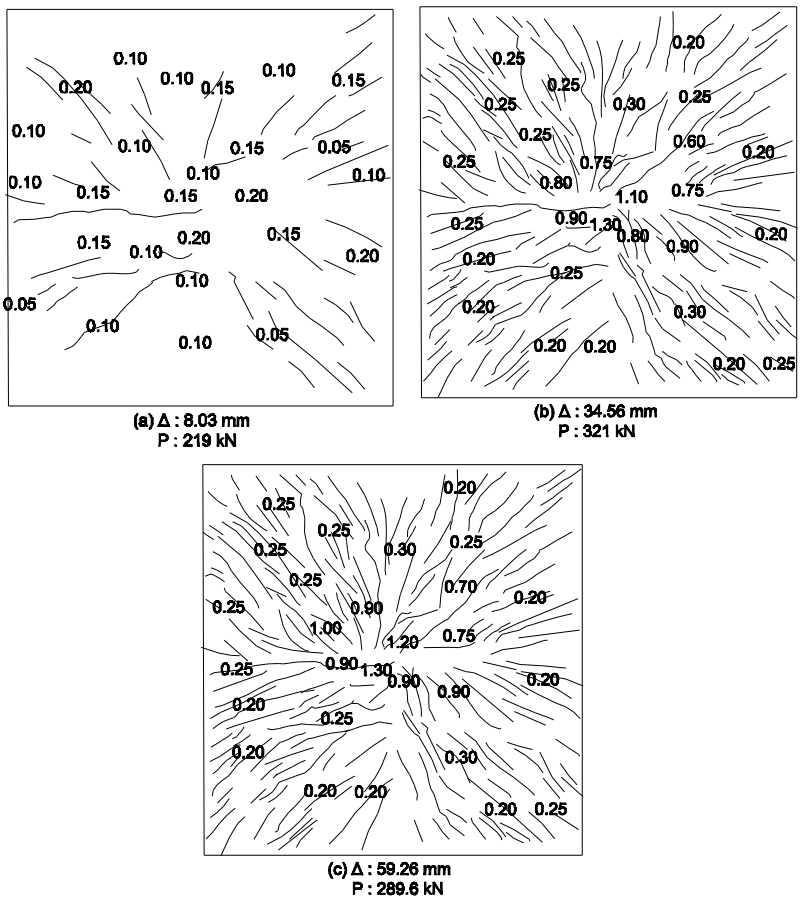

Figure 3.23. Crack patterns at the tension side of specimen SY200f15-a, (a) after 1st stop; (b) after 2nd stop; (c) after 3rd stop (Given numbers are crack widths in millimeter.)

3.6.6. YA200fa (Arsan, 2014)

Specimen YA200fa reached displacement of 25 mm and 298 kN load carrying capacity before failure. Crack distribution and the width of the cracks are presented in Figure 3.24.

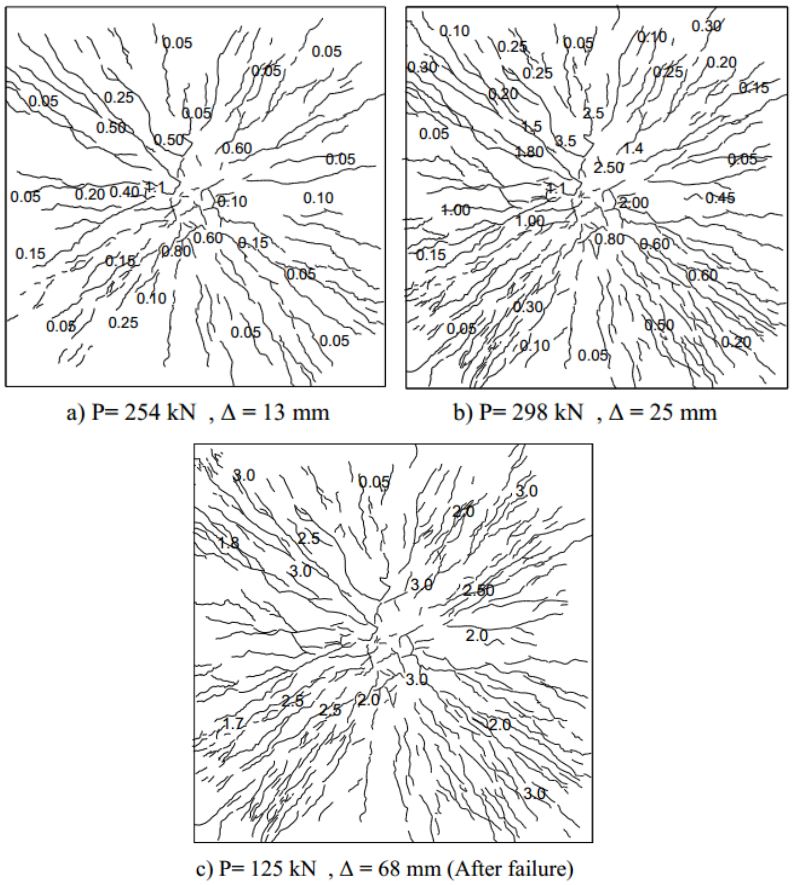

Figure 3.24. Crack patterns at the tension side of specimen YA200fa, (a) after 1st stop; (b) after 2nd stop; (c) after 3rd stop (Given numbers are crack widths in millimeter.)

3.6.7. BB100a (Batarlar, 2013)

Specimen BB100a reached displacement of 24 mm and 248 kN load carrying capacity before failure. Crack distribution and the width of the cracks are presented in Figure 3.25.

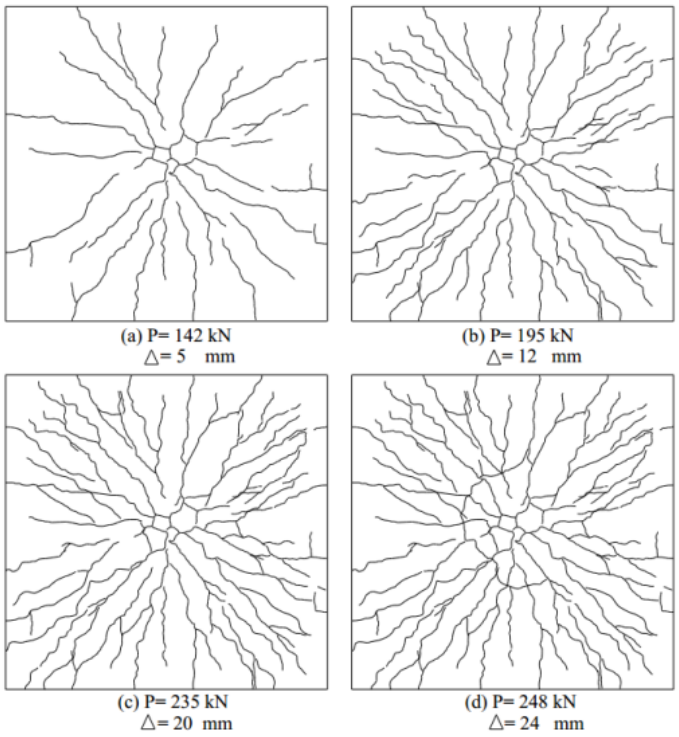

Figure 3.25. Crack patterns at the tension side of specimen BB100a, (a) after 1st stop; (b) after 2nd stop; (c) after 3rd stop; (d) after 4th stop

3.6.8. BB200a (Batarlar, 2013)

Specimen BB200f00-a reached displacement of 43 mm and 161 kN load carrying capacity before failure. Crack distribution and the width of the cracks are presented in Figure 3.26.

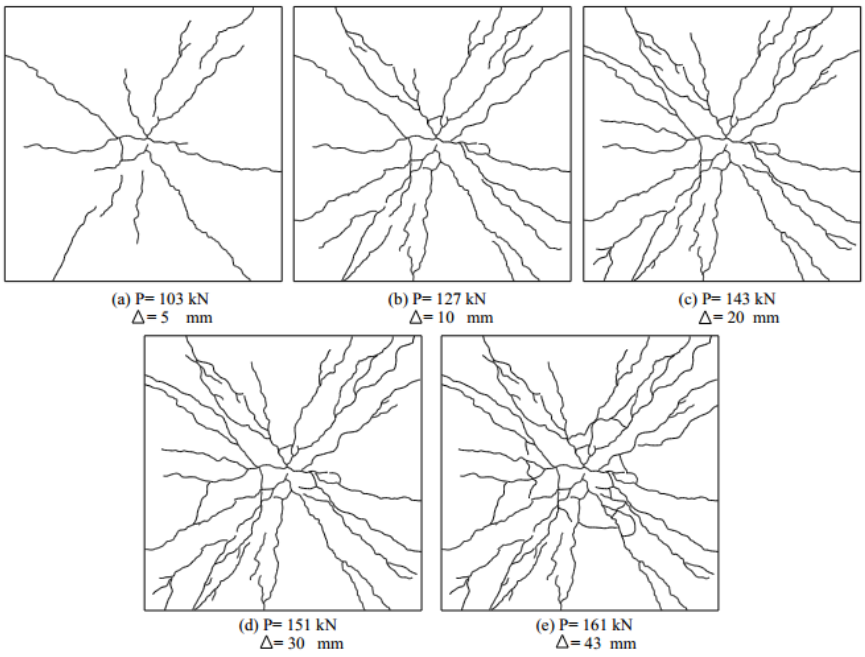

Figure 3.26. Crack patterns at the tension side of specimen BB200a, (a) after 1st stop; (b) after 2nd stop; (c) after 3rd stop; (d) after 4th stop; (e) after 5th stop

3.7. Dynamic Testing

3.7.1. SY100f05-b

For the first impact, drop weight of 320 kg was dropped from 250 cm, and for the second and third impacts drop weight of 555 kg was dropped from the height of 244 cm. Crack distribution on the bottom face of the specimen is presented in Figure 3.27. After each impact, hairline cracks were formed on the top side of the specimen. Distributions of those cracks were in a circular manner and their widths were less than 0.05 mm (Figure 3.28).

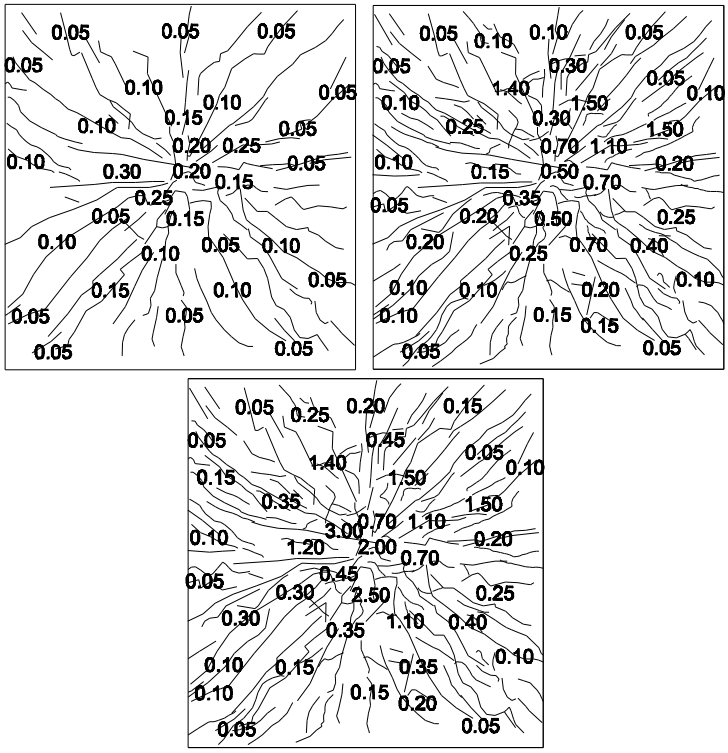

Figure 3.27. Crack patterns at the bottom side of specimen SY100f05-b after 1st, 2nd and 3rd impacts (Given numbers are crack widths in millimeter.)

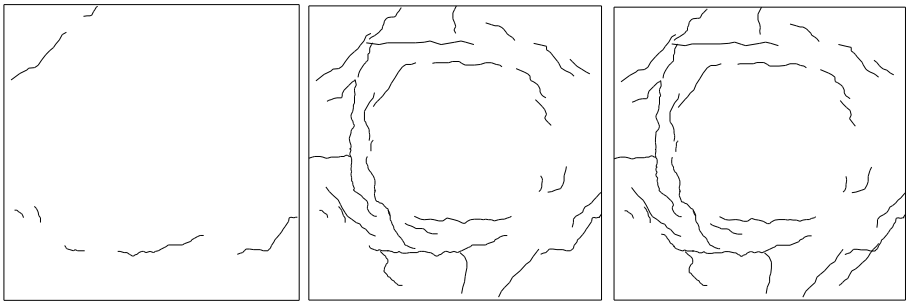

Figure 3.28. Crack patterns at the top side of specimen SY100f05-b after 1st, 2nd and 3rd impacts

3.7.2. SY100f10-b

For the first impact, drop weight of 320 kg was dropped from 250 cm, and for the second and third impacts drop weight of 555 kg was dropped from the height of 244 cm. After the third drop, some scabbing has occurred at the bottom side of the specimen (Figure 3.29(c)). Although after the first impact no crack was observed on the impacted

face of the specimen, circular cracks were observed after the second and the third drops. (Figure 3.30) Furthermore, hairline cracks were formed after second and third drops. Crack distribution on the bottom face of the specimen is presented in Figure 3.29.

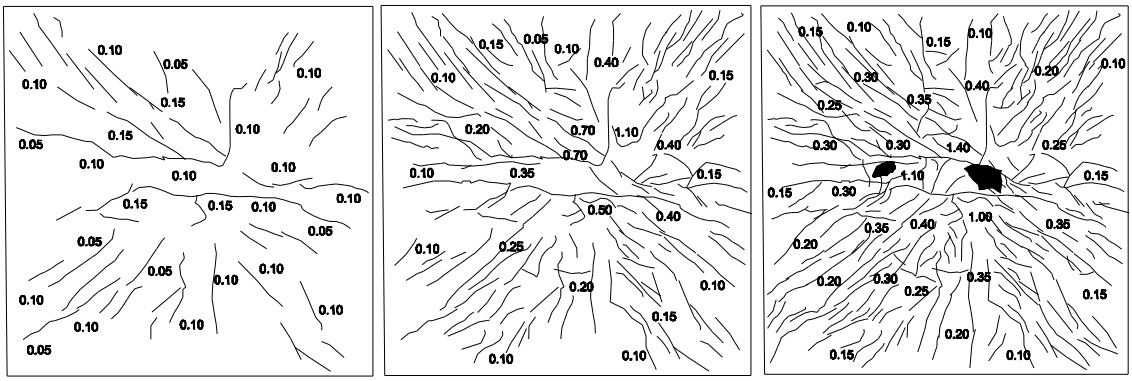

Figure 3.29. Crack patterns at the bottom side of specimen SY100f10-b, (a) after 1st drop; (b) after 2nd drop; (c) after 3rd drop (Given numbers are crack widths in millimeter.)

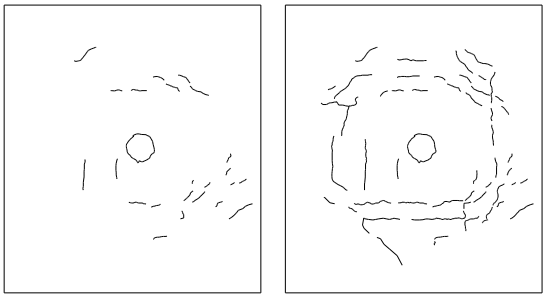

Figure 3.30. Crack patterns at the top side of specimen SY100f10-b, (a) after 1st drop; (b) after 2nd drop

3.7.3. SY100f15-b

For the first impact, drop weight of 320 kg was dropped from 250 cm, and for the second and third impacts drop weight of 555 kg was dropped from the height of 244 cm. Although after the first impact no crack was formed on the impacted face, circular cracks were observed after the second and the third drops. (Figure 3.32) Hairline cracks, with widths less than 0.05 mm, were formed after the second and the third impact. Crack distribution on the bottom face of the specimen is presented in Figure 3.31.

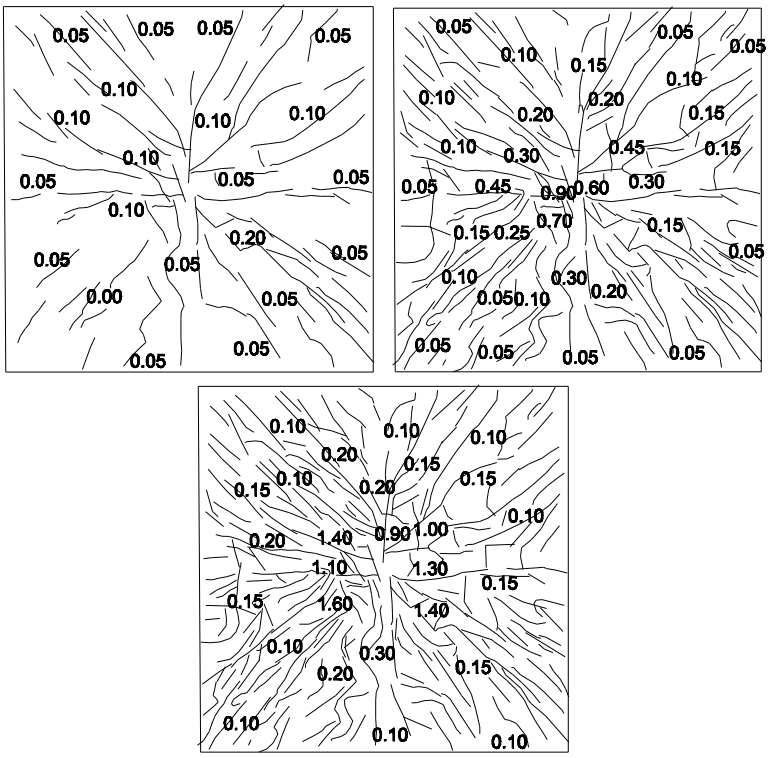

Figure 3.31. Crack patterns at the bottom side of specimen SY100f15-b, (a) after 1st drop; (b) after 2nd drop; (c) after 3rd drop (Given numbers are crack widths in millimeter.)

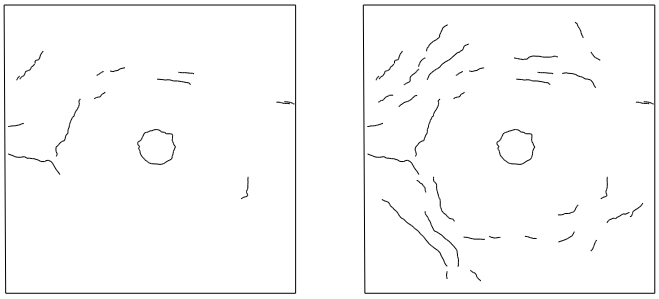

Figure 3.32. Crack patterns at the top side of specimen SY100f15-b, (a) after 2nd drop; (b) after 3rd drop

3.7.4. SY200f05-b

For the first impact, drop weight of 320 kg was dropped from 250 cm, and for the second impact drop weight of 555 kg was dropped from the height of 244 cm. After two drops, the slab reached its ultimate displacement and failed. Circular cracks were formed at the impacted face after both the first and the second drops. (Figure 3.34)

Crack widths and the distributions of the cracks on the top face of the specimen are presented in Figure 3.34. Crack distribution on the bottom face of the specimen is presented in Figure 3.33.

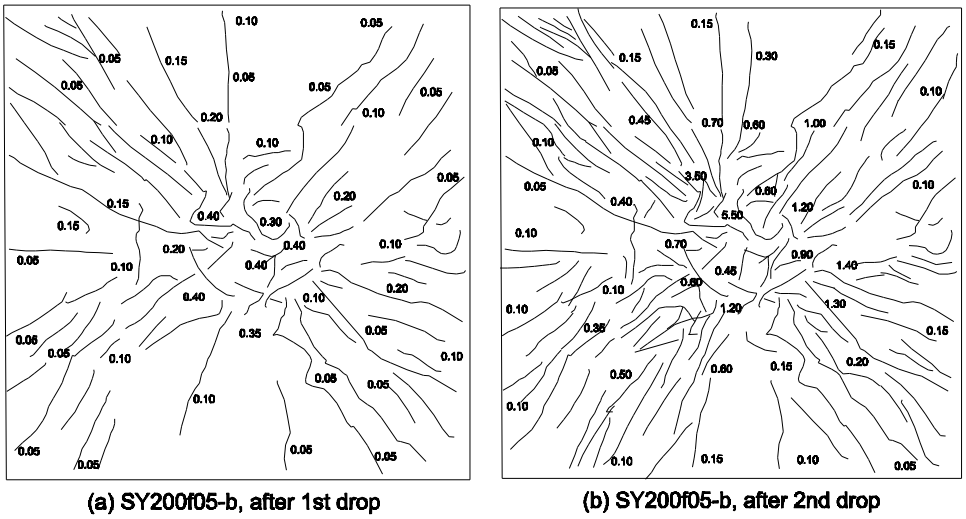

Figure 3.33. Crack patterns at the bottom side of specimen SY200f05-b, (a) after 1st drop; (b) after 2nd drop

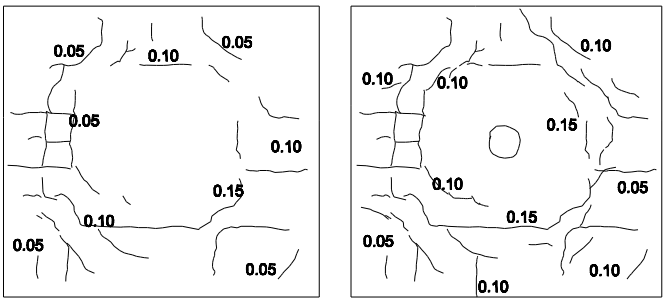

Figure 3.34. Crack patterns at the top side of specimen SY200f05-b

3.7.5. SY200f15-b

For the first impact, drop weight of 320 kg was dropped from 250 cm, and for the second and third impacts drop weight of 555 kg was dropped from the height of 244 cm. After the third drop, some scabbing has occurred at the bottom side of the specimen Figure 3.35 After each drop, circular cracks with very narrow widths, less than 0.05

mm, were observed at the top face of the specimen. (Figure 3.36) Crack distribution on the impacted face is presented in Figure 3.36.

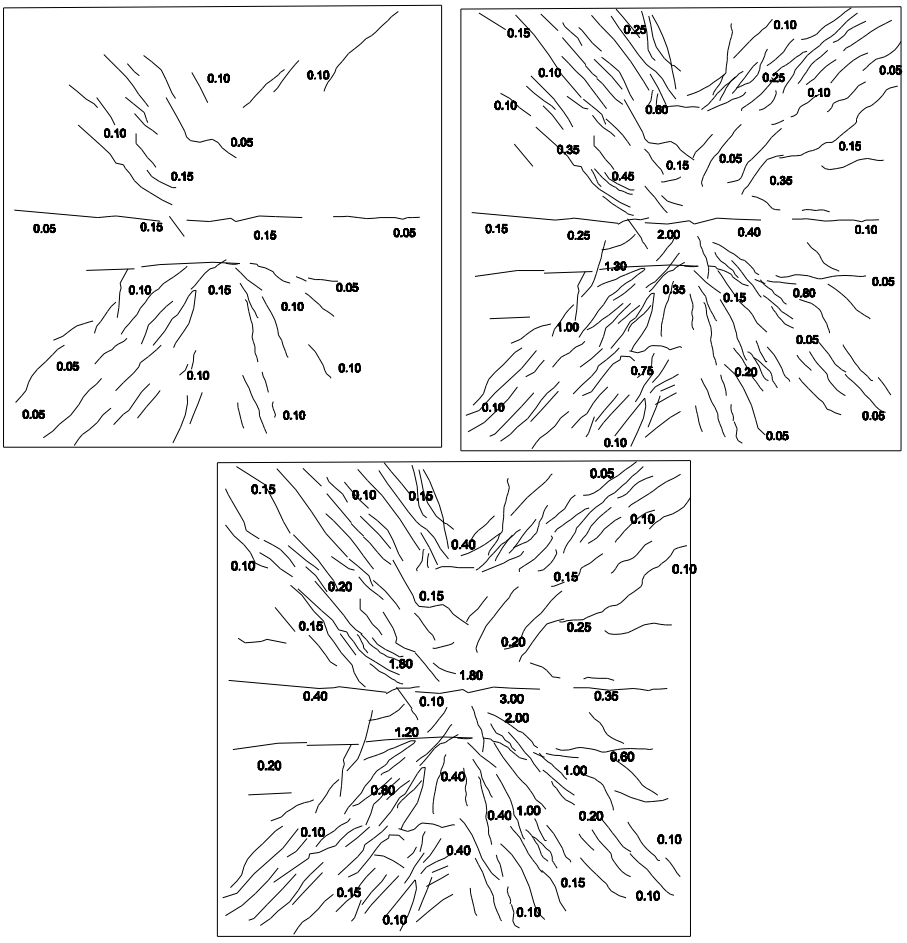

Figure 3.35. Crack patterns at the bottom side of specimen SY200f15-b, (a) after 1st drop; (b) after 2nd drop, (c) after 3rd drop (Given numbers are crack widths in millimeter.)

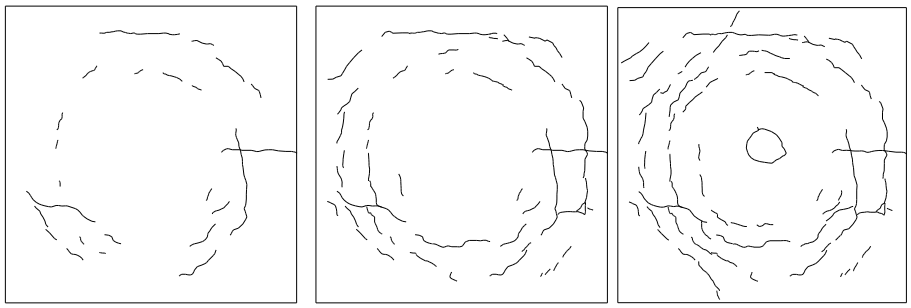

Figure 3.36. Crack patterns at the top side of specimen SY200f15-b, (a) after 1st drop; (b) after 2nd drop, (c) after 3rd drop

3.7.6. YA200fb (Arsan, 2014)

Impact loading was applied by the 320 kg drop weight free-falling from 250 cm, resulting 7 m/s contact velocity. After two impacts, scabbing was observed. Circular cracks were obtained on the top face of the specimen after each impact loading. (Figure 3.38). Crack distribution of the bottom side of the specimen is presented in Figure 3.37.

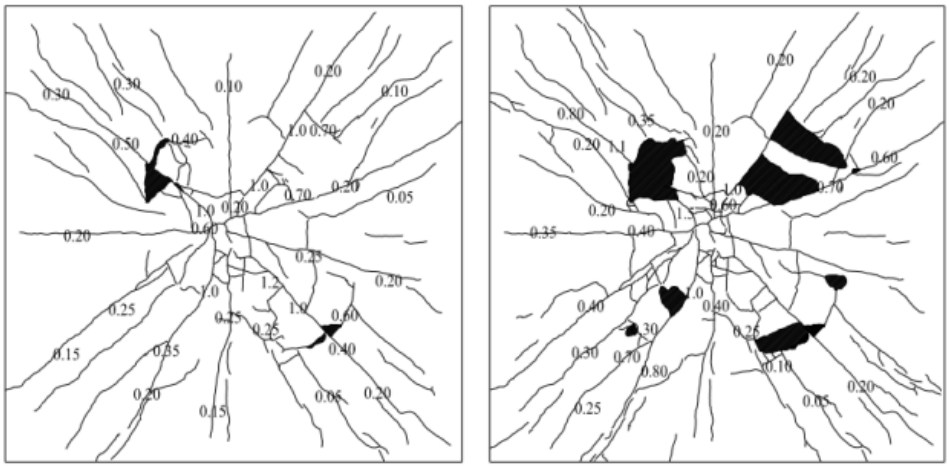

a) YA200b-1 b) YA200b-2

Figure 3.37. Crack patterns at the bottom side of specimen YA200f10-b, after 1st and 2nd drop (Given numbers are crack widths in millimeter.)

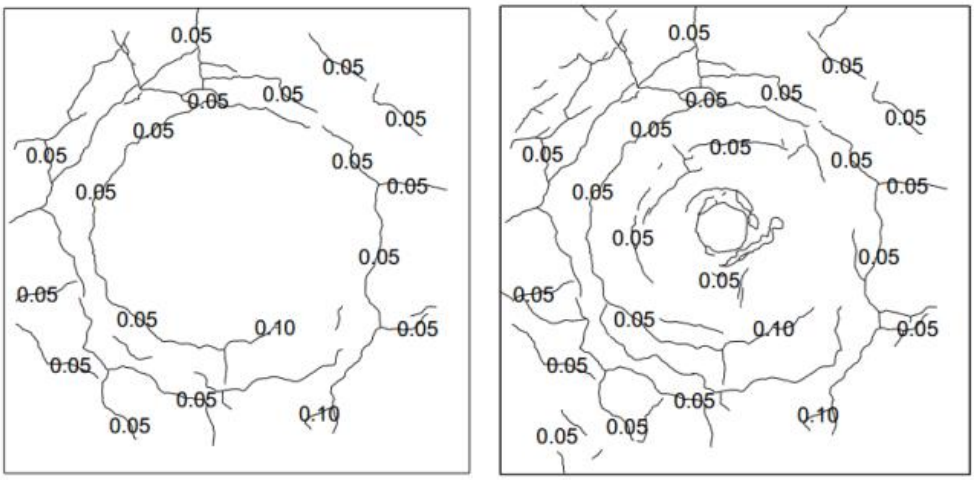

a) YA200b-1 b) YA200b-2

Figure 3.38. Crack patterns at the top side of specimen YA200f10-b, (a) after 1st drop; (b) after 2nd drop (Given numbers are crack widths in millimeter.)

3.7.7. BB100b (Batarlar, 2013)

BB100fb was subjected to impact loading three times. First impact loading was applied by the 210 kg drop weight and 7 m/s contact velocity; other impact loads were applied by the 320 kg drop weight. After the third impact, significant spalling was observed. Crack distribution of BB100b is presented in Figure 3.39

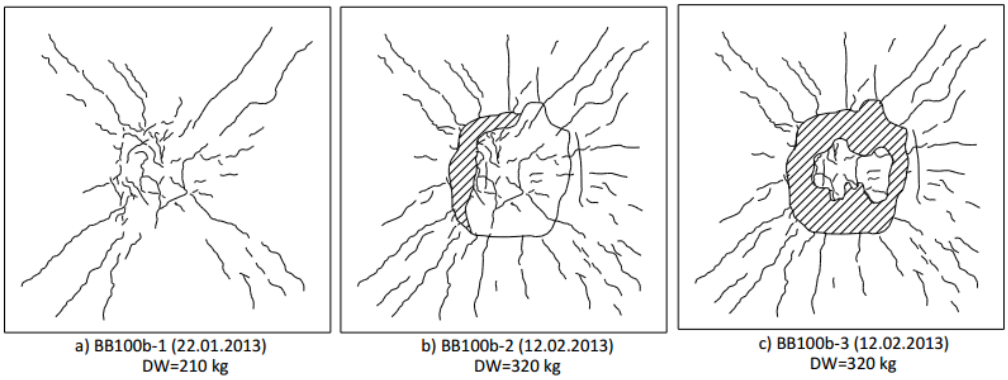

Figure 3.39. Crack patterns at the bottom side of specimen BB100f00-b, (a) after 1st drop; (b) after 2nd drop; (c) after 3rd drop (Given numbers are crack widths in millimeter.)

3.7.8. BB200b (Batarlar, 2013)

BB200f00-b was subjected to impact loading by the 320 kg drop weight twice. Crack distribution on the bottom side of the specimen is presented in Figure 3.40

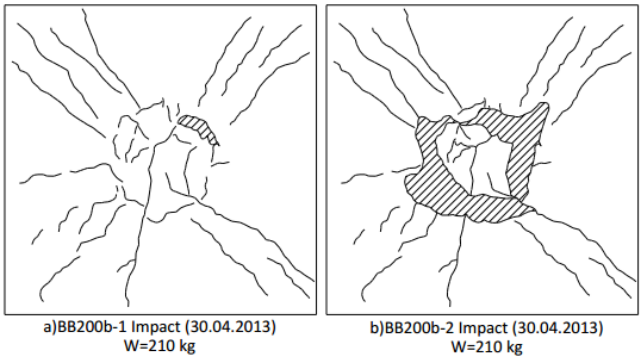

Figure 3.40. Crack patterns at the bottom side of specimen BB200f00-b, (a) after 1st drop; (b) after 2nd drop (Given numbers are crack widths in millimeter.)

CHAPTER 4

DISCUSSION OF RESULTS

In this chapter, crack distributions, peak loads, midpoint displacements at the peak load, modes of failure, failure load and midpoint displacement at failure load of the specimens in both static and dynamic loading are presented and findings are discussed in detail.

4.1. Static Tests

Monotonically increasing load was applied to the bottom center of the specimens by a 50 ton capacity hydraulic piston (Figure 3.7). In order to measure the crack width and record the crack distribution, loading process was halted at certain displacements. These halting points can be seen from both Figure 4.1 and Table 4.1. Load - displacement behavior was presented in Figure 4.1, and more precise values at the halted points and final state was presented in Table 4.1. In Figure 4.1, the points where load suddenly decreased were the stopped points, and the final drop of the load meant the failure of the member. The peak loads and related displacements for all specimens were presented in Table 4.2.

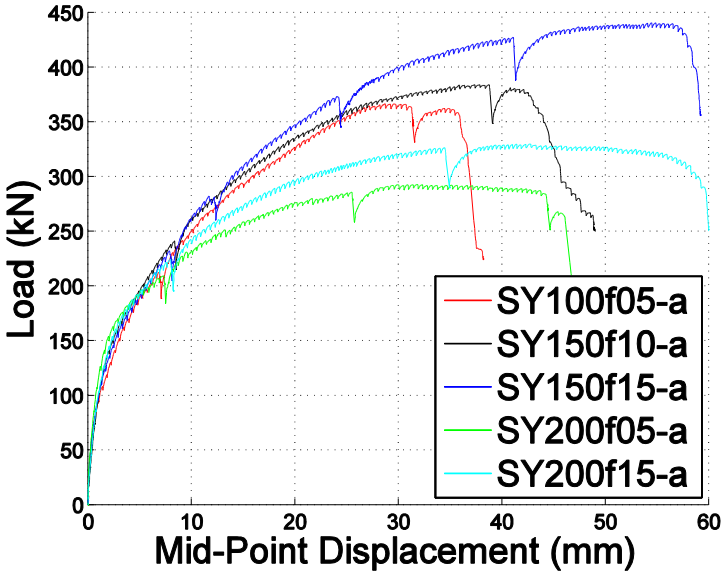

Figure 4.1. Load vs. midpoint displacement responses for static loading

Table 4.1. Stopping displacements and related loads

Name	First Step		Second Step		Third Step	
	Displacement (mm)	Load (kN)	Displacement (mm)	Load (kN)	Displacement (mm)	Load (kN)
SY100f05-a	6,929	214	31,34	358,7	37,57	235,6
SY150f10-a	8,47	237,3	38,87	379,7	47,7	267,1
SY150f15-a	8,02	223,9	41,17	421,3	58,54	401,3
SY200f05-a	7,41	202,5	25,56	278,7	46,95	190
SY200f15-a	8,03	219	34,56	321	59,26	289,6

Table 4.2. Peak loads and related displacements

Specimen	Group	Peak Load (kN)	Displacement (mm)
SY100f05-a	#1	367,89	28,73
SY150f10-a	#1	383,87	37,88
SY150f15-a	#1	440,54	54,89
BB100a	#1	248,31	24,06
SY200f05-a	#2	292,67	31,81
SY200f15-a	#2	329,64	42,66
BB200a	#2	161,1	42,65
YA200f-a	#2	328,63	37,51

To compare the effect of the fibers, specimens were divided into two groups according to their longitudinal reinforcement ratios. (Table 4.2) First group consisted of SY100f05-a, SY150f10-a, SY150f15-a and BB100-a (Batarlar, 2013), which had a 0.4% longitudinal reinforcement ratio, whereas the second group consisted of SY200f05-a, SY200f15-a, YA200fa (Arsan, 2014) and BB200a (Batarlar, 2013), which had a 0.2% longitudinal reinforcement ratio. Properties of the each specimen were presented in Table 3.1.

4.1.1. SY100f05-a SY150f10-a SY150f15-a BB100-a

All four slabs had the same longitudinal reinforcement ratio but different fiber contents. BB100a was the control specimen with no fiber addition. SY100f05-a, SY150f10-a and SY150f15-a had fiber content of 0.5%, 1.0% and 1.5%, respectively. SY100f10-a and BB100a had longitudinal reinforcement with 8 mm diameter, whereas SY150f10-a and SY150f15-a had longitudinal reinforcement with 10 mm diameter. Crack distribution and widths are presented in Figure 4.3, Figure 4.4 , Figure 4.5 and Figure 4.6 for each specimen.

It can be seen in Table 4.3 and Table 4.4 that, peak load, final load and related displacements at those loads were increased with increased fiber contents. It was also observed in Figure 4.2 that, specimens with higher fiber contents became more ductile.

Figure 4.2 demonstrated that presence of fiber change the mode of failure from brittle to ductile manner. Further, both the failure loads and related displacements at those loads were increased. In Table 4.3 it was presented that, the increase in the peak load in SY100f05-a, SY150f10-a and SY150f15-a with respect to control specimen BB100a were 48%, 55% and 77%, respectively. It is observed that peak loads did not increase with the same ratio as the fiber content. As expected, the displacement at the peak load was increased with the higher fiber contents (Table 4.3). As a result of increased fiber content, rate of increase in peak displacement was increased, contrary to the case observed for the peak loads. Further, no increase was observed in initial stiffness of the specimens as a result of increased fiber content. In Table 4.3 it was presented that, the increase in the displacement at the peak load with respect to control specimen BB100a in SY100f05-a, SY150f10-a and SY150f15-a are 19%, 57% and 128%, respectively. Due to the presence of the fibers in higher fractions in concrete

mix, the average crack widths of the specimens were reduced, increasing the efficiency of the fibers. Yet, the failure mechanism of the steel fibers was not investigated due to the difficulties involved.

Table 4.3. Peak load and relative displacement of the specimen Group 1

Specimen	Peak load (kN)	Displacement (mm)	Difference in Peak load (%)	Difference in Displacement (%)
BB100a	248,31	24,06	-	-
SY100f05-a	367,89	28,73	48	19
SY150f10-a	383,87	37,88	55	57
SY150f15-a	440,54	54,89	77	128

Increase in the final displacements and final loads of the specimens relative to the control specimen were presented in Table 4.4. From Table 4.4, it was seen that, final load of SY100f05-a, SY150f10-a and SY150f15-a were 45%, 52% and 76% higher than that of control specimen BB100a, respectively. Furthermore, maximum displacements of the specimens SY100f05-a, SY150f10-a and SY150f15-a were 49%, 75% and 137% higher than that of control specimen, respectively. As a result of increased fiber content, the rate of the increase of the final load was dropped. On the other hand, the rate of the increase of the final displacement was increased with higher fiber content.

Table 4.4. Increase in the failure load and failure displacement

Specimen	Failure Load (kN)	Failure Displacement (mm)	Difference in failure load (%)	Difference in displacement (%)
BB100a	248,3	24,06	-	-
SY100f05-a	359,5	35,82	45	49
SY150f10-a	377,2	42,16	52	75
SY150f15-a	436,3	57,03	76	137

Unlike control specimen BB100a, all the specimens with fiber content showed a ductile behavior before failure. Thus, the presence of fiber in concrete mix changed the mode of failure of the specimens from brittle to ductile manner.

Cracks were observed on the tension side of the specimens (opposite to the face where the load was applied), and no visible crack was formed at the compression side of the specimen. As expected, cracks closer to the loading region were wider than the others. Cracks were radially extending from the loading point to edges of the specimen. As the applied load was increased, inherited cracks were widened and new cracks were formed.

For SY100f05-a, like other specimens in this group, cracks closer to the loading region were wider than the others. As a result of less amount of fiber in the mix, average crack width was larger than specimens SY150f10-a and SY150f15-a. On the contrary, the average crack width was less than that of control specimen BB100a due to the fiber content.

Midpoint displacements vs. load curves for SY150f10-a and SY100f05-a are almost identical until SY150f05-a failed (Figure 4.2). SY150f10 failed under larger load and larger midpoint displacement compared to the specimen SY150f05-a. Thus, total energy absorbed by SY150f10-a was more than that of specimen SY100f05-a. In other words, with increased fiber content the energy absorption capacity of the specimen was enhanced. SY150f15-a reached the maximum peak load and corresponding displacement. Among other three specimens, SY150f15-a had the narrowest cracks. The control specimen BB100a failed in a brittle manner due to punching. Final state of the specimen is presented in Figure 4.6.

In Table 4.4 relative increment of final displacements and related load with respect to controls specimen BB100a are presented. It was also observed from Table 4.4 that, the rate of the increment of the displacement was higher than that of load carrying capacity.

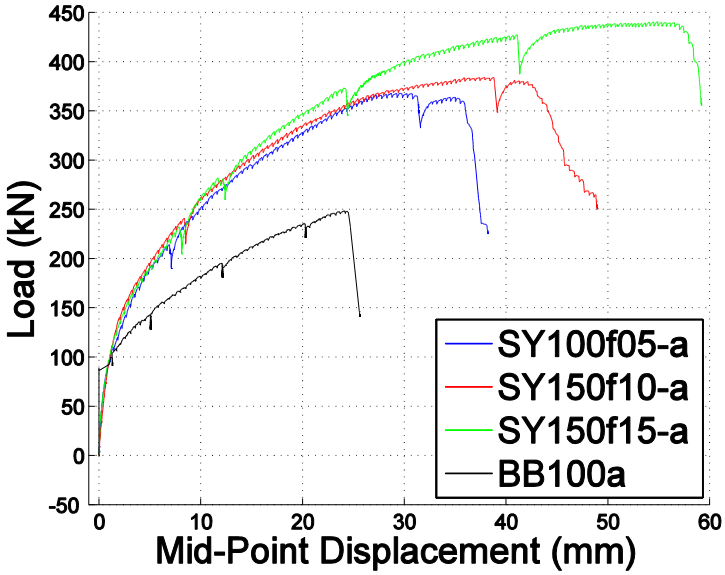

Figure 4.2. Midpoint deflection vs. applied load responses for specimens SY100f05-a, SY150f10-a, SY150f15-a and BB100-a

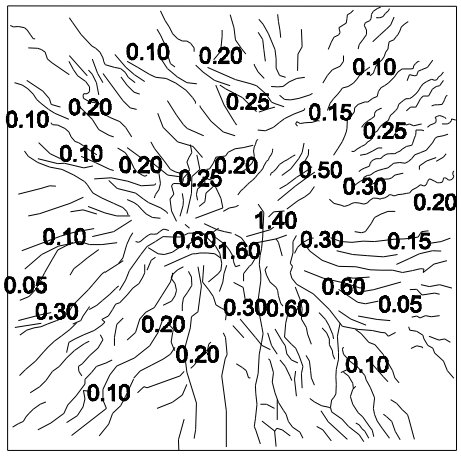

Figure 4.3. Tension face of specimen SY100f05-a after testing (Numbers indicate crack widths in millimeters)

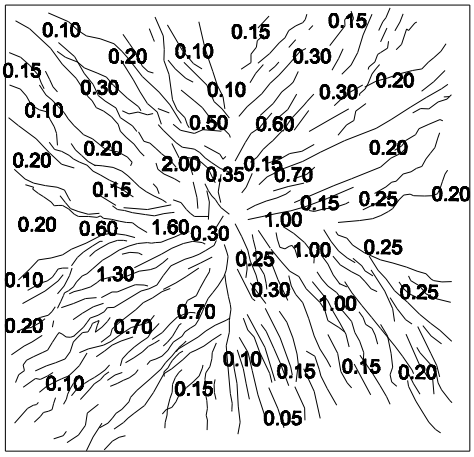

Figure 4.4. Tension face of specimen SY150f10-a after testing (Numbers indicate crack widths in millimeters)

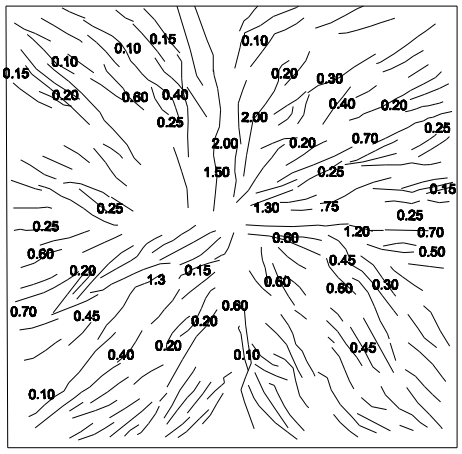

Figure 4.5. Tension face of specimen SY150f15-a after testing (Numbers indicate crack widths in millimeters)

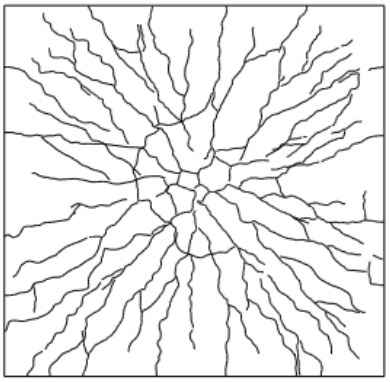

Figure 4.6. Tension face of control specimen BB100-a after testing

4.1.2. SY200f05-a SY200f15-a YA200fa BB200a

All four specimens in this group had a reinforcement ratio of 0.2% and varying steel fiber content (Table 3.1). Crack distributions and widths observed in static tests are presented in Figure 4.8, Figure 4.9, Figure 4.10 and Figure 4.11 for each specimen.

In Figure 4.7 it was presented that, adding fiber resulted in increased load carrying capacity and increased midpoint displacement. In other words, the energy absorption capacity was increased. In Table 4.5 the peak loads and corresponding displacements of all the specimens in this group were presented. The increase in the peak load in specimens SY200f05-a, SY200f15-a and YA200fa with respect to the control specimen BB200a were 181%, 204% and 203%, respectively. The change in the displacement at the peak load of the specimens SY200f05-a, SY200f15-a and YA200f-a with respect to the control specimen BB200a were -27%, 0.5% and -12%, respectively.

As seen in Figure 4.7, Table 4.5 and Table 4.6, SY200f15-a and YA200fa showed an almost identical behavior. On the other hand, peak load, final load and corresponding displacements of specimen SY150f15-a was higher than those of specimen SY150f10-a (Figure 4.2). Thus, for these tests, it could be concluded that behavior of the specimens with lower longitudinal reinforcement ratio was not affected by the fiber content as much as the behavior of specimens with higher reinforcement ratio.

Table 4.5. Peak load and corresponding displacement of the specimen Group 2

Specimen	Peak Load (kN)	Displacement (mm)
SY200f05-a	292,67	31,81
SY200f15-a	329,64	42,66
YA200f-a	328,63	37,51
BB200a	161,1	42,65

Table 4.6. Increase in the failure load and failure displacement relative to BB200a

Specimen	Failure Load (kN)	Failure Displacement (mm)	Difference in failure load (%)	Difference in displacement (%)
SY200f05-a	286	43,77	77	3
YA200f-a	325,4	50,99	102	20
SY200f15-a	325,7	51,12	102	20

As can be seen in Figure 4.7, adding fibers changed the mode of failure from brittle to ductile manner. Although significant increase in the peak loads was observed, no significant increase was observed in case of corresponding displacements. Thus, specimens were resisted more load with less displacements.

By observing Table 4.3, Table 4.4, Table 4.5 and Table 4.6 it could be concluded that with increasing fiber content, peak load, final load and corresponding displacements were increased. Furthermore, in Table 4.5 and Table 4.6 it was presented that final load, final displacement and peak load were increased with higher fiber content.

By comparing Figure 4.5 and Figure 4.9 it was observed that, in case of final displacement and final load cases, longitudinal reinforcement ratio was a significant factor. It was also observed that, specimens with higher reinforcement ratios absorbed more energy with increased fiber content. On the contrary, rate of increase in the final loads were decreased with increased reinforcement ratio (Table 4.7).

Table 4.7. Final load and related displacement of all the specimens

Specimen	Failure Load (kN)	Failure Displacement (mm)	Rate of the increase of failure load (%)	Rate of the increase of failure Displacement (%)
BB100a	248,31	24,06	-	-
SY100f05-a*	359,5	35,82	45	49
SY150f10-a*	377,2	42,16	52	75
SY150f15-a*	436,3	57,03	75	137
BB200a	161,1	42,65	-	-
SY200f05-a**	286	43,77	77	3
SY200f15-a**	325,7	51,12	102	20
YA200fa**	325,4	50,99	102	20

(*****: with respect to BB100a, ******: with respect to BB200a)

All cracks were observed on the tension side of the specimens. Cracks closer to the loading region were wider. Cracks were radially extending from loading point to edges of the specimen, concentrating on the diagonals. As expected, average crack widths decreased as steel fiber content increased.

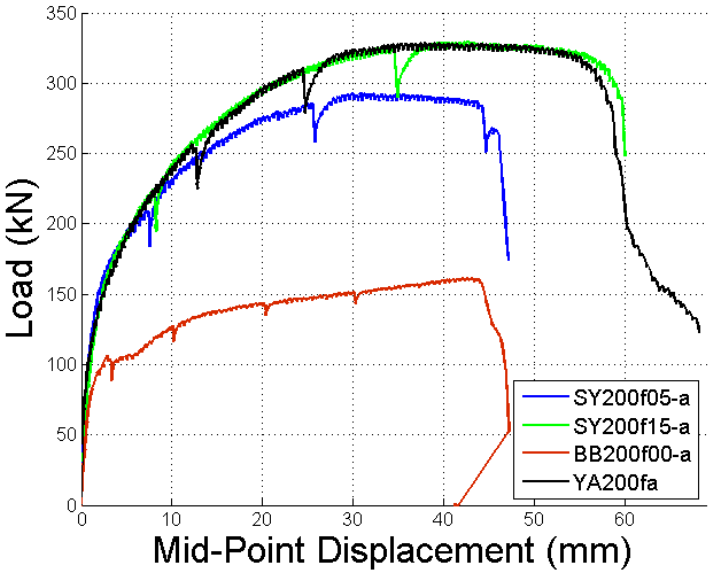

Figure 4.7. Midpoint deflection vs. applied load responses for specimens SY200f05-a, SY200f15-a, YA200f00-a, YA200f-a and BB200-a

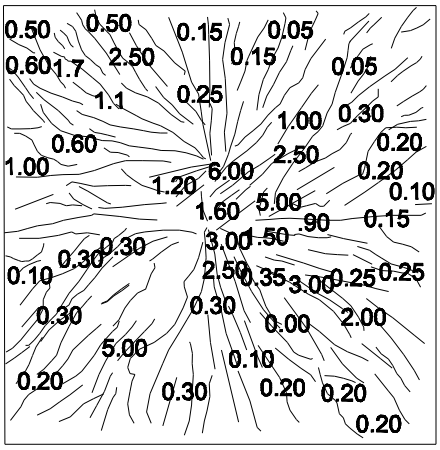

Figure 4.8. Tension face of specimen SY200f05-a after testing (Numbers indicate crack widths in millimeters)

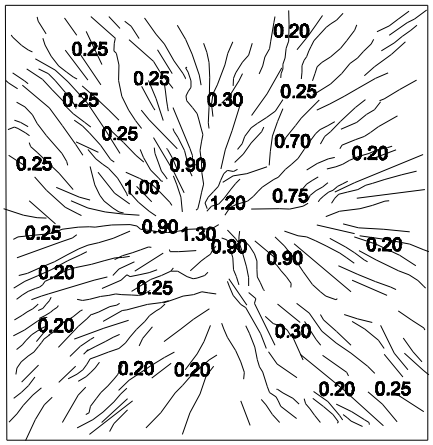

Figure 4.9. Tension face of specimen SY200f15-a after testing (Numbers indicate crack widths in millimeters)

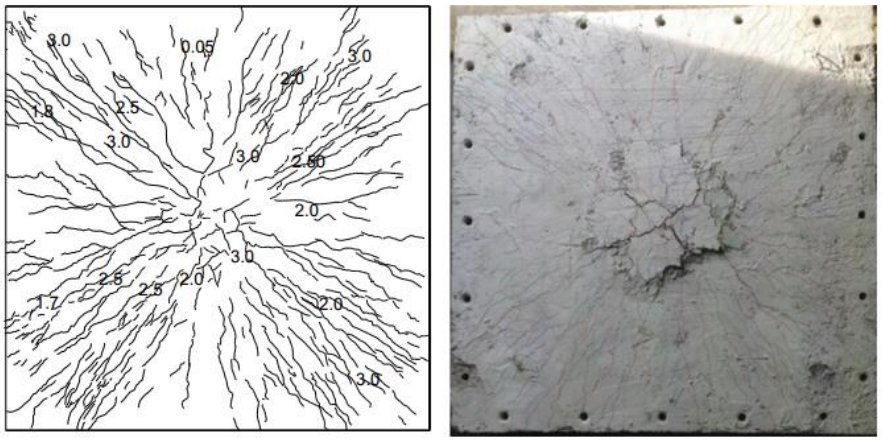

Figure 4.10. Tension face of the specimen YA200fa, after testing (Numbers indicate crack widths in millimeters)

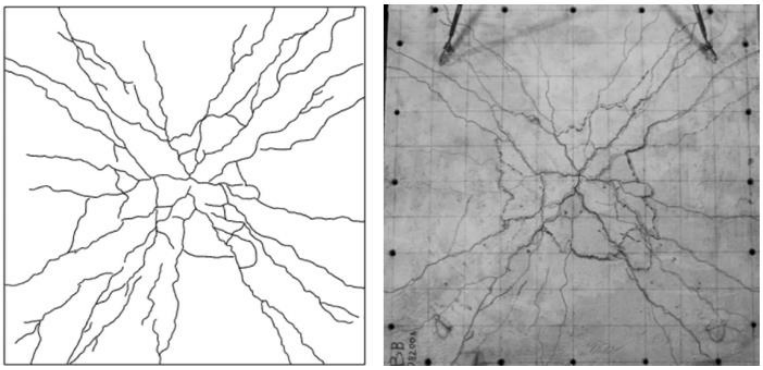

Figure 4.11. Tension face of the control specimen BB200a, after testing

4.2. Impact Tests

Impact loads were generated by dropping the drop weights from 244 or 250 cm to the center top of the specimens. In this study two different drop weights were used. For the first impacts 320 kg drop weight was used, whereas following impacts were generated by the 555 kg drop weight. Details of the used drop weight and drop height were presented in Table 4.8. In this section, deformation characteristics and crack distributions of the specimens will be compared and discussed.

Table 4.8. Drop weight and drop heights for specimens

Specimen	1st Impact		2nd Impact		3rd Impact		4th Impact		Total Energy Imparted (kJ)
	Height (cm)	Mass (kg)	Height (cm)	Mass (kg)	Height (cm)	Mass (kg)	Height (cm)	Mass (kg)	
BB100b*	250	210	250	320	250	320	-	-	20,85
SY100f05-b	250	320	244	555	244	555	-	-	34,42
SY100f10-b	250	320	244	555	244	555	-	-	34,42
SY100f15-b	250	320	244	555	244	555	-	-	34,42
BB200b*	250	210	250	210	-	-	-	-	10,30
SY200f05-b	250	320	244	555	244	555	-	-	34,42
YA200fb**	250	320	244	555	244	555	244	555	47,70
SY200f15-b	250	320	244	555	244	555	-	-	34,42

(*: Batarlar, 2013; **: Arsan, 2014)

4.2.1. SY100f05-b, SY100f10-b, SY100f15-b, BB100b

As presented in Table 4.8, different drop weights were used from different drop height in order to generate impact loading.

Impact load was applied to the specimen SY100f05-b three times. Drop weights of 320 kg and 555 kg were used for impacts. After the first impact, narrow cracks were formed on both impacted and bottom face. After second and third impacts new cracks were formed and inherited ones were widened. Cracks closer to the impacted region were wider than other cracks. Cracks out of the impacted region were narrow with similar crack widths. As a result of the presence of the steel fibers in concrete mix, no punching shear failure was observed and resistance of the specimen against impact

loading was increased. Furthermore, due to the presence of steel fibers, nearly no scabbing or spalling was observed. As expected, average crack distribution of specimen SY100f05-b was larger than that of specimens both SY100f10-b and SY100f15-b. The width and the distribution of the cracks at the bottom face of the specimen SY100f05 are presented in Figure 4.12.

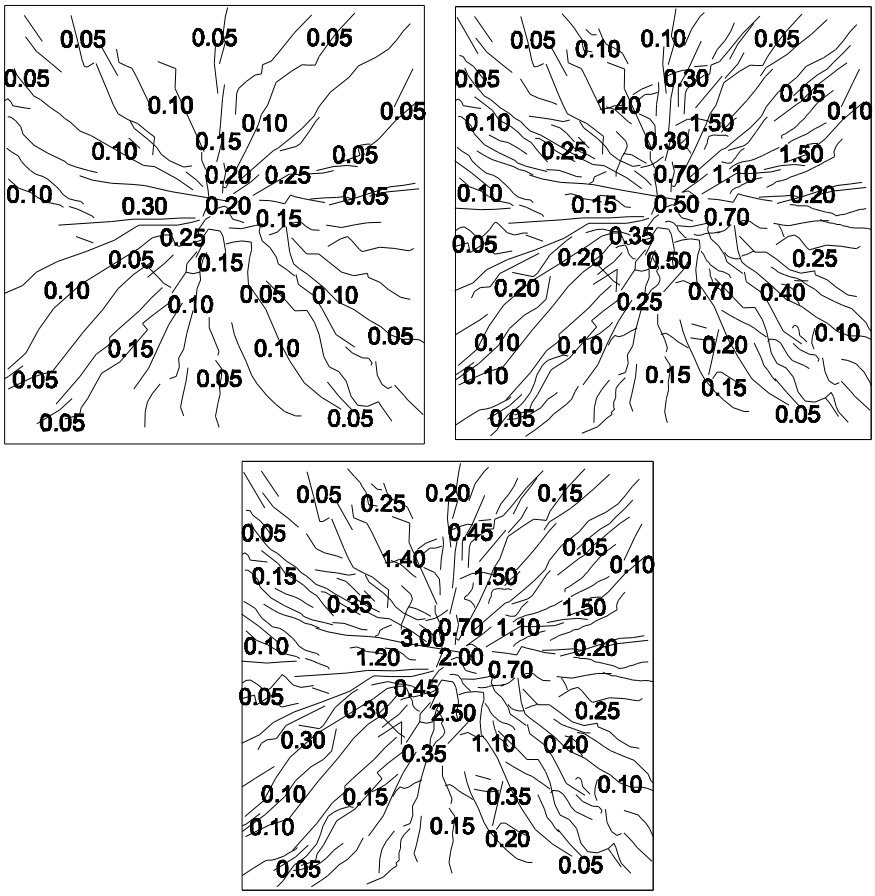

Figure 4.12. Bottom face of SY100f05-b after 1st, 2nd and 3rd impacts (Given numbers are crack widths in millimeter.)

After applying impact loads, some narrow cracks were formed at the impacted face of specimen SY100f05-b. The widths of those cracks were less than 0.05 mm, which was the minimum value of the scale that was used to measure the width of the cracks. The distribution of the cracks at the impacted face of the specimen SY100f05 is presented in Figure 4.13.

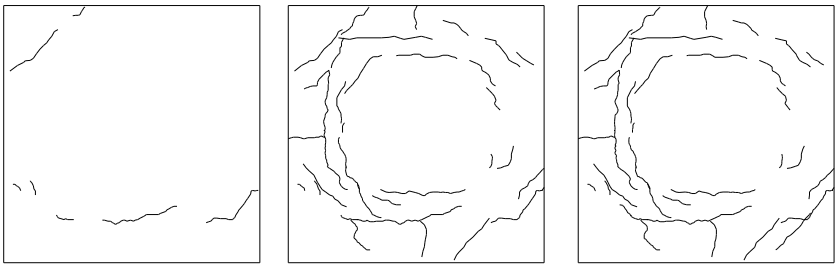

Figure 4.13. Impacted face of SY100f05-b after 1st, 2nd and 3rd impacts

Impact loads with drop weights of 320 and 555 kg were applied on the specimen SY100f10-b three times. After the first impact narrow cracks were formed on the bottom face. After the second and the third impact, new cracks were formed and inherited ones were widened. Cracks closer to the impacted region were wider than other cracks. Cracks out of the impacted region were narrow with similar crack widths. As a result of the presence of the steel fibers in concrete matrix no punching shear failure was observed, and the resistance of the specimen against impact loading was increased. No scabbing or spalling was observed due to the presence of the fiber in the matrix. Crack distribution and the widths of the cracks on the bottom face of specimen SY100f10-b are presented in Figure 4.14.

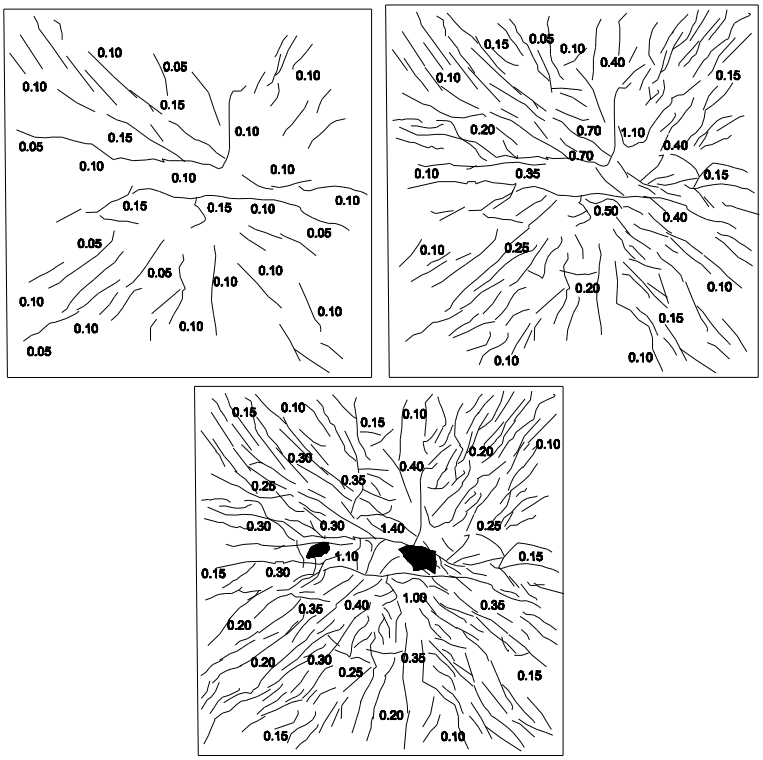

Figure 4.14. Bottom face of SY100f10-b after 1st, 2nd and 3rd impacts (Numbers indicate crack widths in millimeters)

After the first impact no crack was formed on the impacted face. After the second and the third impacts, circular cracks were formed on the impacted face. The widths of the cracks on the impacted face of the specimen SY100f10-b were less than the minimum value of the scale that was used to measure the width of the cracks. Thus, no detailed measurements were done. The distribution of the cracks at the impacted face of the specimen SY100f10-b is presented in Figure 4.15.

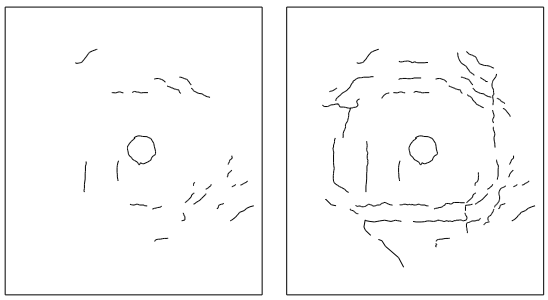

Figure 4.15. Impacted face of SY100f10-b after 2nd and 3rd impacts

Impact load with drop weights of 320 and 555 kg were applied to the specimen SY100f15-b three times. After the first impact, narrow cracks were formed on the bottom face. After the second and the third impacts, new cracks were formed and inherited cracks were widened. Cracks closer to the impacted region were wider than other cracks. Cracks out of the impacted region were narrow with similar crack widths. As a result of the presence of the steel fibers in concrete mix, no punching shear failure was observed and resistance of the specimen against impact loading was increased. Due to the presence of higher amount of fibers in concrete mix, crack formation of SY100f15-b was denser than that of both SY100f10-b and SY100f05-b. Unlike specimens SY100f05-b and SY100f10-b, the rate of new crack formation in specimen SY100f15-b was not reduced between subsequent impacts. As a result of the formation of new cracks after each impact, some of the old cracks were not widened. Thus, average crack width of SY100f15-b was less than that of both SY100f05-b and SY100f10-b. No scabbing on spalling was observed due to the presence of the fiber in the mix. Crack distribution and the widths of the cracks on the bottom side of specimen SY100f15-b are presented in Figure 4.16.

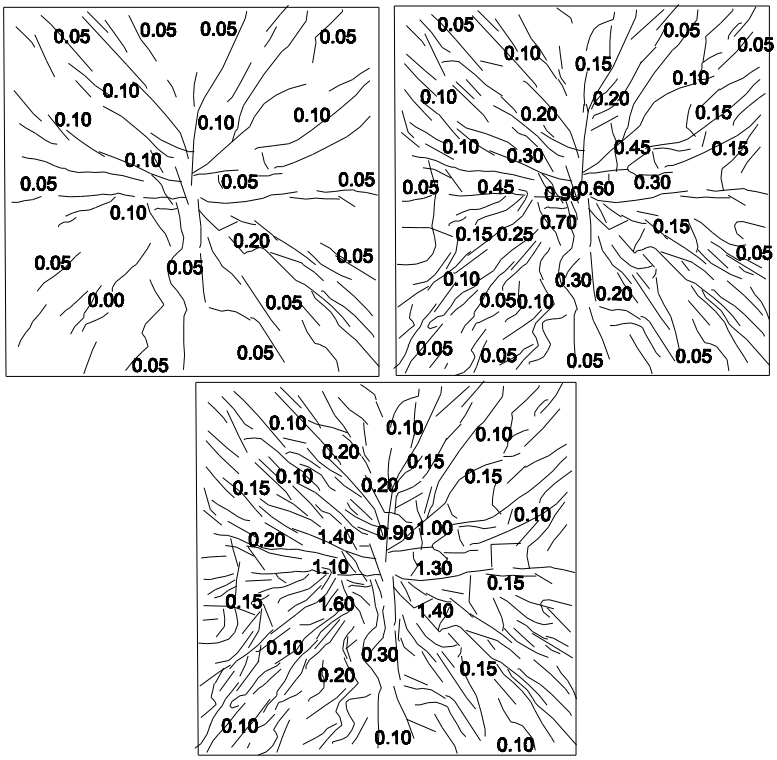

Figure 4.16. Bottom face of SY100f15-b after 1st, 2nd and 3rd impacts (Numbers indicate crack widths in millimeters)

After the first impact, no crack was formed on the impacted face. On the contrary, after the second and the third impact, circular cracks were formed on the impacted face. The widths of the cracks on the impacted face of specimen SY100f15-b were less than the minimum value of the scale that was used to measure the width of the cracks. Thus, no detailed measurements were done. The distribution of the cracks at the impacted face of the specimen SY100f15-b is presented in Figure 4.17.

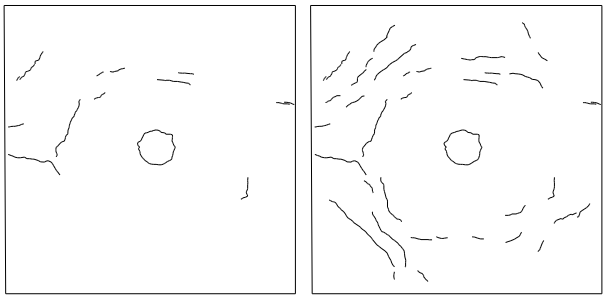

Figure 4.17. Impacted face of SY100f15-b after 2nd and 3rd impacts

Impact was applied to the specimen BB100b with two different drop weights. First drop weight was 210 kg and the second one was 320 kg. First impact was not sufficient to induce a sizable damage on the specimen. Thus, for the second and third impacts, drop weight of 320 kg was used. After three drops, significant scabbing was observed at the bottom face of the specimen. Furthermore, penetration was formed on the impacted region. As presented in Figure 4.18, a sparse crack distribution was observed.

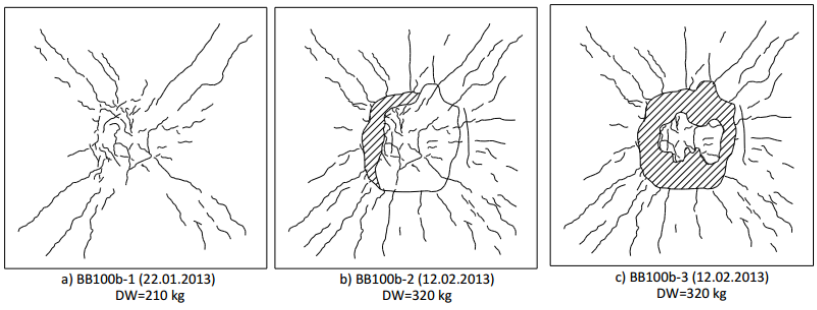

Figure 4.18. Crack profiles of bottom face for BB100b
(Source: Batarlar, 2013)

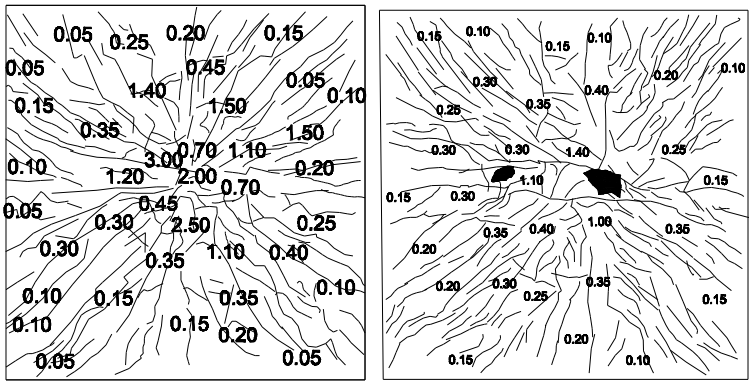

Figure 4.19. Bottom face of (a) SY100f05-b, (b) SY100f10-b and(c) SY100f15-b at final state (Numbers indicate crack widths in millimeters)

In Figure 4.19 crack distribution of specimens SY100f05-b, SY100f10-b and SY100f15-b at their final state after all applied impacts were presented. As expected, between those three specimens, SY100f05–b had the largest crack widths and SY100f15-b had the highest number of cracks. With increased fiber content, number of cracks was increased as well. As the fiber ratio increases, fibers can transfer more tensile load across a crack delaying it's widening, which causes more cracks to open elsewhere to accommodate the imposed deformations. Therefore, with increased fiber content, more cracks with lower widths were formed.

4.2.2. SY200f05-b SY200f15-b YA200fb BB200b

As presented in Table 4.8, different drop weights were used from different drop heights in order to generate impact loading.

Impact load by the drop weight of 320 and 555 kg were applied to the specimen SY200f05-b twice. After the first impact, narrow cracks were formed on the bottom face of the specimen. As expected, closer to the impacted region wider cracks were formed. Number of the cracks on the bottom face of specimen SY200f05-b (Figure 4.20) was less than that of specimen SY100f05-b (Figure 4.12). On the contrary, average crack width on the bottom face of specimen SY200f05-b was larger than that of specimen SY100f05-b. As a result of smaller longitudinal reinforcement ratio, tensile stresses were not well distributed, concentrating imposed deformations on existing cracks. Therefore, wider cracks were formed in specimens with smaller longitudinal reinforcement ratio. Like SY100f05-b, cracks out of impacted region were narrow with similar crack widths. As a result of the presence of the steel fibers in concrete mix, no punching cone was formed and resistance of the specimen against impact loading was improved. No scabbing or spalling was observed as well due to the presence of the fiber in the mix. Crack distribution and the widths of the cracks on the bottom face of specimen SY200f05-b are presented in Figure 4.20.

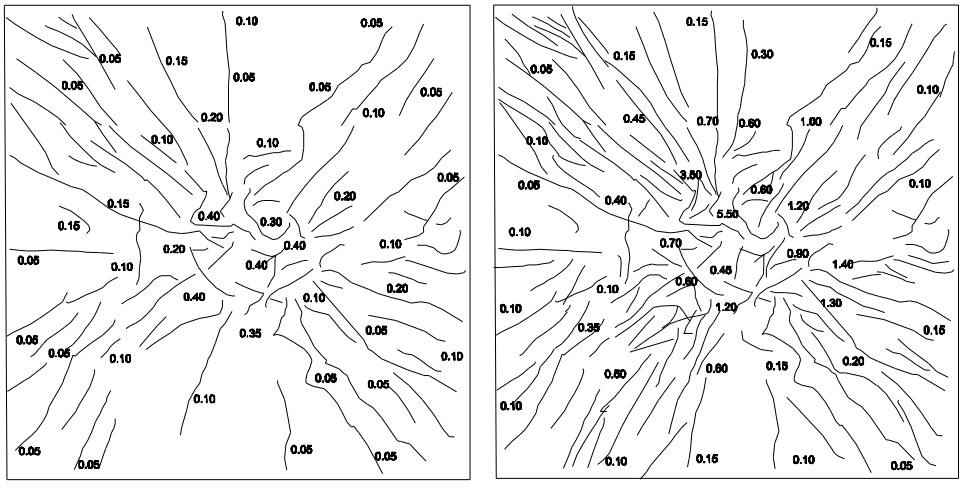

Figure 4.20. Bottom face of specimen SY200f05-b after 1st and 2nd impacts (Numbers indicate crack widths in millimeters)

After the first impact circular cracks were formed on the impacted face of specimen SY200f05-b (Figure 4.21). Number of new cracks after the second impact was less than that of specimen SY100f05-b (Figure 4.13). Instead, inherited cracks were widened after the second impact. Average crack width of specimen SY200f05-b on the impacted face was larger than that of specimen SY100f05-b. The width and the distribution of the cracks at the impacted face of the specimen SY200f05-b are presented in Figure 4.21.

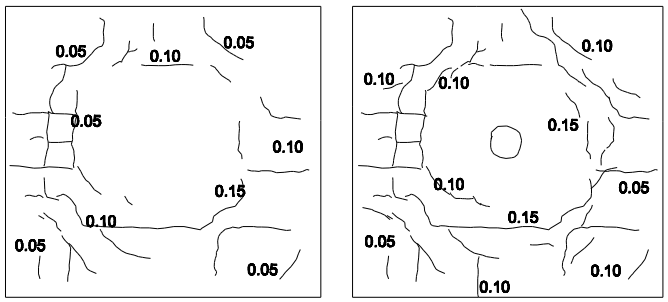

Figure 4.21. Top face of specimen SY200f05-b after 1st and 2nd impacts (Numbers indicate crack widths in millimeters)

Impact load by the drop weight of 320 and 555 kg was applied to the SY200f15-b three times. After the first impact, narrow cracks were formed on the bottom face of the specimen SY200f15-b. As expected, wider cracks were formed closer to the impacted region. Number of the cracks on the bottom face of specimen SY200f15-b (Figure 4.22) was less than that of specimen SY100f15-b (Figure 4.16). On the contrary, average crack width on the bottom face of specimen SY200f15-b was wider than that of specimen SY100f15-b. Like SY100f15-b, cracks out of impacted region were narrow with similar crack widths. In the final state, most of the cracks on the bottom face of the specimen SY200f15-b were on the diagonal axis. As a result of the presence of the steel fibers in concrete matrix, no punching shear failure was observed and the resistance of the specimen against impact loading was improved. No scabbing or spalling was observed due to the presence of the fiber in the matrix. Crack distribution and the widths of the cracks on the bottom face of specimen SY200f15-b are presented in Figure 4.22.

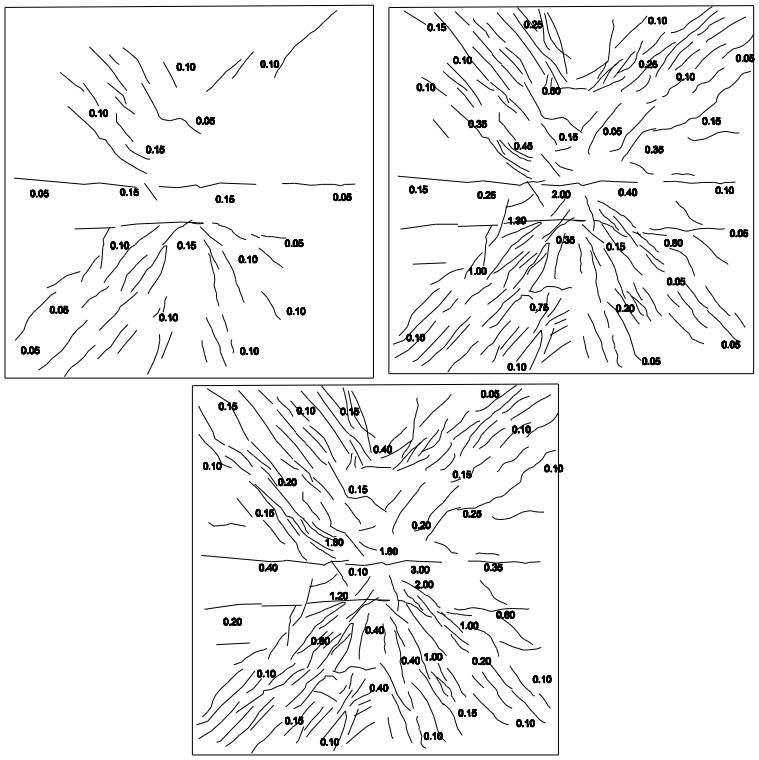

Figure 4.22. Bottom face of specimen SY200f15-b after 1st, 2nd and 3rd impacts (Numbers indicate crack widths in millimeters)

After the first impact circular cracks were formed on the impacted face of specimen SY200f15-b. Very few cracks were formed after the third impact. Instead, inherited cracks were widened after the third impact. In other words, after second impact cracks on the impacted face were widened and little amount of new cracks were formed. Average crack width of specimen SY200f15-b on the impacted face was larger than that of specimen SY100f15-b. The width and the distribution of the cracks at the impacted face of the specimen SY200f15-b are presented in Figure 4.23.

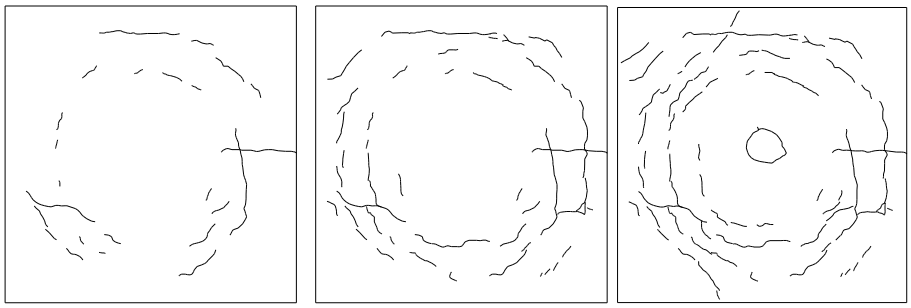

Figure 4.23. Impacted face of specimen SY200f15-b after 1st, 2nd and 3rd impacts (Numbers indicate crack widths in millimeters)

For the control specimen BB200b, impact load was applied by the 210 kg drop weight. After the first impact, diagonal cracks were formed and slight scabbing was observed on the bottom face of the specimen. Circular cracks were also formed on this face. After the second impact, number of the cracks was did not increase, but inherited cracks were widened and excessive scabbing was observed at the bottom face of the specimen. Crack distribution on the bottom face of the specimen BB200b is presented in Figure 4.24. As expected, among all specimens, BB200b had the widest crack width due to lack of fibers and smaller longitudinal reinforcement ratio.

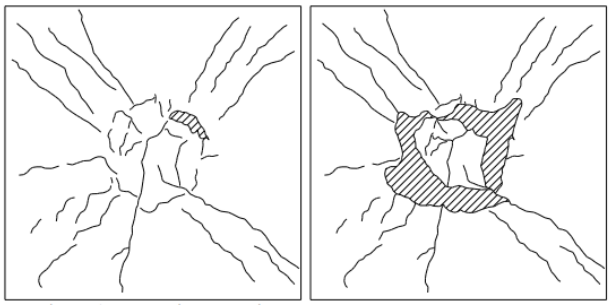

Figure 4.24. Bottom face of specimen BB200b after 1st and 2nd impacts (Source: Batarlar, 2013)

For the specimen YA200fb, impact load was applied once by the 320 kg drop weight dropped from 250 cm and three times by the 555 kg drop weight dropped from 244 cm. As expected, cracks closer to the impacted region were wider than other cracks. Cracks at the out of impacted region were narrow and had similar crack widths. Number of the cracks at the bottom face of specimen YA200fb was more than that of specimen SY200f15-b. However, this can be attributed to the difference in the total applied energy between two specimens, as YA200b was subjected one extra impact by the 555 kg drop weight compared to SY200f15-b. Average crack width of the specimen SY200f15b was less than that of specimen YA200fb, as expected. Although the number of cracks in the specimen YA200fb was more than that of specimen SY200f15b, it was almost equal to that of specimen SY100f10-b. Average crack width of the specimen SY100f10-b was less than that of the specimen YA200fb. Denser cracks were formed on the diagonals of the bottom face of the specimen YA200fb. As a result of the presence of the steel fibers in concrete mix, no shear cone formation was observed and the resistance of the specimen against impact loading was improved. No scabbing or

spalling was observed due to the presence of the fiber in the mix. Crack distribution and the widths of the cracks on the bottom face of specimen YA200fb are presented in Figure 4.25.

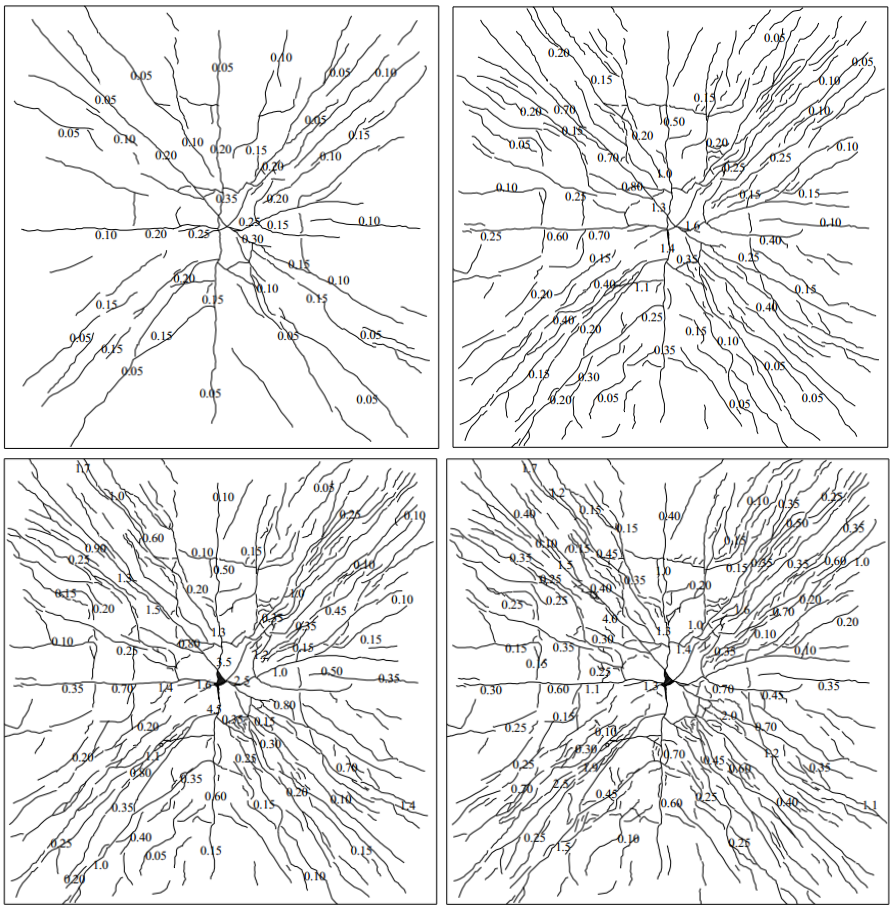

Figure 4.25. Bottom face of specimen YA200f-b after 1st, 2nd, 3rd and 4th impacts (Numbers indicate crack widths in millimeters)

No visible crack was formed on the impacted face of specimen YA200fb after the first impact. After the second impact, circular cracks were formed on the impacted face. After the third impact, cracks on the impacted face were widened and very few new cracks were formed. After the fourth impact, new cracks were formed and inherited ones were widened, as well. Average crack width on the impacted face of specimen YA200fb at the final state was almost equal to that of specimen SY200f05-b. Number of cracks on the impacted face of specimen YA200fb was more than that of specimen SY200f05-b. The width and the distribution of the cracks at the impacted face of the specimen YA200fb are presented in Figure 4.26.

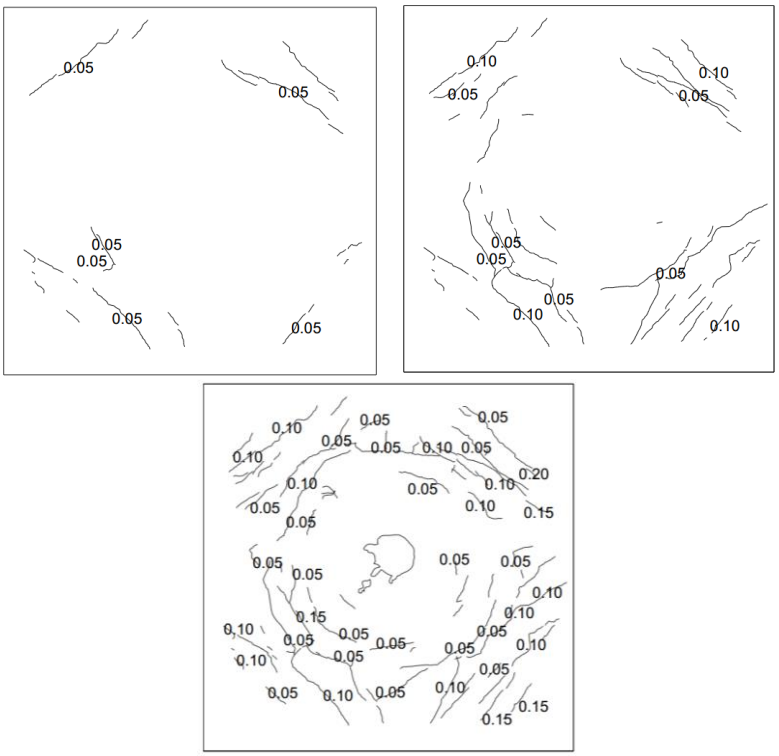

Figure 4.26. Impacted face of specimen YA200fb after 2nd, 3rd and 4th impacts (Numbers indicate crack widths in millimeters)

4.3. Displaced Shapes

A total of 24 RLPTs were mounted under each specimen in order to measure the displacements. As presented in Figure 4.27, RLPTs were concentrated on the North-East quarter of the specimens. Data obtained from those RLPTs were used to plot the deformation profile for each specimen.

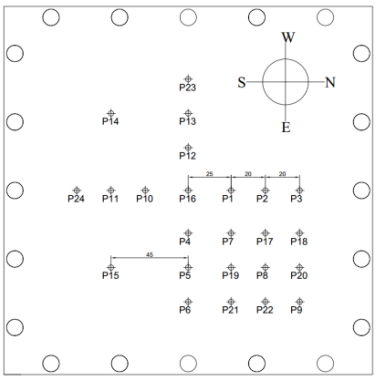

Figure 4.27. Placement of RLPTs on the bottom face of the specimens

The middle axis line in W-E direction was named as *'Axis #1'*, and axis line in S-N direction was named as *'Axis #2'*. Note that connections of some RLPTs dropped in impact tests due to the severity of the impact and no measurement could be taken from such RLPTs. Dropped RLPTs of each specimen for the first impacts were presented in Table 4.9. Among the two axes, the one with less or no dropped RLPTs was chosen to plot the middle axis deformation profile of each specimen. If an RLPT was dropped out, the symmetrical RLPT with respect to middle point of the specimen were used instead. For example, if P4 was dropped, the measurement taken by P12 was used instead. In case of P16, there was no symmetrical RLPT. Thus, if P16 was dropped out, no middle point deflection was obtained. Chosen mid line axis for the first impacts for each specimen is presented in Figure 4.28 and Figure 4.29.

Table 4.9. Dropped RLPTs in each axis of each specimen for the first impacts

Specimen	#1 axis	#2 axis
SY100f05-b	P4, P16	P10, P16
SY100f10-b	P4	P10
SY100f15-b	-	-
SY200f05-b	P4	P10
SY200f15-b	P4	P10

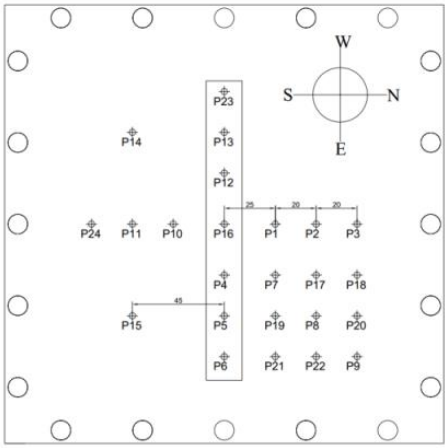

Figure 4.28. Chosen RLPTs for specimens SY100f05-b, SY100f10-b and SY200f05-b for the first impacts

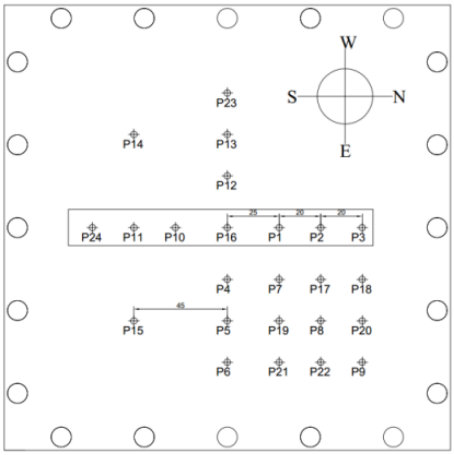

Figure 4.29. Chosen RLPTs for SY100f15-b and SY200f15-b for the first impacts

The maximum deflection in upwards direction, the maximum deflection in downwards direction and the residual displacement of the specimens after first impact are presented in Figure 4.30, Figure 4.31, Figure 4.32, Figure 4.33, Figure 4.34, Figure 4.35, Figure 4.36 and Figure 4.37. Following discussions in this section are made only for the first impacts for brevity.

As presented in Figure 4.30, P16 and P4 were dropped out for specimen SY100f05-b. Thus, for midpoint deflection and for P4's deflection, data obtained from P12 was used. The middle point RLPT of the control specimen BB100b was dropped out as well. Thus, P12 was used instead of P16 (midpoint deflection). Therefore, no exact midpoint displacements were obtained for those specimens. Thus, the displacement measured by a near RLPT was used as midpoint displacement for those specimens.

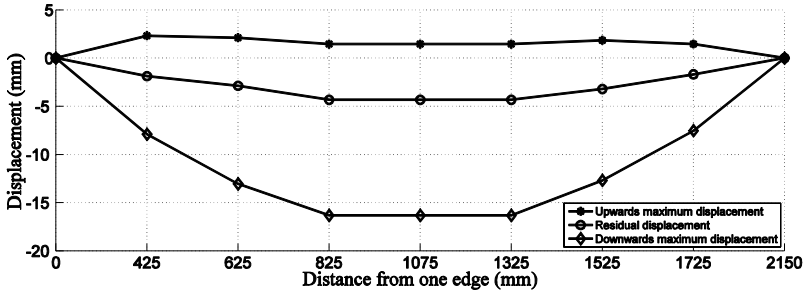

Figure 4.30. Deformation profile of specimen SY100f05-b after 1st impact

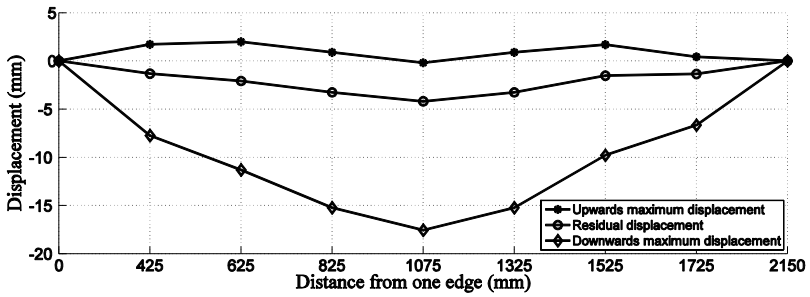

Figure 4.31. Deformation profile of specimen SY100f10-b after 1st impact

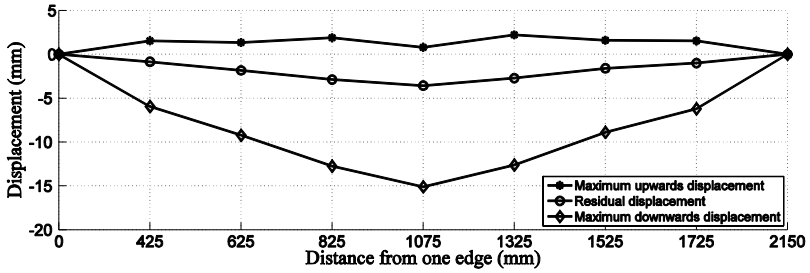

Figure 4.32. Deformation profile of specimen SY100f15-b after 1st impact

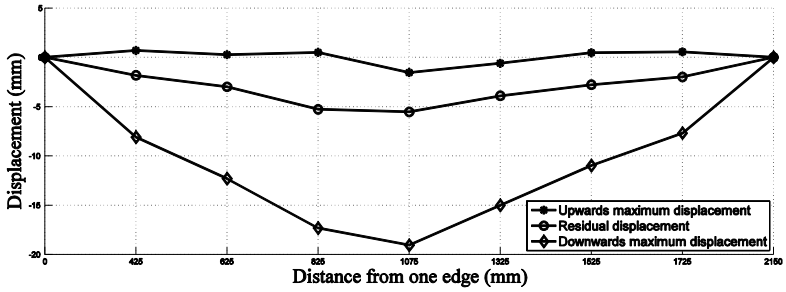

Figure 4.33. Deformation profile of specimen SY200f05-b after 1st impact

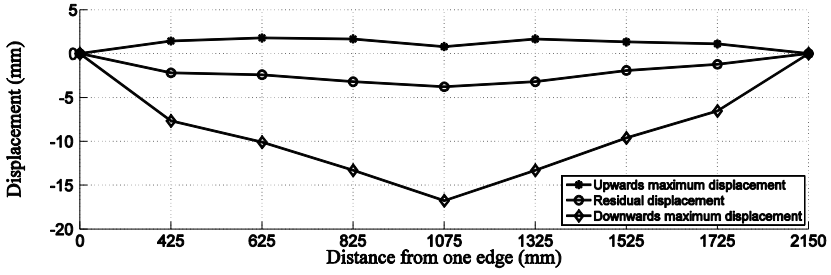

Figure 4.34. Deformation profile of specimen SY200f15-b after 1st impact

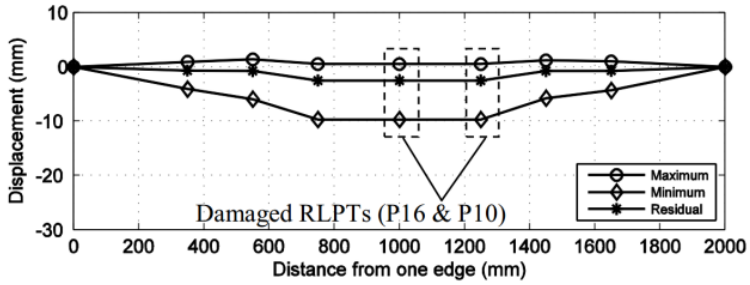

Figure 4.35. Deformation profile of specimen BB100b after 1st impact

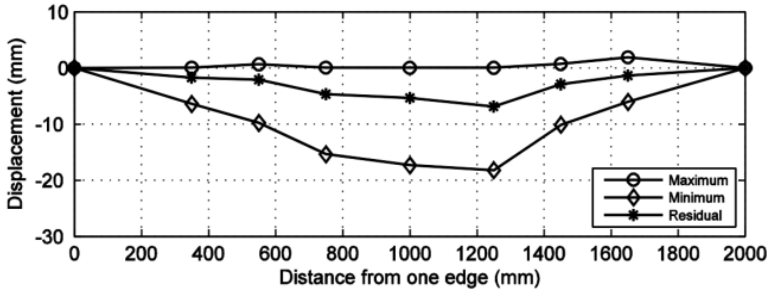

Figure 4.36. Deformation profile of the specimen BB200b after 1st impact

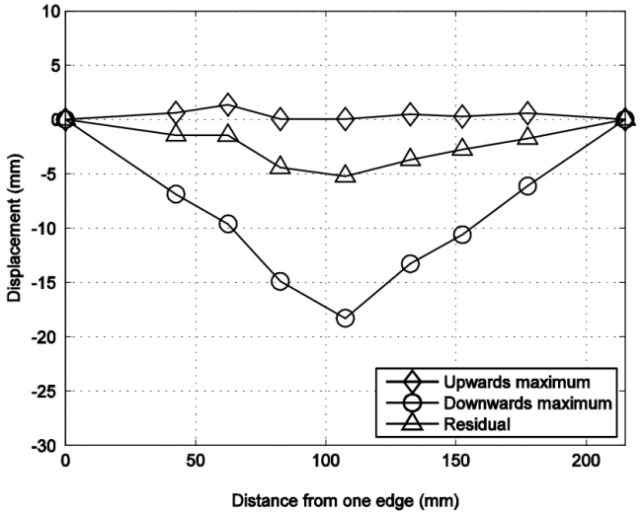

Figure 4.37. Deformation profile of specimen of YA200fb after 1st impact

Table 4.10. Maximum, minimum and residual displacements of each specimen

Specimen	Maximum Upwards Deflection (mm)	Maximum Downwards Deflection (mm)	Residual Deflection (mm)
BB100b*	1,03	-13,11	-2,69
SY100f05-b*	1,45	-16.31	-4,33
SY100f10-b	-0,19	-17,55	-4,19
SY100f15b	0,79	-15,11	-3,58
BB200b	0,74	-17,32	-5,29
SY200f05b	-1,54	-19,06	-5,54
YA200fb	-1,69	-18,3	-5,39
YA200f15b	0,79	-16,77	-3,78

* Midpoint RLPT (P16) of these specimens was dropped.

As a result of increased fiber content, both residual displacements and maximum downwards displacement of specimens were reduced (Table 4.10). Due to the difference in the level of absorbed energy in specimens BB200b and BB100b, these specimens were not included in this (Table 4.8). It must be noted that specimens BB200b and BB100b were failed under lower energy levels. Thus, with fiber addition, energy absorption capacities of specimens were enhanced.

Among specimens with same fiber content, the ones with lower longitudinal reinforcement ratio reached higher maximum downwards and residual displacement values (Table 4.10). This result was in good agreement with the more flexible nature of less reinforced specimens.

Impact loading was applied by the 210 kg drop weight for control specimens BB100b and BB200b. Due to the lower mass of the drop weight, the maximum downwards, the maximum upwards and residual displacement of control specimens were less than that of other specimens.

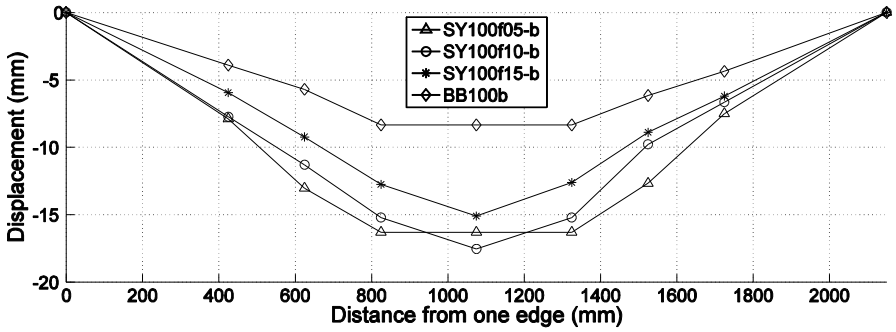

Figure 4.38. Maximum downwards displacement of the specimens with 0.4% longitudinal reinforcement ratio (Group 1)

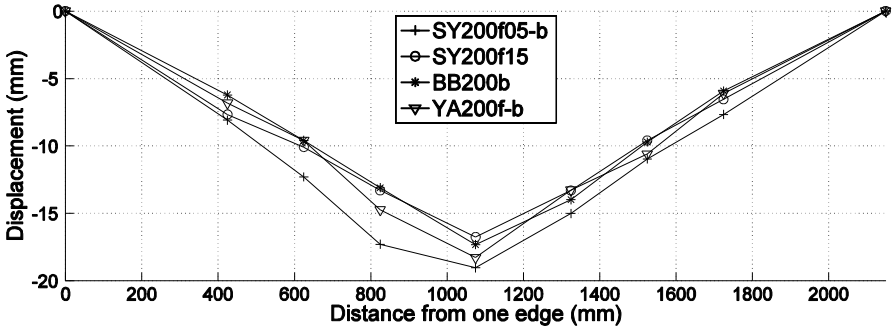

Figure 4.39. Maximum downwards displacement of the specimens with 0.2% longitudinal reinforcement ratio (Group 2)

Displacement profiles for specimens SY100f05-b, SY100f10-b, SY100f15-b and control specimen BB100b was presented in Figure 4.38. The applied energy for each specimen was presented in Table 4.8. The level of the maximum downwards displacement was reduced with increased fiber content. Although the midpoint RLPT of specimen SY100f05 was dropped out, it was clear that the maximum downwards deflection of this specimen would be larger than that of the other specimens in Group 1. It must be noted that, in case of specimen SY100f05-b, midpoint RLPT was pulled out. Here in this specimen, the displacement measured by a near RLPT was used for the midpoint.

Displacement profiles for specimens SY200f05-b, YA200fb, SY200f15-b and control specimen BB200b were presented in Figure 4.39. As expected, the maximum downwards displacement values for specimen Group 2 was more than that of specimen Group 1. Reduction in the maximum downwards displacement as fiber content increase in Group 2 is not as noticeable as in Group 1. Apparently, the effect of fibers in the

rigidity of the member was reduced for the low longitudinal reinforcement ratio. As a result of low longitudinal reinforcement ratio, the average crack width was increased, reducing the efficiency of the fibers by causing either pullout or rupture.

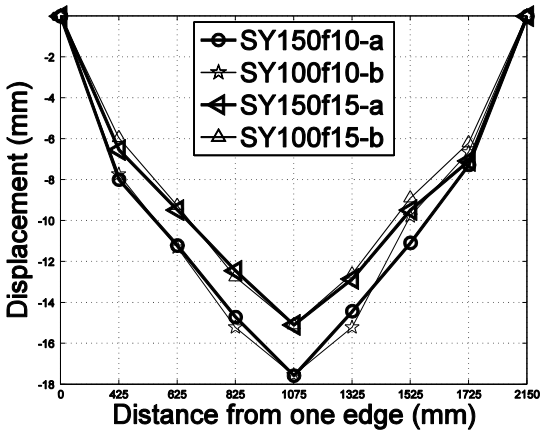

Figure 4.40. Comparison of static and dynamic displacements of specimens for same mid-point displacements

In Figure 4.43 and Figure 4.45 maximum downwards displacements at the impact loading and the corresponding displacements of the specimen at the static loading were presented. In Table 4.11 normalized maximum downwards displacements and residual displacements of the specimens with respect to the specimens with the less longitudinal reinforcement ratio in the corresponding specimen group were presented.

Table 4.11. Normalized maximum and residual displacements of the specimens

Specimen	Maximum Downwards Deflection (%)	Residual Deflection (%)
BB100b	-	-
SY100f05-b	1,24	1,61
SY100f10-b	1,34	1,56
SY100f15b	1,15	1,33
BB200b	-	-
SY200f05b	1,10	1,05
YA200fb	1,06	1,02
YA200f15b	0,97	0,71

The mid-point RLPT of specimen SY100f05-b was fallen. Therefore, no clear compression could be done. From Table 4.11 it was observed that, with lower reinforcement ratio, the residual displacement of specimens under impact loading was reduced more. Apparently, effect of increasing fiber content in specimens with lower longitudinal reinforcement ratio on residual displacements was more than the effect on maximum displacements. Increased fiber content in these specimens did not contribute to the rigidity of the member as much, but it helped to limit the damage and keep the member's resiliency.

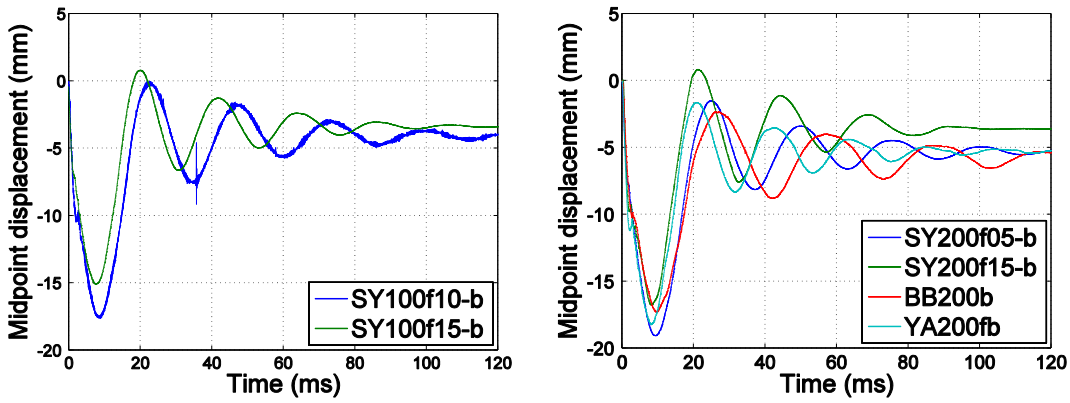

Figure 4.41. Time vs. Midpoint displacements for specimens with 0.2% and 0.4% longitudinal reinforcement ratio

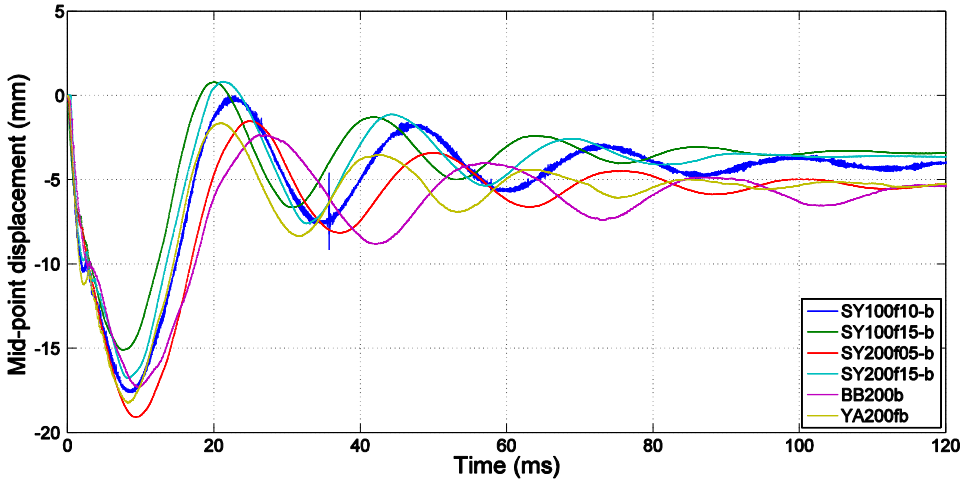

Figure 4.42. Time vs. Midpoint displacements for specimens for all specimens

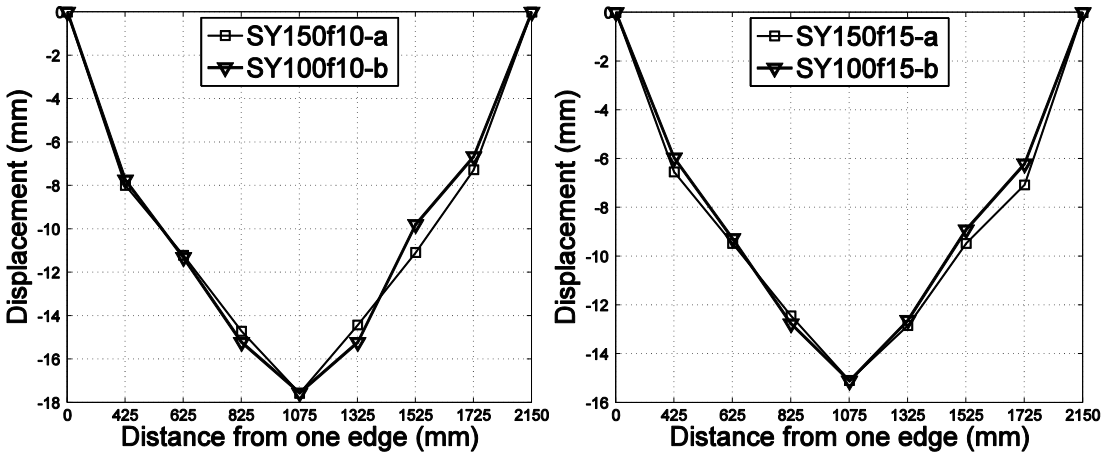

Figure 4.43. Maximum displacements of the specimens withe same longitudinal reinforcements and corresponding static tested control specimens

The maximum downwards displacement profiles for specimens with the longitudinal reinforcement ratio of 0.2% for both static and dynamic testing were presented in Figure 4.43. As mentioned earlier, the midpoint RLPT of specimen SY100f05-b was dropped. Therefore, results for this specimen were not included in Figure 4.43. As a general pattern, it was observed that with increased fiber content the behavior of the specimens became more similar to the behavior under static loading. As seen in Figure 4.43, for the specimen with 1% fiber content, displacements closer to the impact point moved faster whereas the remaining regions lagged behind when compared to the static displacements. This behavior was observed due to the inertia of

the member under rapid (Figure 4.44). On the other hand, this effect was less in the member with 1.5% fiber content. Higher fiber content apparently kept the displacement profile closer to the static profile by preventing the formation of a punching cone.

Figure 4.44. Shape of the specimen under static and impact loading

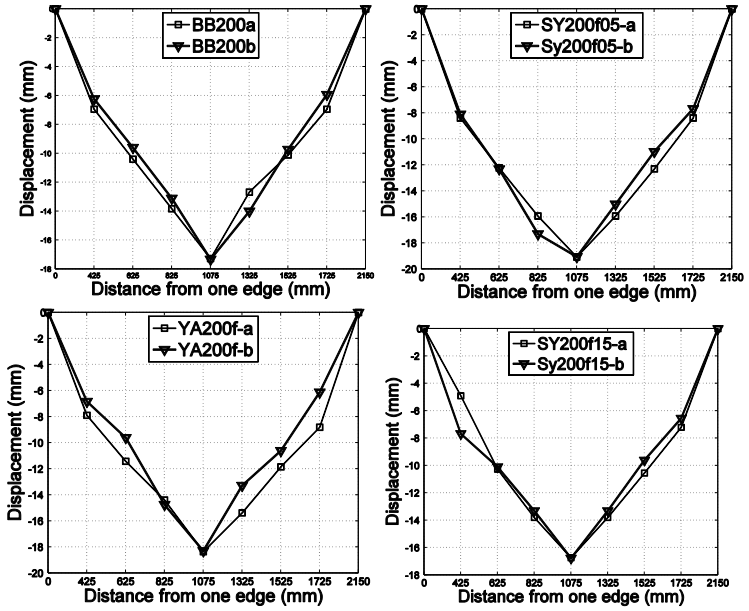

Figure 4.45. Displacement profile of each specimen under impact loading and the corresponding mid-point displacement at static loading

The maximum downwards displacement profiles for specimens with the longitudinal reinforcement ratio of 0.4% for both static and dynamic testing were presented in Figure 4.45. As a result of the increased fiber content, the behavior of the specimen under impact loading became more similar to that of under static loading. As presented in Figure 4.45 the effects of inertia was reduced with increased fiber content and formation of a punching cone was deterred

Table 4.12. Displacement values of the RLPTs under dynamic and static loading

Specimen	1st RLPT	2nd RLPT	3rd RLPT	Mid-point RLPT	5th RLPT	6th RLPT	7th RLPT
SY100f10-b	6,61	9,79	15,3	17,64	15,3	11	7,53
SY100f10-a	7,99	11,21	14,71	17,64	14,42	11,08	7,27
SY100f15-b	5,91	9,15	12,8	15,1	12,6	8,88	6,15
SY100f15-a	6,54	9,47	12,44	15,1	12,84	12,12	7,07
SY200f05-b	7,63	10,99	15,06	19,1	16,63	12,23	8,07
SY200f05-a	8,39	12,23	15,93	19,1	15,93	12,3	8,39
YA200fb	6,63	9,61	14,75	18,3	13,28	10,61	6,12
YA200fa	7,89	11,42	14,39	18,3	15,38	11,85	8,81
SY200f15-b	7,47	9,45	13	16,72	13	9,61	6,51
SY200f15-a	4,91	10,27	15,89	16,72	13,8	10,55	7,21

In Figure 4.12 the maximum mid-point displacement values and the displacement values of the other RLPTs values at that instant were presented. Both increasing the fiber content and increasing the longitudinal reinforcement ratio reduced the maximum displacement values of the specimens. As presented in Figure 4.43, Figure 4.45 and

Table 4.12, with increased fiber content the behavior of the specimens at the instant of the maximum downwards displacement became more similar to that of under static loading.

Displacement profiles of specimens for several moments until the time of maximum displacement under dynamic and static loading for the same mid-point displacement were presented in Figure 4.46, Figure 4.47, Figure 4.48 and Figure 4.49. In most specimens, after around 2.5 ms, impact displacement profile started to catch up with the static displacement profile. Effects of inertia were reduced faster for the specimens with higher fiber fractions.

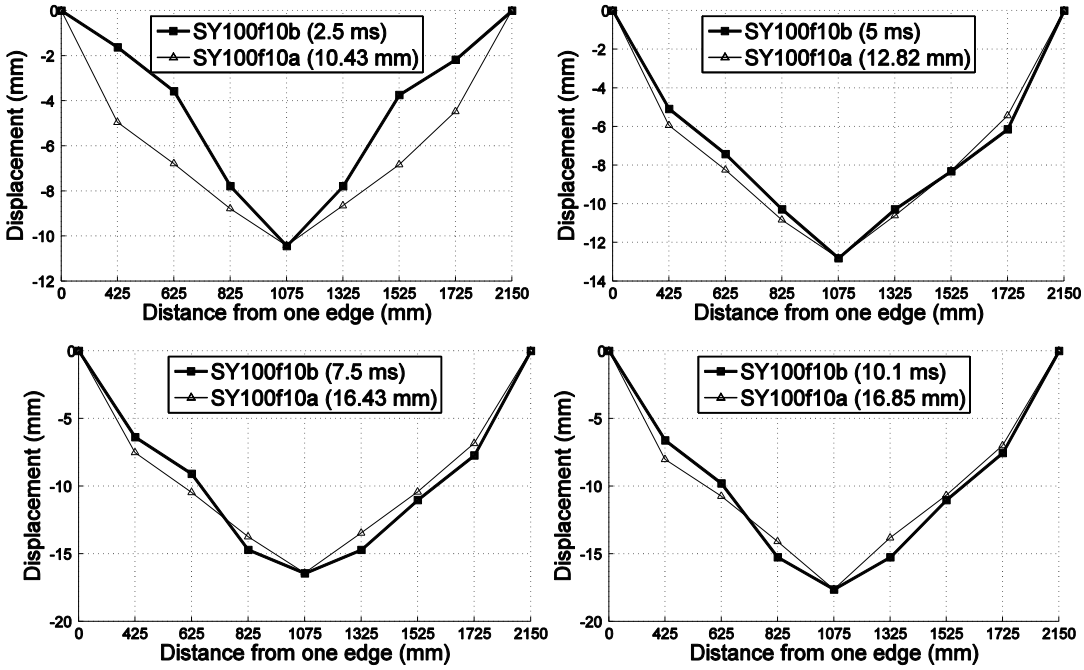

Figure 4.46. SY100f10 dynamic vs static displacements

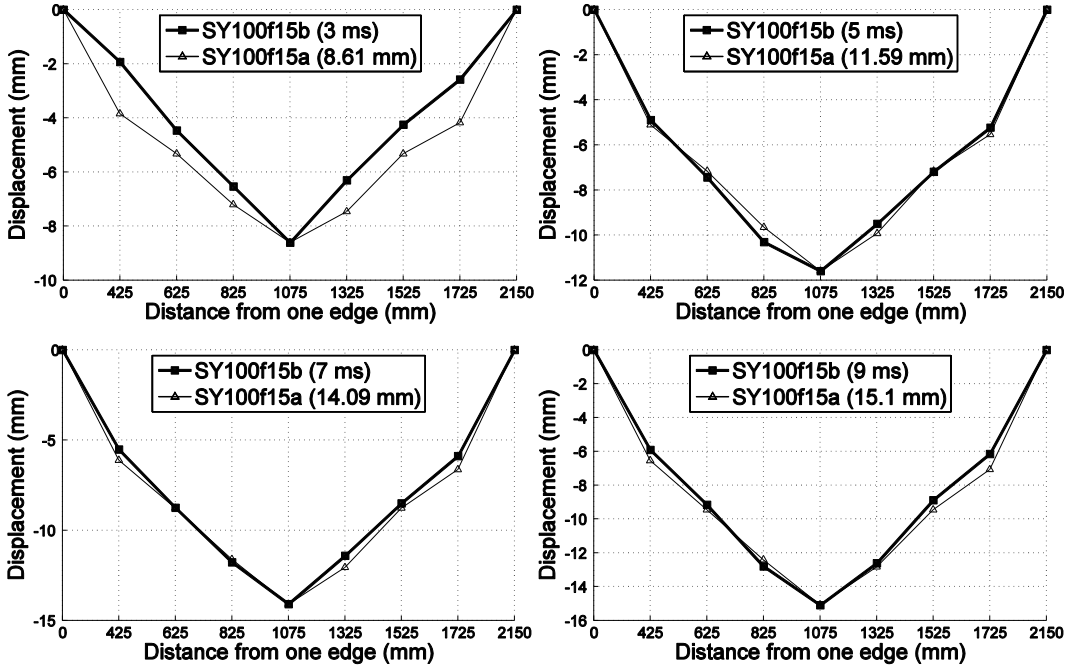

Figure 4.47. SY100f15 dynamic vs static displacements

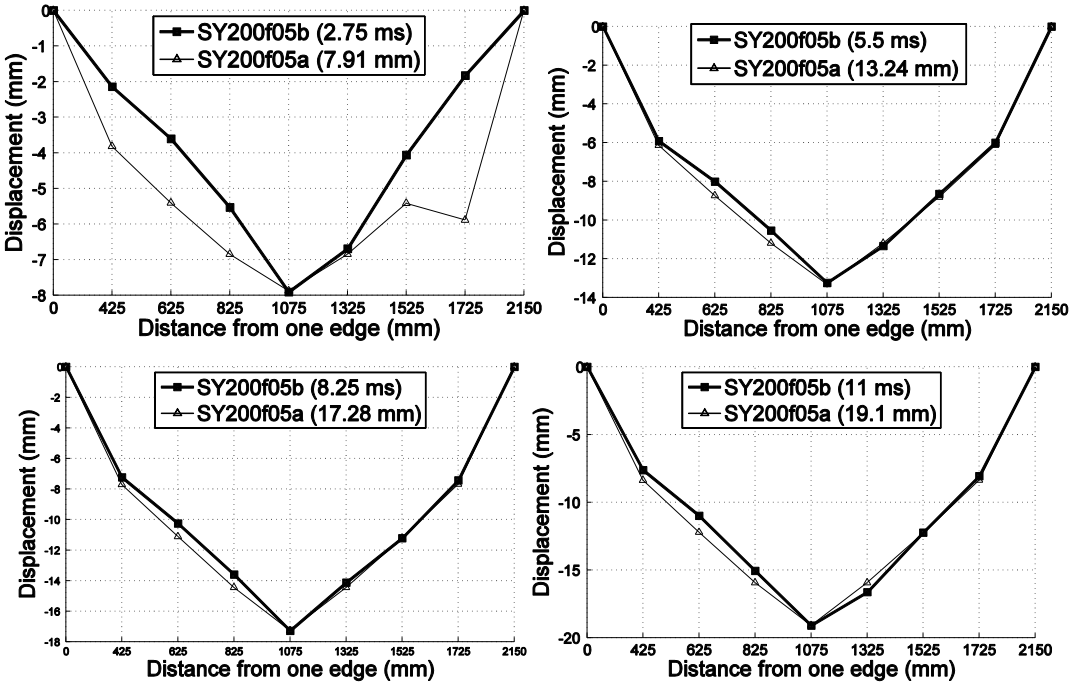

Figure 4.48. SY200f05 dynamic vs static displacements

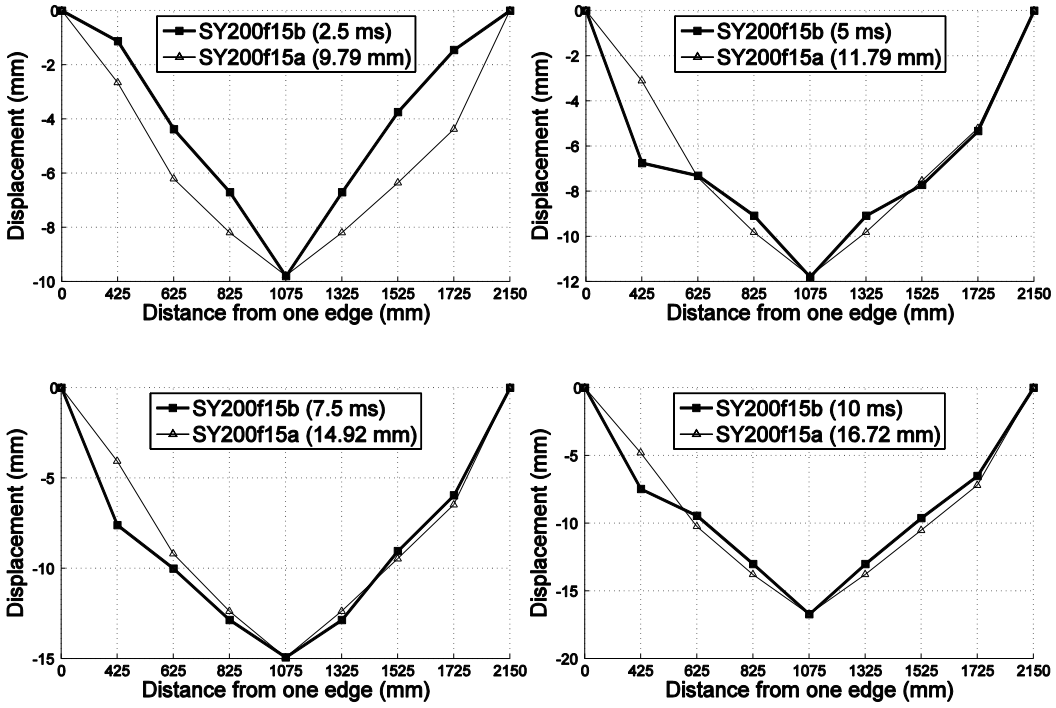

Figure 4.49. SY200f15 dynamic vs static displacements

4.4. Support Reactions

Impact load was resisted by inertia forces and support reaction forces of the specimen. Reaction forces were obtained from the measurements of load cells, whereas inertia forces were obtained from the measurement of the accelerometers on the top of the specimen. Furthermore, the applied impact load was obtained from the accelerometers on the drop weight.

Total reaction forces for each specimen after impacts were presented in Figure 4.50, Figure 4.51, Figure 4.52, Figure 4.53 and Figure 4.54. Unfortunately, total support reaction of specimen SY100f10-b after second impact could not be recorded. Maximum positive and maximum negative support reactions for each specimen were presented in Table 4.13 and Table 4.14.

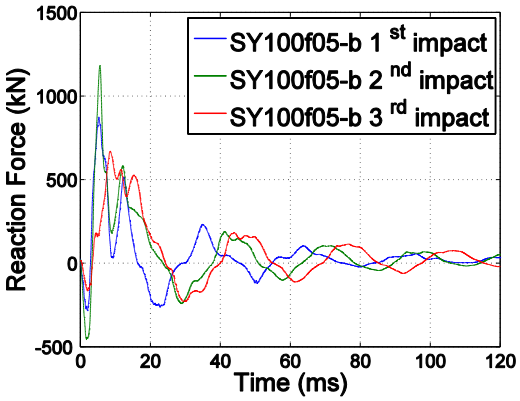

Figure 4.50. Total reaction force – time histories for SY100f05-b after each impact

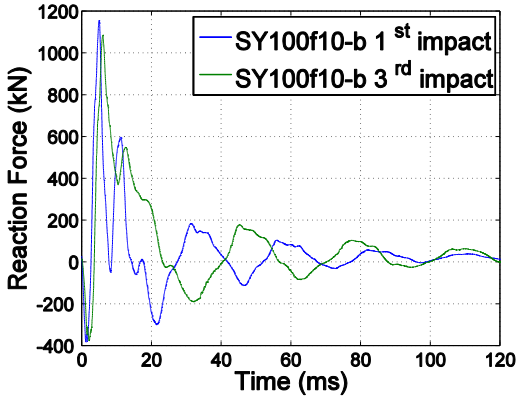

Figure 4.51. Total reaction force – time histories for SY100f10-b after each impact

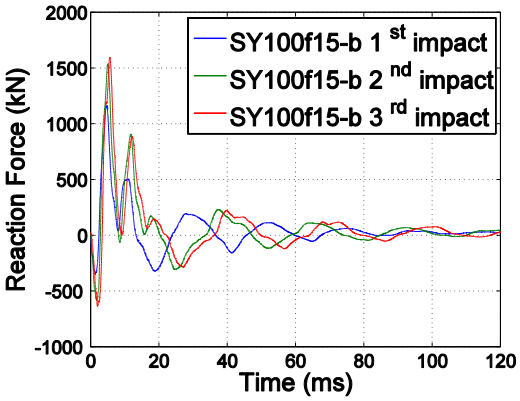

Figure 4.52. Total reaction force – time histories for SY100f15-b after each impact

In Figure 4.50, it was observed that, after the third impact reaction force of specimen SY100f05-b was reduced. This can be attributed to a local failure, probably in the form of a punching cone. There was no similar reduction in specimens SY100f10-b (Figure 4.51) and SY100f15-b (Figure 4.52). Thus, it can be said that, as a result of increased fiber content, such a local failure was prevented. Also in Figure 4.12 and Figure 4.13, no sign about a local failure was observed.

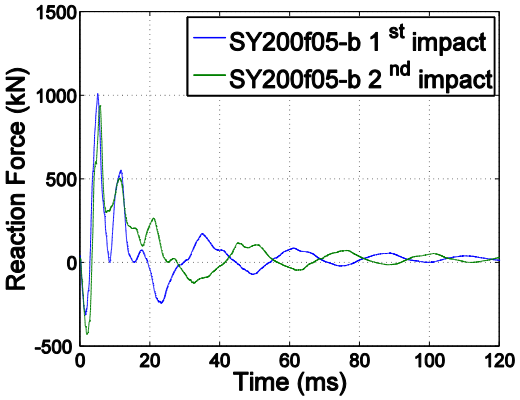

Figure 4.53. Total reaction force – time histories for SY200f05-b after each impact

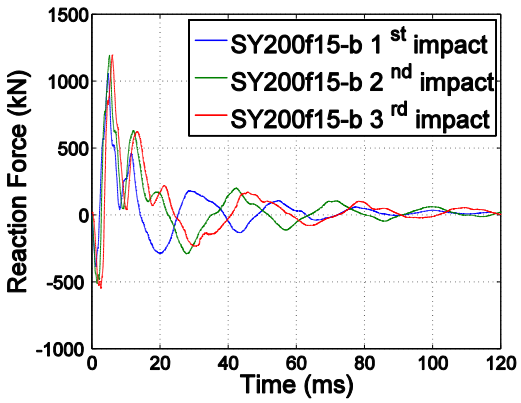

Figure 4.54. Total reaction force – time histories for SY200f15-b after each impact

The maximum positive and the maximum negative reaction forces for all specimens were presented in Table 4.13 and Table 4.14. Typically, if there was not any local punching failure, the maximum total reaction force remained very close under the same impact load between consecutive impacts. For identical fiber contents, specimens with higher longitudinal reinforcement ratio reached higher reaction forces. This could be the result of lower flexibility of specimens with higher reinforcement ratio.

Table 4.13. Maximum positive support reactions after each impact

Specimen	1st Impact (kN)	2nd Impact (kN)	3rd Impact (kN)	4th Impact (kN)
BB100b	661 (210 kg)	750 (320 kg)	971 (320 kg)	-
SY100f05-b	874 (320 kg)	1182 (555 kg)	668 (555 kg)	-
SY100f10-b	1155 (320 kg)	-	1085 (555 kg)	-
SY100f15-b	1161 (320 kg)	1535 (555 kg)	1598 (555 kg)	-
BB200b	683 (210 kg)	561 (210 kg)		-
SY200f05-b	1010 (320 kg)	938 (555 kg)	-	-
YA200fb	1061 (320 kg)	1234 (555 kg)	1136 (555 kg)	1153 (555 kg)
SY200f15-b	1056 (320 kg)	1196 (555 kg)	1195 (555 kg)	-

Table 4.14. Maximum negative support reactions after each impact

Specimen	1st Impact (kN)	2nd Impact (kN)	3rd Impact (kN)	4th Impact (kN)
BB100b	-100 (210 kg)	-180 (320 kg)	-193 (320 kg)	-
SY100f05-b	-285 (320 kg)	-458 (555 kg)	-228 (555 kg)	-
Sy100f10-b	-382 (320 kg)	-	-377 (555 kg)	-
SY100f15-b	-350 (320 kg)	-586 (555 kg)	-637 (555 kg)	-
BB200b	-210 (210 kg)	-215 (210 kg)	-	-
SY200f05-b	-314 (320 kg)	-430 (555 kg)	-	-
YA200fb	-475 (320 kg)	-525 (555 kg)	-603 (555 kg)	-615 (555 kg)
SY200f15-b	-389 (320 kg)	-511 (555 kg)	-549 (555 kg)	-

In order to obtain the acceleration of the drop weight, two accelerometers were mounted on top of the drop weight. Due to the presence of noise in acceleration data, some filtering was applied. Filtering process was done by MATLAB using the *'filtfilt'* command, designed as 5^{th} order Butterworth with 125 Hz cut-off frequency.

Figure 4.55 presents 14 accelerometers placed on the north east quarter of each specimen. Specimens were divided into 14 areas as the tributary area of each accelerometer (Figure 4.55). Then, this area was multiplied by the thickness of specimen, unit weight of reinforced concrete (assumed 2400 kg/m^3) and related accelerometer's measurement to obtain the inertia force on that area. Inertia force for one quarter of the specimen was obtained by summing all inertia forces calculated from each accelerometer and total inertia force on the specimen was obtained by multiplying that force by four. Total reaction force, inertia force and impact force time histories for each specimen were presented in Figure 4.56, Figure 4.57, Figure 4.58 and Figure 4.59. In those figures, the forces for first 20 ms and 60 ms were presented separately. As expected, at the early instant of the impact event, there was no support reaction, indicating that the entire impact load was resisted by the inertia of the specimen only at the first instants of the impact.

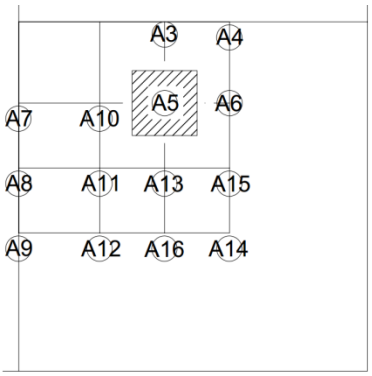

Figure 4.55. Positions of the accelerometers and a typical tributary area used for the calculation of the inertia force of related mass

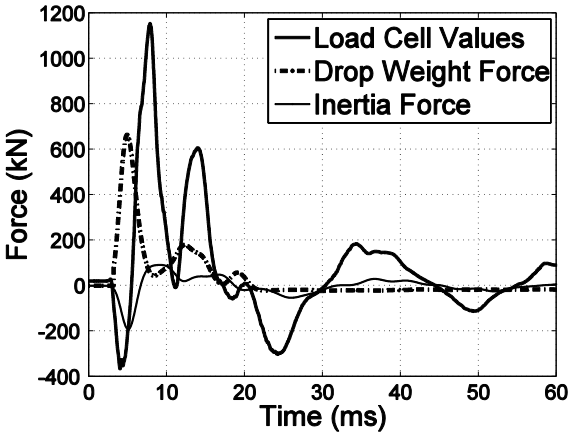

Figure 4.56. Load cell readings, inertia forces and impact forces for specimen SY100f10-b for first 60 ms

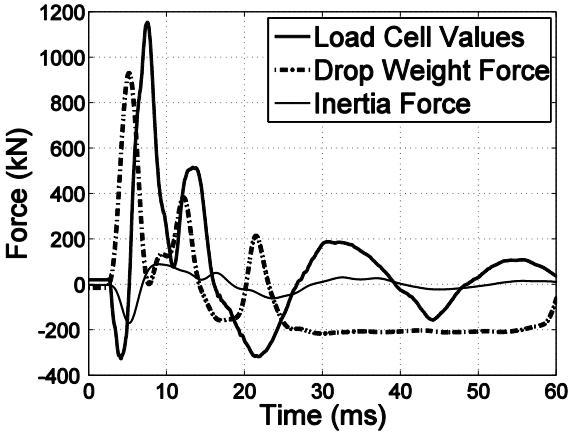

Figure 4.57. Load cell readings, inertia forces and impact forces for specimen SY100f15-b for first 60 ms

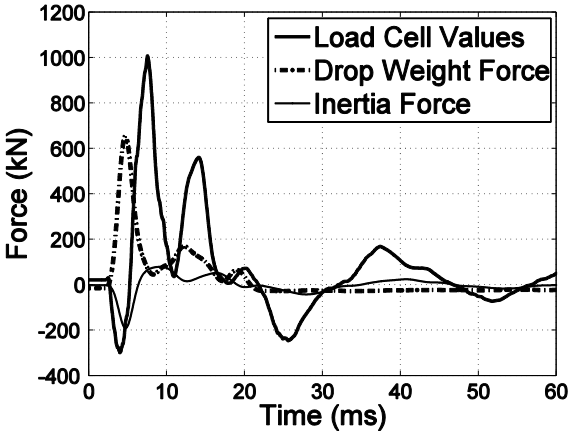

Figure 4.58. Load cell readings, inertia forces and impact forces for specimen SY200f05-b for first 60 ms

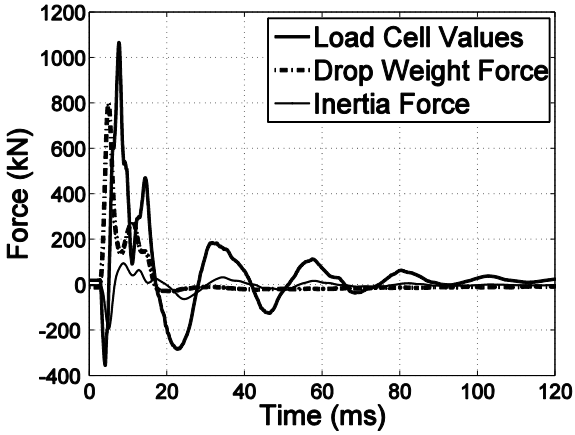

Figure 4.59. Load cell readings, inertia forces and impact forces for specimen SY200f15-b for first 60 ms

CHAPTER 5

CONCLUSIONS

This study investigated the impact behavior of reinforced concrete slabs strengthened for punching shear using steel fibers. For this study, five identical pairs with varying longitudinal reinforcement ratio and varying fiber content were employed to facilitate the comparison of the results for specimens under both static and dynamic loadings. Observations and obtained data were compared with companion studies Batarlar (2013) and Arsan (2014).

According to the results under static loading:

- Unlike specimens without steel fiber, specimens with steel fibers showed ductile behavior.
- Specimens with steel fiber reach higher maximum loads at higher maximum displacement values.
- As a result of the presence of the steel fibers in concrete mix, the number of cracks on the tension side was increased and the average crack width was reduced. Furthermore, an evenly distributed crack formation was obtained.
- As a result of increased fiber content, the rate of the increase of the final load and corresponding displacement dropped.
- For the specimens with higher longitudinal reinforcement ratio, the rate of increase in final displacement was more than that of final load.
- For the specimens with lower longitudinal reinforcement ratio, For specimens with lower longitudinal reinforcement ratio, the rate of increase in final displacement was less than that of final load.
- For specimens with lower longitudinal reinforcement ratio, specimens with 1.0% and 1.5% fiber content showed almost identical behavior. Thus, the efficiency of the fiber after 1.0% was reduced in specimens with 0.4% reinforcement ratio.

According to results under impact loading:

- Control specimens without fiber failed due to punching (Batarlar, 2013).
- Specimens with steel fiber addition resisted more impact loads with higher drop weight than specimens without steel fiber. Thus, specimens with steel fiber absorbed more energy than specimens without steel fiber addition.
- Unlike control specimens (Batarlar, 2013), as a result of the presence of the steel fiber in concrete mix, the behavior of specimens under impact loading was similar to that of under static loading. Displacement profile was changed slightly due to inertial forces.
- As a result of the addition of steel fibers, little or no scabbing was observed.
- With increased fiber content, average crack width was reduced and number of cracks was increased.
- After the first impact, no crack or cracks with the width less than 0.5 mm were formed on the impacted face of the specimen. Thus, as a result of steel fibers in concrete matrix, crack formation on the impacted face was reduced.
- Specimens with less longitudinal reinforcement ratio had wider cracks. In case of specimens with higher longitudinal reinforcement ratio, the number of crack was more than that of specimens with less amount of longitudinal reinforcement ratio.
- Among specimens with same longitudinal reinforcement ratio, maximum downwards displacement and residual displacement of specimens were reduced with increased fiber content.
- As a result of the presence of the steel fibers in concrete mix, punching was prevented and global failure mechanisms were obtained. Furthermore, the risk of spalling was prevented. Thus, secondary effects due to impact were reduced.

REFERENCES

ACI Committee 318, (2005). Building Code Requirements for Structural Concrete (ACI 318-05) and Commentary (318R-05). American Concrete Institute, Farmington Hills, Mich.

Adetifa, B., Polak, M.A., (2005). Retrofit of Slab Column Interior Connections Using Shear Bolts. ACI Structural Journal Title no. 102-S27

Arsan, Y., (2014). Effects of Shear Reinforcement On The Impact Behavior of Reinforced Concrete Slabs. Graduate School of Engineering and Sciences of İzmir Institute of Technology.

Batarlar, B., (2013). Behavior of Reinforced Concrete Slabs Subjected to Impact Loads. Graduate School of Engineering and Sciences of İzmir Institute of Technology.

Bu, W., Polak, M.A., (2009). Seismic Retrofit of Reinforced Concrete Slab-Column Connections Using Shear Bolts. ACI Structural Journal Title no. 106-S49

Cheng, M.-Y., Parra-Montesinos, G.J., (2010). Evaluation of Steel Fiber Reinforcement for Punching Shear Resistance in Slab-Column Connections- Part I: Monotonically Increased Load. ACI Structural Journal Title no. 107-S11

Dinh, H.H., Parra-Montesinos, G.J., Wight, J.K., (2010). Shear Behavior of Steel Fiber-Reinforced Concrete Beams without Stirrup Reinforcement. ACI Structural Journal Title no. 107-S59

El-Salakawy, F., Polak, M.A., Soudki, K.A., (2002). Rehabilitation of Reinforced Concrete Slab-Column Connections. Canadian Journal of Civil Engineering: Vol. 29, 2002.

El-Salakawy, F., Polak, M.A., Soudki, K.A., (2003). New Shear Strengthening Technique for Concrete Slab-Column Connections. ACI Structural Journal Title no. 100-S32

Ghali, A., Youakim, S.A., (2005). Headed Studs in Concrete: State of the Art. ACI Structural Journal Title no. 102-S67

Kiski, N., Kurihashi, Y., Ghadimi Khasraghy, S.,, Mikami, H., (2011). Numerical Simulation of Impact Response Behavior of Rectangular Reinforced Concrete Slabs under Falling – Weight Impact Loading. Applied Mechanics and Materials, Vol. 83, 266-271

LabView (2010). National Instruments, Austin, TX., U.S.A.

Li, Q.M., Reid, S.R., Wen, H.M., Telford, A.R.,(2005). Local impact effects of hard missiles on concrete targets. International Journal of Impact Engineering 32 (2005) 224-284

MATLAB (2009). The MathWorks, Natick, M.A., U.S.A.

Trautwein, L.M., Bittencourt, T.N., Gomes, R.B., Bella, J.C.D., (2011). Punching Strength of Flat Slabs with Unbraced Shear Reinforcement. ACI Structural Journal Title no. 108-S20

Ong, K.C.G., Basheerkhan, M., Paramasivam, P., (1999). Resistance of Fibre Concrete Slabs to Low Velocity Projectile Impact. Cement and Concrete Composites 21 (1999) 391 -401

Xu, H., Mindess, S., (2006). Behavior of Concrete Panels Reinforced With Welded Wire Mesh and Fibres Under Impact Loading. ASCE 2006, Shotcrete.

Zineddin, M., Krauthammer, T., (2007). Dynamic response and behavior of reinforced concrete slabs under impact loading. International Journal of Impact Engineering 34 1517-1534

APPENDIX A

TECHNICAL DATA SHEETS

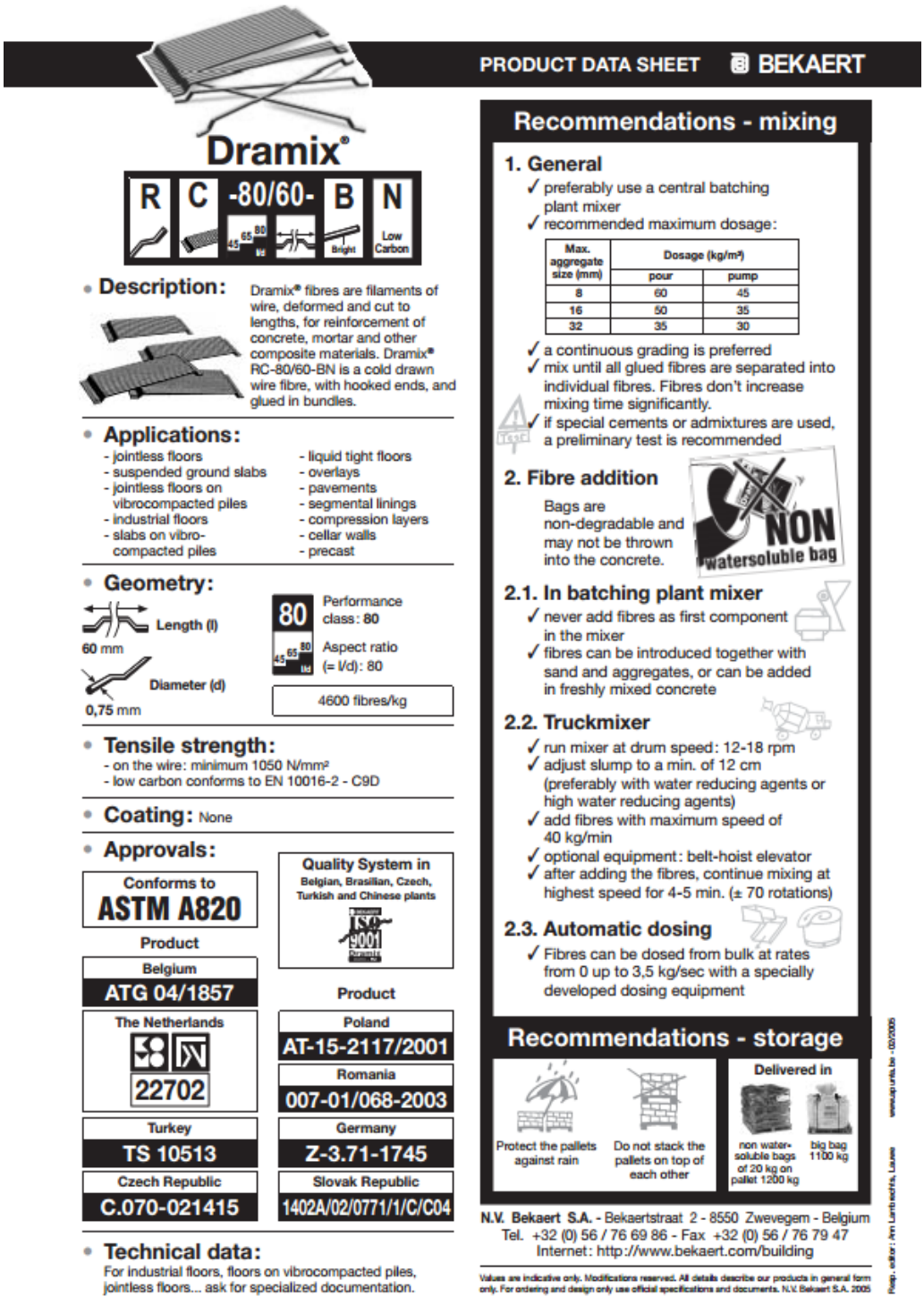

PRODUCT DATA SHEET BEKAERT

Dramix®

R C -80/60- B N

Low Carbon

Description: Dramix® fibres are filaments of wire, deformed and cut to lengths, for reinforcement of concrete, mortar and other composite materials. Dramix® RC-80/60-BN is a cold drawn wire fibre, with hooked ends, and glued in bundles.

Applications:
- jointless floors
- suspended ground slabs
- jointless floors on vibrocompacted piles
- industrial floors
- slabs on vibro-compacted piles
- liquid tight floors
- overlays
- pavements
- segmental linings
- compression layers
- cellar walls
- precast

Geometry:
Length (l) 60 mm
Diameter (d) 0,75 mm
80 Performance class: 80
Aspect ratio (= l/d): 80
4600 fibres/kg

Tensile strength:
- on the wire: minimum 1050 N/mm²
- low carbon conforms to EN 10016-2 - C9D

Coating: None

Approvals:
Conforms to ASTM A820
Quality System in Belgian, Brasilian, Czech, Turkish and Chinese plants

Product		Product	
Belgium	ATG 04/1857	Poland	AT-15-2117/2001
The Netherlands	22702	Romania	007-01/068-2003
Turkey	TS 10513	Germany	Z-3.71-1745
Czech Republic	C.070-021415	Slovak Republic	1402A/02/0771/1/C/C04

Technical data:
For industrial floors, floors on vibrocompacted piles, jointless floors... ask for specialized documentation.

Recommendations - mixing

1. General
- ✓ preferably use a central batching plant mixer
- ✓ recommended maximum dosage:

Max. aggregate size (mm)	Dosage (kg/m³)	
	pour	pump
8	60	45
16	50	35
32	35	30

- ✓ a continuous grading is preferred
- ✓ mix until all glued fibres are separated into individual fibres. Fibres don't increase mixing time significantly.
- ✓ if special cements or admixtures are used, a preliminary test is recommended

2. Fibre addition
Bags are non-degradable and may not be thrown into the concrete.
NON watersoluble bag

2.1. In batching plant mixer
- ✓ never add fibres as first component in the mixer
- ✓ fibres can be introduced together with sand and aggregates, or can be added in freshly mixed concrete

2.2. Truckmixer
- ✓ run mixer at drum speed: 12-18 rpm
- ✓ adjust slump to a min. of 12 cm (preferably with water reducing agents or high water reducing agents)
- ✓ add fibres with maximum speed of 40 kg/min
- ✓ optional equipment: belt-hoist elevator
- ✓ after adding the fibres, continue mixing at highest speed for 4-5 min. (± 70 rotations)

2.3. Automatic dosing
- ✓ Fibres can be dosed from bulk at rates from 0 up to 3,5 kg/sec with a specially developed dosing equipment

Recommendations - storage

Protect the pallets against rain
Do not stack the pallets on top of each other
Delivered in: non water-soluble bags of 20 kg on pallet 1200 kg; big bag 1100 kg

N.V. Bekaert S.A. - Bekaertstraat 2 - 8550 Zwevegem - Belgium
Tel. +32 (0) 56 / 76 69 86 - Fax +32 (0) 56 / 76 79 47
Internet: http://www.bekaert.com/building

Resp. editor: Ann Lambrechts, Leuven www.up-units.be - 02/2005

Figure A.1. Steel fibers' product data sheet

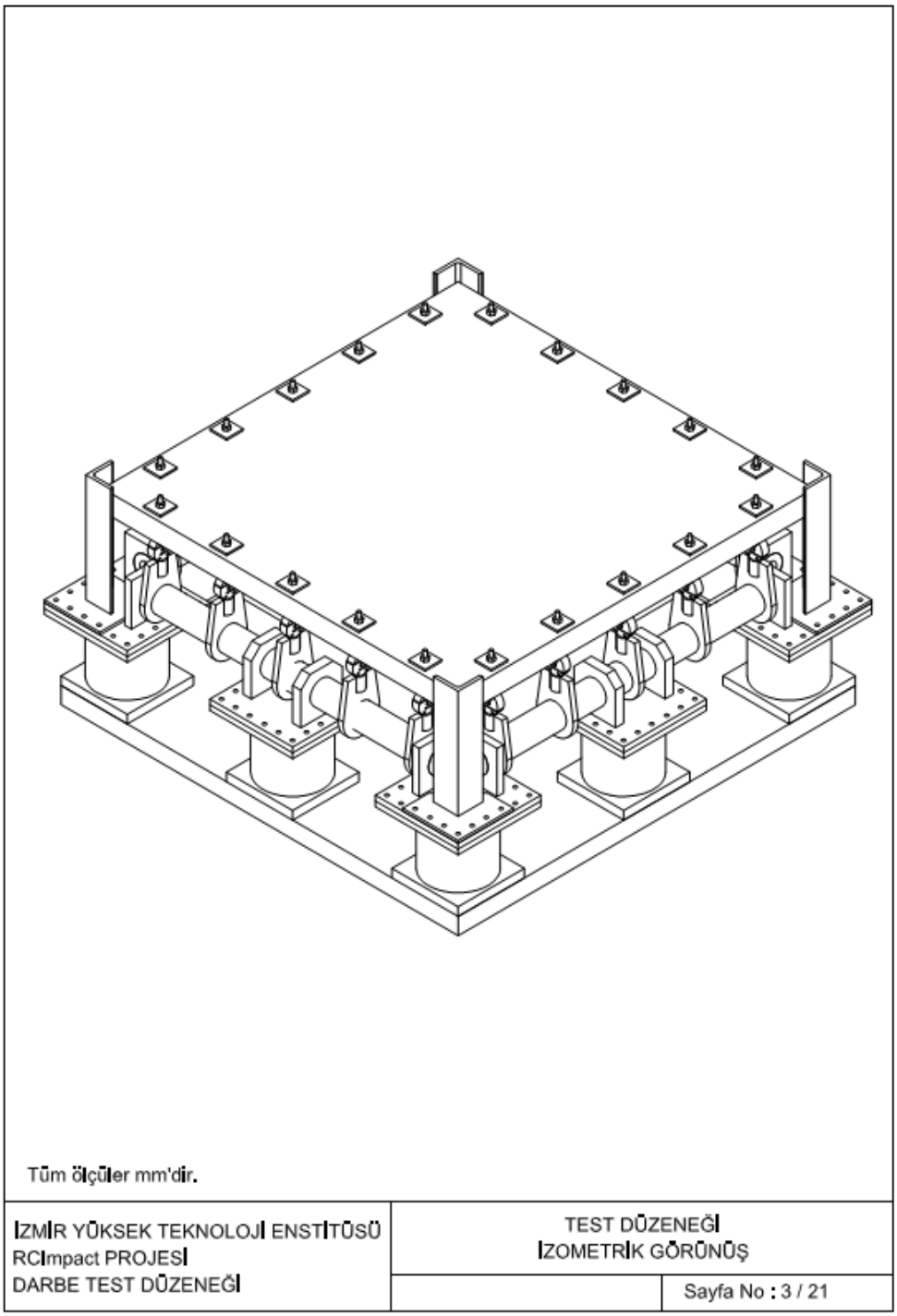

Figure A.2. Isometric view of the test setup